THE UNIVERSITY *of* EDINBURGH

PEBAX-based Mixed Matrix Membranes for Post-Combustion Carbon Capture

Nicholas Bryan

THE UNIVERSITY *of* EDINBURGH
School of Engineering

Doctor of Philosophy

August 2017

Abstract

Polymeric membranes exhibit a trade-off between permeability and selectivity in gas separations which limits their viability as an economically feasible post-combustion carbon capture technology. One approach to improve the separation properties of polymeric membranes is the inclusion of particulate materials into the polymer matrix to create what are known as mixed matrix membranes (MMMs). By combining the polymer and particulate phases, beneficial properties of both can be seen in the resulting composite material.

One of the most notable challenges in producing mixed matrix membranes is in the formation of performance-hindering defects at the polymer-filler interface. Non-selective voids or polymer chain rigidification are but two non-desirable effects which can be observed. The material selection and synthesis route are key to minimising these defects. Thin membranes are also highly desirable to achieve greater gas fluxes and improved economical separation processes. Hence smaller nano-sized particles are of particular interest to minimise the disruption to the polymer matrix. This is a challenge due to the tendency of some small particles to form agglomerations.

This work involved introducing novel nanoscale filler particles into PEBAX MH1657, a commercially available block-copolymer consisting of poly(ethylene oxide) and nylon 6 chains. Poly(ether-b-amide) materials possess an inherently high selectivity for the CO_2/N_2 separation due to polar groups in the PEO chain but suffer from low permeabilities.

Mixed matrix membranes were fabricated with PEBAX MH1657 primarily using two filler particles, nanoscale ZIF-8 and novel nanoscale MCM-41 hollow spheres. This work primarily investigated the effects of the filler loading on both the morphology and gas transport properties of the composite materials. The internal structure of the membranes was examined using scanning electron microscopy (SEM), and the gas transport properties determined using a bespoke time-lag gas permeation apparatus.

ZIF-8 is a zeolitic imidazolate framework which possesses small pore windows

that may favour CO_2 transport over that of N_2. ZIF-8-PEBAX membranes were successfully synthesised up to 7wt.%. It was found that for filler loadings below 5wt.%, the ZIF-8 was well dispersed within the polymer phase. At these loadings modest increases in the CO_2 permeability coefficient of 0-20% compared to neat PEBAX were observed. Above this 5wt.% loading large increases in both CO_2, N_2 and He permeability coefficients coincided with the presence of large micron size clusters formed of hundreds of filler ZIF-8 particles. The increases in permeability were attributed to voids observed within the clusters.

MCM-41 is a metal organic framework that has seen notable interest in the field of carbon capture, due to its tunable pore size and ease of functionalisation. Two types of novel MCM-41 hollow sphere (MCM-41-HS) of varying pore size were incorporated into PEBAX and successfully used to fabricate MMMs up to 10wt.%. SEM showed the MCM-41 generally interacted well with the polymer with no signs of voids and was generally well dispersed. However, some samples of intermediate loading in both cases showed highly asymmetric distribution of nanoparticles and high particle density regions near one external face of the membrane which also showed the highest CO_2 permeability coefficients. It is suspected that these high permeabilities are due to the close proximity of nanoparticles permitting these regions to act in a similar way to percolating networks. It was determined that there was no observable effect of the varying pore size which was expected given the transport in the pores should be governed by Knudsen diffusion.

This work was undertaken as part of an Industrial Cooperative Awards in Science and Technology (CASE) award coordinated by The University of Edinburgh in a partnership with Johnson Matthey and the EPSRC.

Lay Summary

Climate change has the potential to severely alter the world as we know it. Emissions of carbon dioxide (CO_2) are the main culprit of climate change and therefore curbing the continual output of CO_2 offers the most effective means of tackling the challenge of climate change in the immediate future.

While in the future a reality free of carbon emissions will be feasible, it seems inevitable that fossil fuels will continue to be used for energy generation for many years to come. One of the simplest and most effective ways to reduce CO_2 emissions could be to capture the CO_2 from large point sources such as the flue gas of coal and gas-fired power plants by separating the carbon dioxide from the flue gas (mainly nitrogen) and store it in depleted gas reservoirs.

Membrane gas separation is one technology currently being developed to separate CO_2 from the flue gases produced by fossil fuel power stations. Polymeric membranes are a well established technology used for separating mixtures of gases but improvements in current polymer-based membranes would make the process more economically feasible and viable for implementation.

One approach to improving the properties of polymeric membranes is to incorporate solid particles known as fillers into the polymer to combine the best features of both materials. In this work, two nanoscale porous materials were incorporated into a highly selective polymer and the effects of the mass loading of the filler into the materials on both the internal structure and gas separation properties were investigated.

Declaration

I hereby declare that I have written this thesis in its entirety and that the work presented is my own except where indicated. None of the work has been previously submitted for any other degree or professional qualification.

Acknowledgements

First and foremost I must thank my supervisor Chiara Ferrari for her guidance, patience and support over the last fours years. Her help has been invaluable, and I have immensely enjoyed working with and learning from her. My great thanks must also be extended to Stefano Brandani from whom I have learned many things, well beyond these last four years, especially the importance of thermodynamics and cake.

It has been a joy to be a part of the carbon capture group whose camaraderie and collective ability to bake is second to none in the school. Special thanks must go to Elsa Lasseuguette for her friendship and help over the years as the other sole long-standing member of the 'membrane group.'

I must also thank Ludovic Dumee who aside from the work, showed immense kindness during my stay at Deakin and it is a pleasure have met him and to call him a friend.

The last four years have been a lot of fun thanks to the countless friends I have made here in the school of engineering and I could not avoid mentioning Pedro, Alex, Patrick and Arran for leading the way, and Sofia, Nelly, Steven, Charithea, James and Rohan for their company at lunch and suffering too. I trust Davido, Chris and Bruno will carry on the traditions of the IMP PhD students.

Lastly I must thank all my family and friends for their support, encouragement and fun had over the last four years. In particular I am grateful to all of my many many flatmates - Ryan, Doug and Theo, for the countless years of fun, Liam, Anne, Danielle, Josh, Lovisa and Karen (the faffmates), Jude, Damon for never saying no to an adventure, Holly for giving me something to look forward to, and of course both my parents and my sisters for whom I do everything.

Contents

Chapter 1

Introduction

1.1 Climate Change and its Challenges

Climate change is arguably the greatest challenge ever faced by human civilization. It is now of little debate whether climate change is happening but the impact it will have and how fast its effects will come to fruition.[1] The full implications are far from certain; glaciers are melting at unprecedented rates, the risks of flooding, heatwaves, wildfires, and droughts are increasing, hurricanes and tropical storms are occurring ever more frequently and with greater power, and sea levels continue to rise threatening low lying communities.[2–7]

The average global temperature has not only continued to increase since the dawn of the industrial revolution but in recent decades warming has started to accelerate.[8,9] Figure 1.1 shows the extent of warming since the onset of the industrial revolution. Worryingly 2016 has stood out in this trend setting both monthly global temperature records for seven of the first eight months of 2016 since modern records began in 1880, as well as five of the same months setting records for the lowest coverage of Arctic sea ice.[10–12] There is also evidence to suggest there will be positive-feedback type responses to further global temperature increases such as regime changes in Arctic ice conditions and net release of carbon dioxide held within the soil.[13,14] With the potential for such fast alterations to climate systems in the immediate future, the impetus to minimise further CO_2 emissions quickly is crucial.

The paramount driver of climate change is the continued emission of carbon dioxide into the atmosphere. Figure 1.2 shows the increase in atmospheric carbon dioxide concentration since 1960 and this has been undeniably linked to climate change.[1] While emissions of other gases and aerosols as well as other causes such

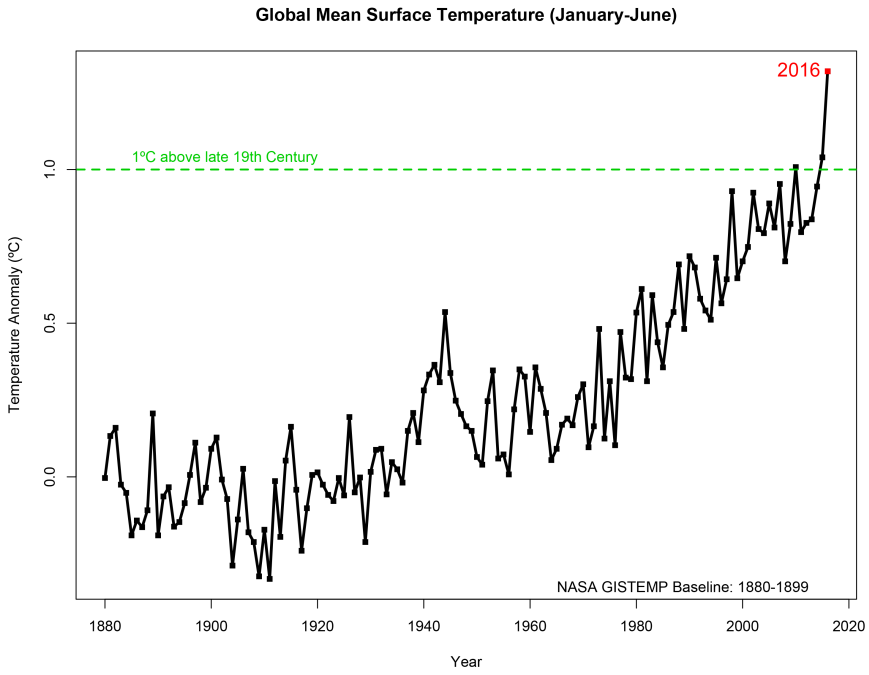

Figure 1.1: Global temperature data highlights the acceleration in the last 30 years.[11,12]

as modification of land use play a role, it is CO_2 from fossil fuel use that is the dominant force in driving climate change.[15,16] Thus it is here we can have the biggest impact in altering the path we are on and attempt to limit climate change. This has been realised for many decades now and numerous international treaties have been agreed on with the purpose of limiting CO_2 emissions.

The United Nations Framework Convention on Climate Change (UNFCCC) was negotiated nearly 25 years ago in 1992 with the aim of minimising further anthropogenic changes to the climate by controlling atmospheric concentrations of greenhouse gases (GHGs). Shortly after the Kyoto Treaty, a binding commitment to reduce GHG emissions, was signed. The 4th of November 2015 marked a significant date in that the Paris Agreement legally entered into force.[18] Article 2 of the Paris Agreement states that it:

> aims to strengthen the global response to the threat of climate change... by holding the increase in the global average temperature to well below 2°C above pre-industrial levels and pursuing efforts to limit the temperature increase to 1.5°C above pre-industrial levels, recognizing that this would significantly reduce the risks and impacts of climate change.[19]

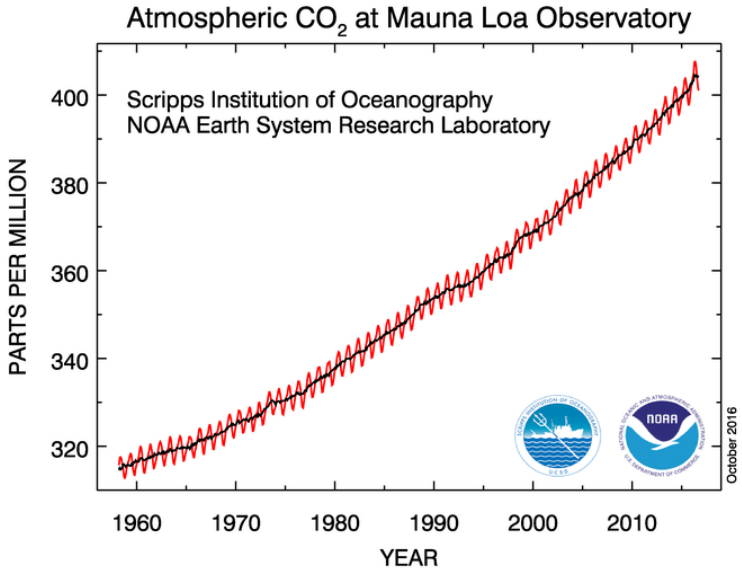

Figure 1.2: Historic atmospheric CO_2 concentrations recorded at Mauno Loa Observatory as of October 2016[17]

These targets are ambitious to say the least, particularly in light of recent temperatures observed already in 2016. Professor Chris Field, Chair of the IPCC working group on adaptation to climate change recently said the 1.5°C target "now looks impossible or at the very least, a very, very difficult task."[20] To limit climate change to 1.5°C, let alone 2°C, will require a global response of a monumental scale.[21]

1.2 A Brief Argument for Carbon Capture

The industrial revolution irrevocably changed the world and led to the exponential explosion of the global population. Since then, the world as we know it has been intertwined with fossil fuels. Modern civilization is currently dependent on fossil fuels for both energy and transport. It is this dependency that makes abatement of carbon dioxide emissions quite so challenging. Fossil fuels are often simply reduced to 'evil' substances which we should discard to the annals of history with immediate effect, however to treat this dependency with such ease of thought is wholly unhelpful. In truth, fossil fuels are still an essential part of energy generation. This is where the most simple case for carbon capture shines through: to still be able to utilise fossil fuels whilst minimising their continued contribution to climate change.

The case for carbon capture has been long debated, there is some argument that it would increase our dependency on fossil fuels, and in the same space of time as it would take to be implemented, alternate, low-carbon energy technologies could be developed.[22] A quote from Lord Oxburgh, published in a recent report by the Parliamentary Advisory Group on CCS sums up often held attitudes to carbon capture:

> I began this study, as I know a number of my colleagues did, quite prepared to advise you to write-off CCS as a part of UK energy policy. As you will see, our report recommends the opposite of this.[23]

In this report they concluded that CCS was essential as part of the lowest cost method to 'decarbonise' the UK. The Committee on Climate Change also recently claimed that any delay in implementing carbon capture in the UK would add significant costs to later carbon abatement.[24]

A similar point, highlighting the increased cost of any delay beyond 2020 in reducing carbon emissions, was also reflected in the 2010 International Energy Agency report Energy Technology Perspectives.[25]These higher costs are related to the scale of action that must be undertaken on a shorter time scale as well as being able to continue to use fossil-fuel power stations which are able to vary their power output.[26] As well as for reasons of cost, a degree of flexibility should be maintained by utilising a diverse portfolio of low carbon technology to allow for changing cost-competitiveness of these various technologies. Further to this, to help guarantee a transition to a low carbon future a diverse energy portfolio will also avoid relying on the success of a few technologies. Thus there are reasons of cost, flexibility and security why CCS technology should be developed and pursued. Quite simply it seems impossible to envisage a scenario where the targets for meeting reductions in CO_2 emissions can be met without CCS.

1.3 Approaches to Carbon Capture

Carbon capture and storage is the process of separating and purifying carbon dioxide and subsequently sequestering it whether it be either in large geological formations or by some other means, the former currently seeming the most viable option due to the quantities involved and the necessary time scale of storage.[27] The purpose of carbon capture is to limit the emissions of CO_2 from large point sources such as fossil fuel power plants or industrial sites such as cement plants. Carbon capture is typically seen as involving 3 distinct steps: the separation and purification of CO_2, the transport of CO_2 to the storage site, and finally the storage itself. Transport would be facilitated by a network of pipelines or potentially

tankers to a large geological storage site, such as a depleted gas field or saline aquifer, where it would be stored. The transport and storage of CO_2 are both complex topics in their own right, far outwith the scope of this work. Thus for the purpose of simplicity, in the remainder of this text 'capture' will be used to refer to the act of separating the CO_2 from flue gas.

Capture from fossil fuel based power plants has been suggested by three differing approaches:[28]

- **Pre-combustion** is the method wherein CO_2 is separated prior to combustion of the fuel. Hydrogen is produced by steam reforming of natural gas or coal. Carbon dioxide is separated from this CO_2/H_2 mixture.
- **Oxyfuel combustion** is the method where the fuel is combusted in a stream of oxygen and recycled flue gases. This means the flue gas is composed of mainly CO_2 and water where other incondensable gases are in impurity quantities making the separation relatively easy.
- **Post-combustion** involves separation of CO_2 from the flue gases after complete combustion of the primary fuel. The incondensable flue gas is mainly a CO_2/N_2 mix with other impurities.

Each have their advantages and limitations. Figure 1.3 shows the operations that are involved in each method. From this it is clear to see the lower number of steps and lessened degree of integration involved in post-combustion. Combined with the fact that currently the large majority of electricity is produced via direct combustion of coal, oil or gas in air, it follows that post-combustion capture is the simplest of the options to retrofit. This is the case as it requires minimal modification to the existing power plant, and, while pre-combustion and oxyfuel technologies may well provide advantages in the future, it is post-combustion that is the most likely to be implemented in the near future.[26,28–30] While the work presented here is not irrelevant to the separations involved in pre-combustion and oxyfuel combustion, it will focus on the CO_2/N_2 separation of post-combustion capture.

1.3.1 Capture from Various Primary Fuels

Coal, oil and gas still make up the large majority of primary fuel usage for electricity generation as can be seen in figure 1.4. While the use of renewables and nuclear power is increasing relatively, it is clear that changes in sources of energy are slow, and that coal, oil, and gas will continue to play a large role for a considerable time.[31]

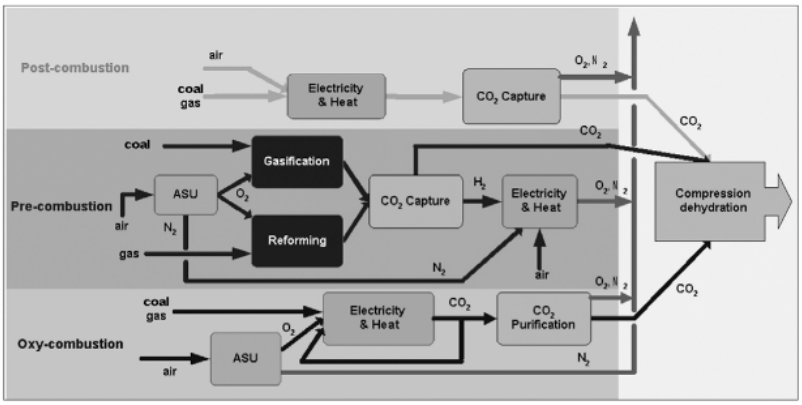

Figure 1.3: Flow chart highlighting the steps involved in each capture process[28]

The fuel used drastically changes the composition of the flue gas and hence has a huge impact on the capture process. The concentration of CO_2 in flue gas is a key factor in the separation. Coal produces the highest concentration of CO_2, typically around 12-14%, oil fired boilers produce gases around 11-13% CO_2, whereas natural gas produces flue gases with a CO_2 concentration of around 3-4%.[32] Thus, energetically, it is much more favourable to capture from a coal flue gas stream, however flue gas is produced at very near atmospheric pressure, hence the partial pressure of CO_2 is very low and the driving force for mass transfer is relatively low. While coal provides the highest partial pressure of CO_2, it often contains relatively more impurities and dust requiring post treatment units such as electrostatic precipitators and sulphur dioxide removal, possibly to a greater degree than what is already implemented.

In the future, capture from biofuel may be a potential option for 'negative emissions' i.e. reducing the overall atmospheric CO_2 concentration by fixing the CO_2 from air through the growth of biomass and subsequently sequestering said CO_2. Ultimately direct air capture - the idea of separating CO_2 directly from atmosphere - may even be a possibility.

1.3.2 Carbon Capture Technologies

The actual separation of CO_2 requires a great deal of energy, in the range of 25-40 % of the fuel energy of a power plant and could be responsible for 70% of the costs of CCS.[27] Thus it is vital technology is researched to reduce this burden and make CCS as economically palatable as possible. There are currently numerous technologies being researched for the purposes of post-combustion carbon capture including:

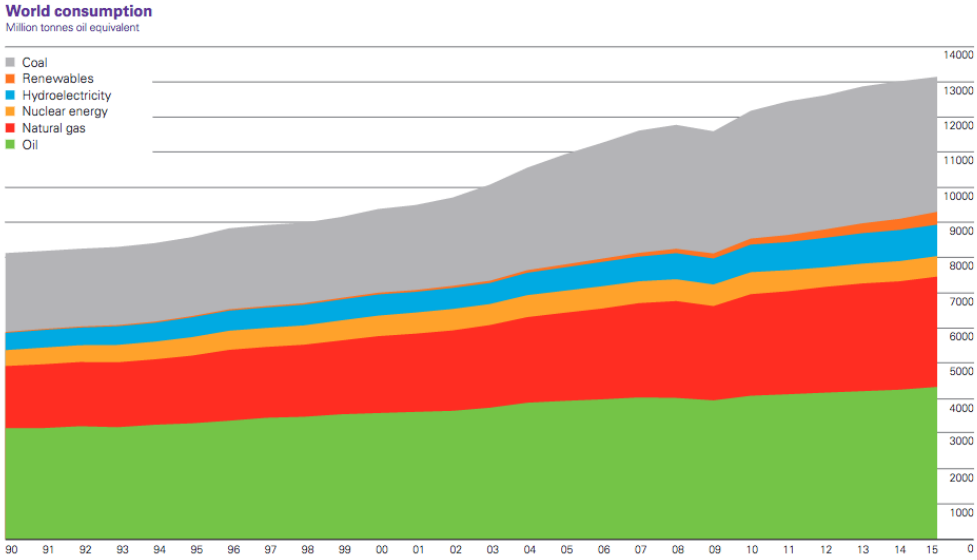

Figure 1.4: World energy consumption based on fuel type[31]

- Absorption, typically using amine-based solvents or ionic liquids,
- Adsorption using solid sorbents,
- Cryogenic distillation,
- Calcium looping,
- Selective membranes.

Capture using amine-based solvents is currently by far the most developed technology. Since 2014, the first commercial post-combustion coal fired CCS project went into operation at the Boundary Dam in Saskatchewan, Canada.[33,34] However, efficient capture using amines as a retrofit option requires complex heat and power integration with existing plant streams. The high heats of regeneration of amines also mean it is highly energy intensive. In addition, there are also high costs due to degradation of the solvents, and corrosion of equipment.[29,30,35–38]

Pressure and thermal swing adsorption are proven gas separation technologies utilising solid sorbents which have seen a lot of interest for the purposes of carbon capture. These techniques also show potential to be cost competitive with amine solvents and the main focus of research is in developing novel sorbents and improving process configurations to further reduce costs.[36]

Cryogenic distillation does not appear to be feasible for dilute streams of such great volume due to inherent heat transfer issues.

Calcium looping is an interesting technology involving the use of calcium oxide

as a sorbent in large circulating fluidised beds that shows potential as a low cost carbon option that is resistant to impurities in gas streams and may also integrate well with industry, particularly cement manufacture where calcium oxide is used as a raw material. However, it is currently beset with various issues affecting the longevity of limestone sorbents as well as problems with scale up.[39]

Membranes are another possible low cost alternative to amine-solvents. They are also a proven gas separation technology that could be well suited for post-combustion carbon capture. Requiring only electrical power to attain a partial pressure difference, they would be relatively straightforward to integrate into a currently operating power plant. Similar to adsorbents, membrane material properties and process optimisation are key in minimising costs.[29,40] In a review of capture from flue gases, Aaron and Tsouris[38] determined in 2005 that while liquid absorption was the most promising at the time, the development of membranes would yield a much more efficient separation. Further studies have supported this claim such as Brunetti et al. who predicted that membranes could better amine-based separations in terms of both energy penalty and cost per ton of CO_2 avoided.[41]

Membranes also have other advantages compared with absorption technology such as: the relative simplicity of retrofit, their lack of moving parts, their modularity, their durability and longevity, the fact that the process requires significantly less energy integration: compared with solvent scrubbing towers which require both heat *and* power integration, membranes need power to drive only the compressors, blowers and/or vacuum pumps depending on the process configuration.[32]

1.4 Membranes for gas separation

The first large scale use of membranes to separate gases dates back to the 1940s. The Manhattan Project utilised microporous metal membranes to enrich uranium via separation of a mixture of uranium fluoride containing both ^{235}U and ^{238}U isotopes.[42,43] Commercially, membranes were not used to separate gases for some time after this - until the 1980s, partly due to the secrecy surrounding the Manhattan Project. The first commercial process saw hydrogen separated from ammonia streams. Since then membranes have been used for a wide range of separations such as an alternative to cryogenic separation of air, and separation of CO_2 from H_2 and CH_4. At the forefront of commercial membranes MTR (Membrane Technology and Research) produce products to separate both nitrogen (NitroSep^{TM}), and CO_2 from natural gas,[44,45] and Fujifilm's Apura^{TM} is used for natural gas sweetening.[46]

Membranes for gas separation can exist in many different forms: they can be

made of polymers, metals, ceramics, or anything that can feasibly be fabricated into a membrane; they can be porous or dense, non-porous materials; anisotropic or isotropic. For the purposes of laboratory testing membranes often exist as a simple flat sheet but in a process environment would exist either in a spiral wound configuration or as hollow fibres.

As is discussed in greater length in chapter 2, process simulations have shown that membrane separations could well rival, and even better, absorption for post-combustion carbon capture in terms of both cost *and* energy usage.[29,47,48] However due to limitations in polymeric materials in which they fundamentally experience a trade-off between two vital properties for gas separation, permeability and selectivity, new materials should be developed for this reality to be achieved.[49]

1.4.1 Limitations of Polymeric Membranes

Polymers, the mainstay material of gas separation membranes, exhibit a trade-off between permeability and selectivity. This trade-off is clearly demonstrated by what is commonly known as the Robeson upper limit, an empirical upper limit on the selectivity of a membrane for a given permeability.[50,51] This relationship has been shown to exist for a number of gas pairs. Figure 1.5 shows data for the CO_2/N_2 separation with data points from a collaborative database put together by Thornton et al.[52] and the 2008 Robeson upper bound. It is generally found that a competitive membrane must have a selectivity of anywhere in the region of 20 to 100 and a permeability greater than 5000 Barrer.[29,47,48] Despite this range, the values for selectivity and permeability that would permit capture using membranes to compete with absorption, lie *above*, or very near to, the Robeson upper bound. While there are a few polymeric membranes that perform at this limit, as can be seen in Figure 1.5, these high performing membranes must also meet the other requirements such as cost, durability and the ability to be easily processed into membranes.

1.5 Overcoming the Upper Bound with Novel Polymeric-based Membranes

To overcome the limitation highlighted by the Robeson upper bound a multitude of new classes of polymers, and adaptations to polymer membranes, have been suggested such as thermally rearranged polymers, polymers of intrinsic porosity, also known as PIMs, polymerized room-temperature ionic liquids (poly(RTIL)s),

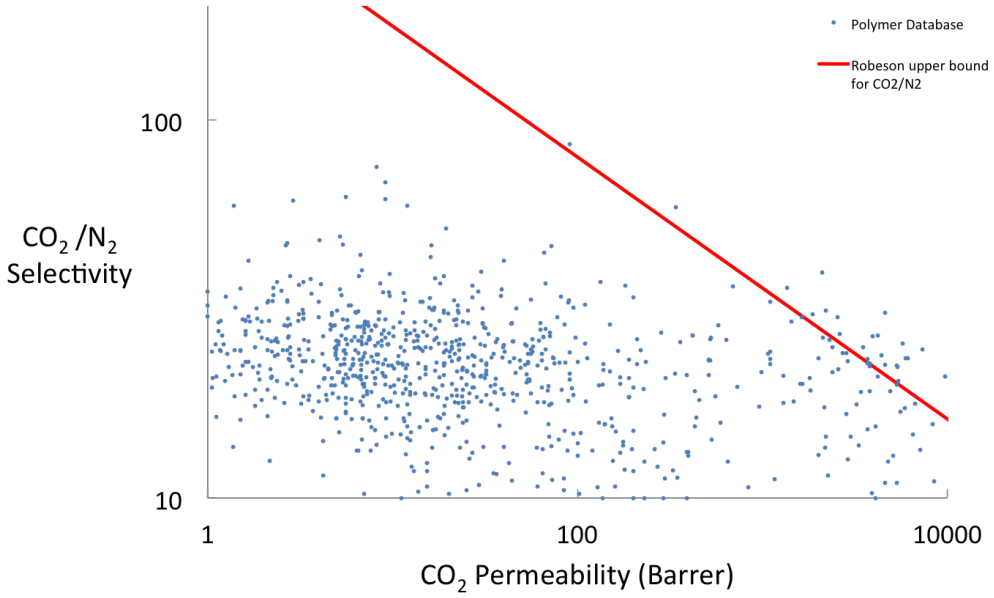

Figure 1.5: Plot showing a collaborative database of polymer selectivity vs permeability (blue circles),[52] the 2008 Robeson upper bound (red line)[51]

and facilitated transport membranes.[53–63] One of the most promising and active domains of these new polymer based materials is in mixed matrix membranes (MMMs).[64–73]

Mixed matrix membranes (MMMs) are composites formed from polymers and dispersed particulate materials, known as fillers. By combining the two phases MMMs can benefit from the separation properties of both materials.[63] Filler materials that would otherwise be too brittle, or expensive, to form into membranes can also be utilised. There are challenges in developing these materials as they often suffer from unpredictable defects with detrimental effects at the interface between the polymer and particulate fillers.[49,62] A plethora of polymer and filler materials have been tested in combination to create mixed matrix membranes, but in general principles regarding the behaviour of these defects are poorly understood.

The ability to produce thin membranes is also a valued property as these permit greater gas fluxes and limit the demands on material property development. As such nanoparticles are of particular interest as fillers in MMMs as they theoretically allow for thinner membranes to be produced, however controlling dispersion of nanoparticles in MMMs can be challenging.

Given the trade-off between permeability and selectivity, the two general methods of MMM development are to combine highly selective polymers with fillers that will increase their permeability, or to combine highly permeable polymers with highly

selective fillers.[74] In this work, PEBAX MH1657 was used as the sole polymer for making MMMs. This polymer was chosen primarily due to its inherently high selectivity and its relative inexpense, as any membrane must have both good separation properties and be cost effective. It also has other virtuous properties such as its mechanical robustness, its prior use in MMMs, and its availability.[75] Utilising only one polymer further had the benefit of reducing the number of variables being altered, such that any noted behaviours or trends could be attributed to the different fillers and their loadings.

Two main fillers were used in this work. They were ZIF-8, an amine-modified ZIF-8 sample, and two variations of novel hollow-sphere MCM-41. ZIF-8 was selected for use in this study due to flexible structure and possible gating behaviours which may make it highly selective in the CO_2/N_2 separation. This is discussed further in Chapter 3. At the outset utilising nanoscale ZIF-8 in PEBAX was also a novel undertaking and to learn about the dispersion of ZIF-8 in PEBAX was of much interest. It was found the ZIF-8 had a tendency to form agglomerations at loadings above 5 wt.%, and so a novel ethylenediamine-modified ZIF-8 (ED-ZIF-8), developed by co-workers at Deakin University, Australia, was used to try and improve the dispersion.

MCM-41 is a mesoporous silica which has seen much interest for gas separation purposes and carbon capture, primarily as an adsorbent. Its highly tunable pore size, its high surface area, and ease of functionalisation are all notable beneficial properties for gas separation. Novel hollow spheres of MCM-41 with pores perpendicular to the surface were utilised in this study as their geometry is of great interest in mixed matrix membranes. The reason the hollow, spherical geometry is of such interest is because if the shell of the sphere is reasonably selective, transport of one species can be greatly promoted relative to the other, since the more favoured species can travel quickly through the hollow centre of the sphere, whilst the other species must bypass the spheres creating a much more tortuous path. Spherical geometries can also produce better dispersions of particles as the geometry limits particle-particle interactions lessening the chance of agglomerations forming.[76] Three variations of MCM-41 hollow sphere (MCM-41-HS) were used in this work: 160 nm spheres with a 3.8 nm pore size, 160 nm spheres with a 4.4 nm pore size, and 450 nm spheres with a 4.4 nm pore size, investigating both the influence of the pore size and the particle size.

Further information on the materials can be found in chapter 3

1.6 Aims and Objectives

The aim of the study undertaken was to investigate novel nanoscale filler materials in PEBAX-based mixed matrix membranes for carbon capture applications. One of the prime goals was to develop an understanding of the morphological interactions between the polymer and filler materials, and the influence of these interactions on the gas transport behaviour. This was achieved by synthesising mixed matrix membranes using a solution casting method, and investigating the effects on the morphology and transport properties of varying the loading, or mass fraction, of these materials. The morphology was primarily investigated using scanning electron microscopy and the gas transport properties determined using a constant-volume variable-pressure apparatus.

The objectives were to:

- successfully develop a reliable technique for fabricating mixed matrix membranes using PEBAX MH1657 as the polymer phase, and ZIF-8, ED-ZIF-8, variations of MCM-41 hollow spheres as fillers.
- examine the morphology of the synthesised membranes using scanning electron microscopy, examining the dispersion of nanoparticles and interface between phases in particular.
- measure the gas permeation properties utilising a constant volume-variable pressure permeation system.
- attempt to relate the gas transport properties to the observed morphologies.
- compare the morphology and gas transport properties of the PEBAX-ZIF-8 and PEBAX-ED-ZIF-8 mixed matrix membranes.
- compare the morphology and gas transport properties of the variations of PEBAX-MCM-41-HS mixed matrix membranes and in particular the influence of the MCM-41 pore size, and filler size.

1.7 Outline

This thesis discusses the synthesis and characterisation of novel MMMs using PEBAX MH1657 as the polymer matrix. The thesis is arranged as detailed below:

- **Chapter 2** gives a background to membrane separations, mixed matrix membranes for post-combustion carbon capture, and highlights the necessity for improved membrane materials.
- **Chapter 3** gives a background to the materials used in this work.
- **Chapter 4** outlines the methods and theory behind the experimental techniques used to synthesise and characterise the MMMs under investigation.
- **Chapter 5** presents the results on the work looking at nano-sized ZIF-8 in PEBAX. In this chapter both untreated ZIF-8 and ZIF-8 that has been functionalised with amines are discussed.
- **Chapter 6** presents the results on the work investigating the effects of the addition of novel hollow-sphere MCM-41 into PEBAX. In this chapter variation in the pore size of the MCM-41 is investigated.
- **Chapter 7** contains the conclusions of the work presented and final remarks.

The work in this thesis was undertaken as part of a Industrial Cooperative Awards in Science and Technology (CASE) award coordinated by The University of Edinburgh in a partnership with Johnson Matthey and the EPSRC.

Chapter 2

Membranes for Gas Separation and Mixed Matrix Membranes

The fundamental principle of membranes used for separation of gases is to allow one component in a mixture to permeate at a greater rate than that of its counterparts. In a gas separation, a mixture of gases is supplied to the feed, or upstream side, of the membrane. The permeate, at a lower pressure, is removed from the downstream side. In a membrane separation the pressure is constant, equal to the feed pressure, and it is the chemical potential gradient that is the driving force for the separation. This is effectively a gradient in concentration within the membrane.[42]

Generally the separation of gases using membranes is based on one of the following transport mechanisms:[42,43,77]

- **Knudsen-diffusion** wherein the pore size is smaller than the mean free path of the gas molecules resulting in selectivity equal to the ratio of square roots of the gases;
- **solution-diffusion** occurs in non-porous membranes when transporting molecules in the gaseous phase dissolve into the surface of the membrane and subsequently diffuse through the free volume in the polymer. This will be discussed in greater detail below in the current section;
- **molecular-sieving** in which ultramicroporous membranes separate on the basis of molecular size;
- **facilitated transport** where permeation is promoted for one species which selectively reacts with a carrier molecule which greatly improves the solubility and diffusion across the membrane.[78]

While molecular-sieving and facilitated transport membranes are domains of active research, solution-diffusion is the sole, current, commercially viable technology. In Knudsen-diffusion, without a high difference in molecular weight, in which case alternative separation techniques would likely be more appropriate, the selectivity is much lower than in a competitive solution-diffusion membrane.[43] Ultramicroporous membranes are highly susceptible to fouling issues due to the inherent nature of their pore size.[77] Much work has gone into researching facilitated transport membranes which can exhibit separation properties well above the Robeson upper bound in laboratory environments. However they have not achieved commercial viability due to instability of carrier species and thus a lack of longevity.[43,78] With the exception of the Manhattan Project, all large scale polymer-based membrane gas separations have utilised dense polymer membranes where the transport was via the solution-diffusion mechanism.

2.1 Transport in Dense Polymer Membranes

Transport in dense polymer membranes occurs via the solution-diffusion mechanism.[79] The permeating gases dissolve into the surface of the membrane and subsequently diffuse across it. The quantity of gas dissolving into the membrane can be described by Henry's Law as in equation 2.1 or by dual-mode sorption model in glassy polymers[80] as in equation 2.2 :

$$C_i = p_i \cdot S_i \tag{2.1}$$

where C_i is the concentration of species i in the membrane at the gas-membrane interface, p_i is the partial pressure of species i, and S_i is the solubility of species i.

$$C_i = k_{D,i}\ p_i + \frac{C'_H\ b_i\ p_i}{1 + b_i\ p_i} \tag{2.2}$$

where $k_{D,i}$ is the Henry's Law coefficient,C'_H is the hole saturation constant, and b_i is the hole affinity constant.

Diffusion can be described by Fick's law as in equation 2.3:

$$J_i = -\frac{D_i \cdot C_i}{RT}\frac{\partial \mu}{\partial x} \tag{2.3}$$

where J_i is the flux across the membrane, D_i is the diffusivity, C is the concentration, R is the ideal gas constant, T is the temperature, μ is the chemical potential, x the direction of transport across the membrane, and i denotes species i.

Where the gas can be approximated as behaving as an ideal gas this can be reduced to equation 2.4

$$J_i = -D_i \frac{\Delta C_i}{L} \tag{2.4}$$

where ΔC_i is the concentration gradient across the membrane and L is the thickness of the membrane.

Two fundamental parameters can characterize the separation performance of any given membrane. These are the permeability coefficient and the selectivity. The permeability coefficient is a useful metric that describes the gas flux per unit area through a membrane normalised for the thickness and the partial pressure gradient across the membrane as shown in equation 2.5.

$$Permeability = \frac{flux \cdot thickness}{pressure_{upstream} - pressure_{downstream}} \tag{2.5}$$

The common unit of permeability is the Barrer, defined as 1 Barrer = $10^{-10}\ cm^3_{STP}\ cm\ \ cm^{-2}\ cmHg^{-1}\ s^{-1}$.

The permeability is the product of an equilibrium term, the solubility, and a kinetic term, the diffusivity, as shown in equation 2.6:

$$P = D \cdot S \tag{2.6}$$

The ideal selectivity is the ratio of permeability coefficients of two gases, as represented by equation 2.7.

$$\alpha_{\frac{A}{B}} = \frac{P_A}{P_B} = \frac{D_A\ S_A}{D_B\ S_B} \tag{2.7}$$

where P_A is (*nearly* always) the permeability coefficient of the more permeable gas and P_B the permeability coefficient of the less permeable gas.

2.2 Process design considerations: The reasons for new materials

In a membrane separation process several parameters affect the cost and energy performance of the process. The key parameters are the:

- Permeance,[1]
- Selectivity,
- Cost of membrane,
- Pressure ratio,
- Number and configuration of stages,
- Capture requirements.

These parameters can be defined as membrane properties, operational parameters, and process parameters. Process design and optimisation is a complex subject where extensive work has been done specifically aimed at the subject of carbon capture using membranes.[41,47,48,81–83]

In any single gas separation stage the three parameters that dictate the performance are the selectivity, α, given previously by equation 2.7, the stage-cut, θ, given by equation 2.8, and the feed to permeate pressure ratio, φ given by equation 2.9:[42]

$$\theta = \frac{Q_{permeate}}{Q_{feed}} \tag{2.8}$$

$$\varphi = \frac{p_0}{p_l} \tag{2.9}$$

where $Q_{permeate}$ and Q_{feed} are the flows of the permeate and feed streams, and p_0 and p_l are the total upstream and downstream pressures, the subscript l denoting the thickness of the membrane measured from the upstream face.

The selectivity is inherently significant, being the ratio of permeabilities of the species being separated, and thus the very basis on which the separation is possible. Higher selectivities lead to higher permeate purities, although as is mentioned later there are limiting cases when this is not always beneficial.

[1] the permeance is often used in place of the permeability in process situations. The permeance is the permeability divided by the thickness. It can be thought of as the flux per unit area for a given pressure gradient. It is measured in gas permeation units, or gpu: 1 gpu = $10^{-6} cm^3_{STP} cm^{-2} cmHg^{-1} s^{-1}$. A membrane 10 µm thick with a permeability of 1000 Barrer will have a permeance of 100 gpu.

The pressure ratio is vital to the gas separation. The partial pressure of a component must be higher on the feed side than that on the permeate side to allow flux across the membrane. How this is achieved, whether it is through compressing the feed or utilising vacuum pressures on the permeate side is virtually solely a matter of process optimisation. Examining the case in which a gas mixture with a concentration of species i in the upstream side is $c_{i,0}$, and that of the downstream is $c_{i,l}$, where l is the thickness of the membrane, the following relationship can be established for a gas flux:[42]

$$c_{i,0}\ p_0 \geq c_{i,l}\ p_l \tag{2.10}$$

which upon rearranging shows the maximum separation in terms of concentration ratios is always less than or equal to the pressure ratio:

$$\frac{c_{i,l}}{c_{i,0}} \leq \frac{p_l}{p_0} = \varphi \tag{2.11}$$

As Baker explains in the book Membrane Technology and Applications,[42] an elaborate relationship can be established between the selectivity of the membrane and the pressure ratio using Fick's law which highlights two limiting cases: one, in which the selectivity is much greater than the pressure ratio, $\alpha \gg \varphi$, is known as the pressure-ratio-limited region where the selectivity plays little to no role and the performance is dictated by the pressure ratio; the second is when the selectivity is much less than the pressure ratio,$\alpha \ll \varphi$, referred to as the selectivity-limited region where the separation is determined only by the selectivity. In between these two limiting cases both play a role in the separation performance, where increasing either leads to an increase in the permeate concentration of the more permeable species. These considerations are significant as there are practical limits on the achievable pressure ratios largely due to the capital and operational costs of maintaining a high pressure ratio, associated with larger compressors or vacuum pumps, and their running costs. While Baker states that pressure ratios of 5 - 20 are typical of membrane separations, for post-combustion carbon capture purposes, values of around 5 - 10 have been shown to be more economical due to processing the vast volumes of gas in a coal power station flue gas stream.[29,41,42]

The third and final parameter of any membrane unit operation stage is the stage-cut. The stage-cut is the ratio of the permeate to the retentate flow and is a function of permeance and area of the membrane utilised. The significance of the stage-cut is a trade-off between enrichment in the permeate and removal from the feed gas. This is because as the stage-cut is increased and more of the product, or species to remove, transfers to the permeate stream, and so the concentration in the retentate stream decreases. To continue increasing the stage-cut would mean separation from a more dilute stream. As the stage-cut is increased, both the retentate and

permeate streams become more dilute. This is better envisaged by picturing the hypothetical near limits of stage-cut in a binary separation of species a and b where a is the more permeable species ($\alpha = P_a/P_b > 1$). As the stage-cut approaches zero ($\varphi \to 0$), very little of either species permeates but component a clearly does so more than b and thus you have very little recovery but a high purity permeate stream. In the other limit where the stage-cut nears infinity ($\varphi \to \infty$) ie virtually all the the feed is in the permeate, you have complete recovery but the permeate has the same concentration as the feed.[29,42]

As previously mentioned the current frontrunner in post-combustion carbon capture technologies is absorption using amines. In this process the flue gas is desulpherised and cooled, before being introduced to a absorption column utilising blowers to surpass the pressure drops in the column. The CO_2 dissolves and is chemically bound to the solvent. To remove the CO_2 from the solvent, the solvent is pumped into a stripping tower where heat from steam is used to overcome the chemical bonds and release the CO_2, after which the CO_2 lean solvent can be recycled into the absorption column. While there has been much work into the heat and energy integration of such processes, the high heats of regeneration involved in recovering the CO_2 from the solvent, and the associated high reboiler duties are significant. In process simulation studies of coal and gas power stations with retrofitted amine post-combustion carbon capture units, it is typical for it to drain 20-35% of the power from the plant.[35] Quoting numbers from the MIT CCS Project Database,[84] regarding the currently operating capture facility at Boundary Dam, the gross power output and net power output after CO_2 capture are 160 and 110 MW respectively which is slightly over a 30% penalty. Predicted costs for capture in absorption capture systems vary but range from 40 - 100 $\$/t_{CO2}$ avoided.[29,85]

Thus for membrane separations to be a viable post-combustion capture technology they must be able to meet or better the costs of capture using absorption. Process optimisation of carbon capture using membranes is a highly active avenue of current research.

In 2008, Zhao et al.[81] carried out a parametric analysis of CO_2/N_2 separations for post-combustion carbon capture using a single stage separation. In line with fundamental theory they found that increasing the membrane area in their simulations decreased the product purity, but increased the degree of separation. In the case of post-combustion carbon capture, the goal is to remove a high proportion of CO_2 from the flue gas and concentrate it to a high purity, the typical standard as being greater than 90% capture with a CO_2 concentration of 95%.[29] As previously discussed there is an inherent trade-off between enrichment and recovery making this a notable challenge. In their simulations, even with a pressure ratio of greater than 30 (Feed pressure = 1 bar, permeate pressure 30 mBar) and a selectivity of 200, Zhao et al. demonstrated that 90% capture with a 95% purity CO_2 stream in a

single stage was not possible. This was due to the low partial pressure of CO_2 in the flue gas stream.[28] They concluded that the membrane properties: the permeability, selectivity and the membrane area were vital in the separation performance as well as the operating conditions such as the pressure ratio and mole fraction of CO_2 in the feed.

Further work by the same group in 2010[47] looked at 2 simple two-stage configurations with and without recycle streams to further investigate the energetic and economic implications in such systems. They identified that in such a system the membrane area of the first membrane was significantly greater than the second, which heuristically makes sense as the best solution was for the first membrane to perform a bulk separation, thus requiring a high stage-cut to achieve sufficient recovery, and the second membrane stage purified the CO_2 stream, thus requiring a low stage-cut and a low area. In their cost analysis they noted the required area of the membranes was dominated by the CO_2 permeance of the materials, with little change in the required specific energy of the system. This revealed the permeance of such materials has a large impact on the capital cost. They found that increases in selectivity greatly reduced the required power ($\alpha \rightarrow\sim 40$) but saw diminishing returns above this ($40 \leqslant \alpha \leqslant 80$). Interestingly they noted the role nitrogen played in the permeate stream to maintain the driving force: at very high selectivities N_2 was not easily permeated resulting in a higher CO_2 permeate partial pressure, lowering the driving force and leading to higher energy requirements. Merkel et al. in a paper studying similar topics in 2010 drew similar conclusions regarding the influence of the permeance and selectivity on membrane area and power consumption.[29]

In this work, Merkel et al.[29] also drew conclusions regarding further design considerations for a multi-stage membrane system. The noted that utilising vacuum pressures on the permeate side required significantly less energy than compressing the feed which they attributed to the significant volumes in a typical flue stream. They claimed that if sufficiently permeable or cheap membranes could be developed, the most energetically favourable option would be to utilise no feed compression. They estimated utilising membranes with a permeance of 1000 gpu and a selectivity of 50 their design could meet capture requirements only using 16% of the plants energy at a cost of $\$23/t_{CO2}$ captured (compared with amines which are typically have an energy penalty of 20-30% and a capture cost of above $\$40/t_{CO2}$).

This paper was also one of the earliest to discuss the concept of recycling some of a CO_2 permeate stream into the boiler/combustor/turbine to artificially increase the CO_2 partial pressure in the flue stream. This has developed into a range of studies known as selective exhaust gas recirculation as they refer to in their 2013 paper.[29,86]

More recently in 2016, Arias et al.[87] carried out work in which they aimed to optimize the number of stages, membrane area and power requirements for a capture process using a fixed permeance and selectivity of approximately 1000 gpu and $\alpha = 50$. One of their most notable conclusions was that the number of required stages was heavily dependant on the desired CO_2 concentration in the final CO_2 stream, and independent of the capture requirement. For 90 to 93% purity they determined a two-stage separation with one recycle stream was optimal; for 94 to 96%, three stages with two recycle stream were most efficient. They determined for a two-stage cycle a capture cost of 40 $\$/t_{CO2}$.

In 2016 Roussanaly et al.[74] undertook a study investigating specifically the membrane properties permeance and selectivity, that would be required to allow membrane post-combustion capture to compete in terms of cost with amine-technologies. Using a numeric approach to test 1600 membrane properties, or pairs of selectivities and permeabilities, using a simple two-stage setup they identified the membrane properties that would be required to rival absorption technology. They found that membranes with high permeances of at least 1100 gpu and selectivities of at least 65 would be required for this technology to compete with established capture costs of amines. The did concede that with more advanced configurations that permeances with around 370 gpu and selectivities of 30 could be competitive.

One common theme in these works is generally the call for improved materials.[29,40,74] The impact of the permeability on the required area and hence capital cost, and the selectivity on the power requirements are significant. They must also be able to be processed sufficiently thin enough to maintain high permeances, and importantly, be affordable.[88] Despite huge advancements in membrane process optimization, the necessity of improved materials is paramount if capture using membranes is to be realised.

2.3 Mixed Matrix Membranes

The first mention of mixed matrix membranes developed for the purposes of gas separation was in 1973, when Paul and Kemp[89] combined zeolite 5A with polydimethyl siloxane (PDMS) while investigating the CO_2-CH_4 separation. In 1988, Kulprathipanja et al. filed a patent detailing the use and methodology of synthesis of mixed matrix membranes for the separation of fluids, noting the inclusion of adsorbent type materials into organic polymers to improve the steady state permeability and selectivity.[90] The following ten years saw relatively little work into mixed matrix membranes, what was done mainly revolving around the inclusion of zeolites into MMMs.[63,91–94] Highlighting the infancy of MMMs in the early '90s, a reasonably comprehensive review of membrane gas separations written by Koros and Fleming in 1993[77] made no mention of anything resembling mixed matrix membranes, as they were far from an established vein of membrane research at the time. After around 1997, the number of papers published on MMMs began to noticeably grow and today a swathe of polymer and filler materials have been investigated regarding their use for MMMs.

Conceptually mixed matrix membranes are simply the combination of a dispersed phase, commonly referred to as 'fillers,' with a polymeric phase to produce a single, composite membrane. The idea is to fabricate a membrane with advantageous properties of both phases, for example the processability, relatively low cost, strength and durability of polymers, and the superior separation properties of some filler materials. As previously mentioned a huge range of polymers and filler materials have been tested; notable materials that have been investigated as fillers include:[62,63,95]

- zeolites,[93,96–102]
- carbon molecular sieves,[103,104]
- carbon nanotubes (CNTs),[105–109]
- metal organic frameworks.[64,71,110–114]

One of the key challenges in creating effective MMMs lies at the polymer-filler interface wherein performance hindering defects can occur, and thus how to control and minimise these phenomena. While the properties of a mixed matrix membrane are obviously heavily and primarily influenced by their constituent materials, these effects at the interface frequently play a significant role and can drastically affect the expected gas permeation properties. Further these effects are often notoriously difficult to predict. These interfacial defects can take several forms:[62]

- **chain rigidification** happens when the mobility of the polymer chains at the interface is hindered, thus reducing or ceasing transport into the filler

material;

- **pore blockage** occurs when the polymer chains intrude into or otherwise block the pores of the filler material, reducing the transport in the filler phase as well as throughout the overall material;
- **voids** wherein there is separation between the polymer and dispersed phases; this results in gas being able to pass around the filler, thus reducing, if not negating, their presence.

The synthesis route and material selection are key in minimising these defects.

Zimmerman et al.[63] presented work in 1997 on theoretical MMMs based on the inclusion of zeolite 4A and commercial carbon molecular sieves in Ultem and Udel concluding that only with the right combination of materials could significant improvements on the polymer properties be achieved. Zimmerman also noted that without the discrete phase forming any continuous network, the resulting membrane performance was heavily dominated by the properties of the polymer. Heuristically this makes sense as even in the hypothetical limiting case in which an infinitely permeable discontinuous phase is used, the gas must always travel through the continuous phase.

The use of nanoparticles as fillers allows for thinner membranes to be produced, compared with larger fillers. This is of great benefit to membrane separations as thin membranes are desirable to maintain high fluxes. However the dispersion of nanoparticles can be a challenging subject. Nanoparticle-polymer composites have been the subject of much interest long before MMMs for gas separation was even conceived. The dispersion of nanoparticles in a solvent alone is complex enough: the phenomenon of nanoparticle dewetting is a field of scientific study in its own right. Controlling the dispersion of nanoparticles in polymers is one of the greatest obstacles to such materials. In block copolymers nanoparticles can influence the morphology of the copolymer domains as has been shown by Lee et al.[115] The effect of dispersion of the nanoparticles can significantly influence the macroscopic properties[116] and thus poses a notable challenge, and potential boon if well controlled, for mixed matrix membranes.

At higher loadings it may be possible for the discontinuous phase to form continuous networks and even percolating clusters, that is a continuous network of particles that connects both sides of the membrane. Forming such a membrane has its own challenges, as such a membrane made up of a high proportion of discrete particles will possibly posses inherent structural weaknesses without strong interaction between particle and polymer.

2.4 Models for Predicting MMM Behaviour

A wide variety of approaches have been undertaken to try and predict the effective permeability of gases in mixed matrix membranes.[117] The models can largely be grouped into ideal, and non-ideal, models. Ideal models rely on the assumption of two discrete phases with no imperfections that do not account for any interactions with the other phase. These include the Maxwell, Bruggeman, Lewis-Nielsen, and Pal models, as well as many others. As mentioned in section 2.3, there are a number of interfacial defects that commonly occur in mixed matrix membranes such as voids, chain rigidification, and pore blockage. Non-ideal models, also known as three-phase models, attempt to account for these morphologies.[118]

One of the most commonly used ideal models is the Maxwell model. It was initially developed in 1873 to predict the "permittivity in a heterogeneous dielectric," or the conductivity of composite materials.[119] Using potential theory for conduction through heterogeneous media, he derived the exact solution for the conductivity of random and non-interacting homogeneous spheres in a continuous matrix.[120] This problem is analogous to gas permeation through a heterogeneous membrane and thus the Maxwell equation can be applied to gas separation properties by replacing the dielectric properties with that of the permeability of the continuous and discontinuous phases.[121] In the Maxwell model the effective permeability of a species, P_{eff} is given by equation 2.12:[122]

$$P_{eff} = P_c \frac{P_d + 2P_c - 2\phi(P_c - P_d)}{P_d + 2P_c + \phi(P_c - P_d)} \tag{2.12}$$

where P represents the permeability coefficient of a given phase, the subscripts c and d represent the the continuous (polymer), and discontinuous (filler) phases respectively, and ϕ represents the volumetric loading.

While the Maxwell model benefits from being very simple to use, its range of validity is limited. Since the Maxwell model is based on a dilute dispersion of homogeneous spheres it accounts for no interaction between particles. As the volumetric loading reaches what is known as the percolation threshold, when the dispersed phase can form a continuous network in contact with either side of the membrane, it is expected that the overall permeability would change drastically. Because the Maxwell model does not account for the flux of the transporting species being influenced by nearby particles, it cannot account for this behaviour and thus is only valid at low volumetric loadings, $\phi < 0.2$.[123] It further relies on the assumption of homogeneous dispersion of particles, something which is not always achieved in reality; for example particles often have a tendency to form agglomerations. Additionally it does not account for particle size distribution, nor variation from

spherical filler shapes.

Despite its limitations, the Maxwell model has been used effectively to match experimental data of mixed matrix membranes. Hao et al.[124] employed the Maxwell model to predict the effect of combining ZIF-8 with a polymerizable room temperature ionic liquid (poly(RTIL)) and saw near perfect agreement, which they attributed to the formation of near ideal interface morphologies and homogeneous filler dispersion. This agreed with their optical observations which showed homogeneity throughout their samples.

The Bruggeman equation was similarly developed for determining the dielectric constant of particulate composite materials.[125] It is thought to more accurately account for the volumetric loading,[123,126] however in practical use its solution often differs only slightly from that given by the Maxwell equation. It is an implicit function and must be solved numerically.[126] The Bruggeman equation is given by equation 2.13:[125]

$$P_{eff}^{\frac{1}{3}} \left(\frac{P_d - P_c}{P_d - P_c P_{eff}} \right) = (1 - \phi)^{-1} \tag{2.13}$$

The Bruggeman model shares the Maxwell model's limitations in that it is only valid at low loadings.

Ebneyamini et al. compared a number of ideal models with experimental data for the pervaporation separation of butanol from binary aqueous solutions using polydimethylsiloxane(PDMS)-activated carbon composite membranes. Both the Maxwell and Bruggeman models showed good agreement with the experimentally determined values. The Bruggeman model showed marginally less deviation from the experimental results but the difference was inconsequential.[117]

The main drawback of the ideal models is that they do not account for interfacial effects such as voids and polymer chain rigidification. Three-phase models have been developed to account for these where the interface is modelled as a third, 'pseudo' phase. These models require additional parameters to model the interfacial region such as the permeability and thickness of the void or rigidified polymer layer. This is the main drawback of the non-ideal models as there are no reliable ways to determine these parameters experimentally and they are often determined by semi-empirical means.[117]

One of the simplest of these models is the modified-Maxwell model which applies the Maxwell equation twice: once to the dispersed phase and the interface to estimate their combined properties, and then again to the polymer phase and the combined dispersed-interface phase.[127] The modified-Maxwell model only requires an additional two parameters: the permeability coefficient and the volume fraction of the interfacial region. This geometry of the interface phase is far from a dilute

homogeneous suspension of spheres, as is the basis of the Maxwell equation and so the modified-Maxwell model is not technically accurate. It has often been used without acknowledgement of this concession however.[97,128] While the modified models are inherently far from perfect, they can serve as a fast and approximate tool for predicting the influence of ternary phases.[123]

More elaborate models accounting for numerous interfacial and other behaviours such as clustering have been developed. Fang et al.[128] investigated ZIF-8/PDMS MMMs for hydrocarbon recovery specifically looking at the propane/N_2 separation. They noted an enhanced selectivity and diminished permeability in return for increasing loadings, a result which contradicted the prediction of the Maxwell model. They suggested these effects were likely due to chain rigidification of the polymer-filler interface. They also noted significant agglomeration of ZIF-8 particles and proposed a model to quantify these behaviours, a schematic of which can be seen in figure 2.1. This model possessed five regions of transport which were the polymer, the ZIF-8 particles, a pore blockage layer in the surface of the particles, a rigidified polymer layer around the particles and the agglomerated nanoparticles in which they estimated a number of parameters such as the pore blockage and polymer chain rigidification lengths, the permeabilities in these regions based on reduction factors, and the ratio of aggregated particles to dispersed particles, among others. In this model, the Maxwell model was utilised three times as well as approximating the transport in the agglomerations using a simple dusty gas model and aggregating the permeabilities of the dispersed particles and clusters by a simple parallel flow model. As previously mentioned, while oft used due to its simplicity, it is well known that utilising the Maxwell model, as in the non-ideal Maxwell mode, to determine properties of the intermediate phases such as voids and rigidified layers is technically not accurate due to the original model relying on the assumption of discrete particles in which the flux is unaffected by other nearby particles, which is clearly not representative of the geometry of a layer surrounding a sphere. Further to this, it also would appear dubious to assume the flux in the clusters and particles can be assumed as parallel given both are surrounded by polymer. Given the number of approximations used in this work, the model developed seems ambitious at best. Due to the number of parameters that were used to fit the experimental data points, due consideration must be given to avoid both overfitting as well as obtaining unrealistic values for such parameters. To confirm the validity of the presented model, Fang et al. used their model to fit three separate cases from literature, which they claim to have done well, thus proving the applicability of their model. However, no information is provided on the parameters used to fit these other models which calls into question the rigour with which this separate data was modelled. While attempting to model this many domains is arguably ambitious, it does highlight the complexity of the transport of

MMMs themselves.

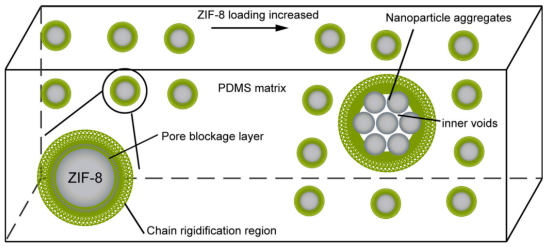

Figure 2.1: Schematic diagram for the proposed model showing the chain rigidification and aggregation of ZIF-8 particles[128]

Possibly the largest challenge in attempting to model MMMs is the unpredictability of the effects that are observed when combining materials. One notable case which is exemplary in making this point is the work done by Merkel et al in 2002.[129] By introducing nanoscale fumed silica particles, which were notably *non-porous*, into a reverse-selective glassy polymer, they noticed improved permeabilities and selectivities for the separation of large organic molecules over non-condensible gases. They attributed these observations to a disruption of the polymer chain packing, thus changing the free volume within the membrane. Thus by introducing impermeable particles into a polymer, they somewhat counter-intuitively improved the gas separation properties. Despite best efforts, it still remains highly difficult to accurately predict the gas transport properties of the composite materials from the properties of the constituent materials, largely due to unpredictable phenomena that can be observed.[66]

Chapter 3

Materials

In this project, PEBAX was used as the polymer phase and ZIF-8 and MCM-41 were used as the main fillers. The following section details these materials used in the project and some background to their prior use in the fields of carbon capture and gas separation.

3.1 PEBAX

Poly(amide-6-b-ethylene oxide) (PEBAX®) has been investigated extensively for gas separation purposes for not only the CO_2/N_2 separation[68,81,130] but also for methane/CO_2,[131] propane/CO_2,[128] as well as other mixtures.[132–134] It has been included as a standalone material as well as being modified with the layering or incorporation of other polymers,[135–137] or as the polymer matrix in MMMs.[68,108,130,138,139] Figure 3.1 shows some previous values for permeability and CO_2/N_2 selectivity on a Robeson plot. While there is a spread in the values obtained for the selectivity, there is consensus that the selectivity remains higher than the bulk of the polymer data. By combining PEBAX with fillers that improve the permeability it is not infeasible that a material could be produced that approaches or even crosses the upper bound.

Poly(ether-b-amide) are a group of block co-polymers which show a high selectivity for polar gases. They are generalised by their structure of polyether and polyamide segments. Various types exist depending on the particular units and ratio that make up the polyether and polyamide sections. The grade of PEBAX used in this work was MH1657, in which the polyether is poly(ethylene oxide) and the polyamide is polyamide 6 (PA 6, a.k.a. nylon 6) in a 60:40 ratio.[140,142]

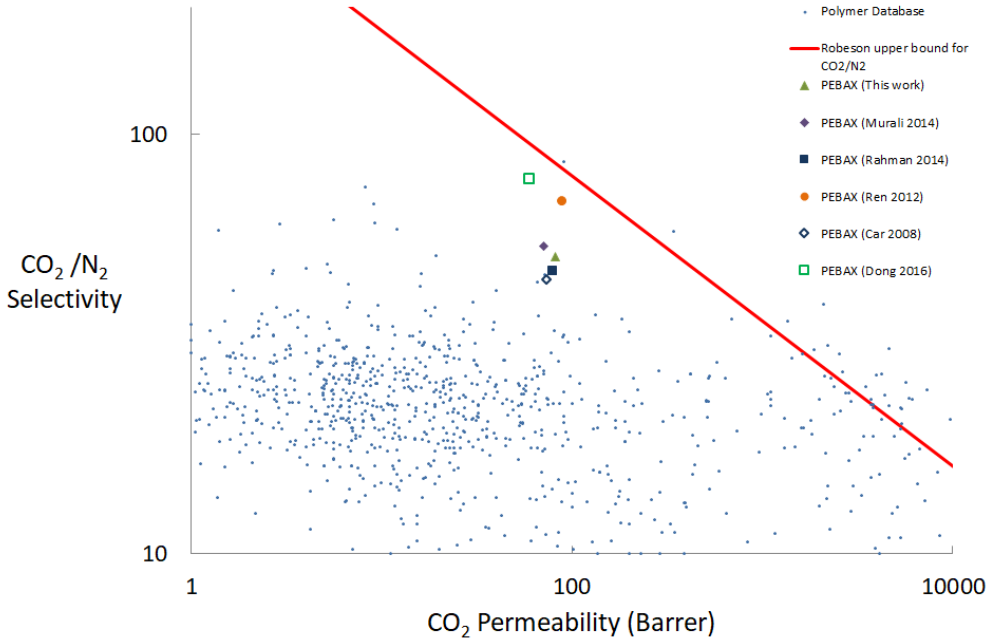

Figure 3.1: Robeson plot showing the permeabilities and selectivities of pure PEBAX membranes previously used in literature.[73,130,136,140,141]

Its wide use is due to its inherent high selectivity for polarizable gases which stem from the strongly polar polyether segments.[75,143] Lin and Freeman[144] noted that the inclusion of polar groups in polymers could greatly increase the solubility of CO_2 and benefit from a high solubility selectivity. They subsequently noted that the polyether segments within polyether block-copolymers contained exactly that.

Work done by Bondar et al.[75] investigating the permeation properties of H_2, N_2 and CO_2 in various grades of PEBAX highlights the notable effects of this solubility selectivity. Despite H_2 possessing a significantly smaller kinetic diameter than CO_2 resulting in a much higher diffusion coefficient, thus $D_{CO2}/D_{H2} < 1$, the PEBAX materials show CO_2/H_2 selectivities greater than one as the diffusion selectivity is not sufficiently great to counter the high solubility selectivity, $S_{CO2}/S_{H2} >> 1$. Thus for CO_2/N_2, not only is CO_2 more soluble, it is also smaller than N_2 (3.30 Å versus 3.64 Å), which both make the permeation of CO_2 more favourable.

3.1.1 Preparation of PEBAX composite membranes

Composite PEBAX membranes are nearly always made via a solution casting-method in which the polymer is dissolved, the filler material is added, mixed and

then cast. The details of this procedure can vary notably. Table 3.1 gives a selection of some of the fabrication details that have previously been used in literature to make both mixed matrix membranes and other PEBAX composites.

A wide variety of solvents have been used. For PEBAX MH1657, a 7:3 by weight mixture of ethanol and water is most commonly employed, although acetic acid and other alcohols can be used. A temperature of nearly 80°C is almost always used for dissolution of the polymer, mainly as it decreases the time for dissolution.

3.2 ZIF-8

Zeolitic imidazolate frameworks (ZIFs) are a subset of MOFs which have structures analogous to that of zeolites. Instead of an aluminosilicate structure they contain transition metal centres with imidazolate linkers. These metal centre-imidazolate links share an identical bond angle of 145° to that of the oxygen links in zeolites which is why structurally equivalent frameworks can be created.[148] They are highly stable due to the strong bonding present between the transition metal centres and the imidazolate linkers.[149] There are also thousands of predicted structures and they can be easily tailored by interchanging the centre or imidazolate linker. They posses other useful properties such as their high surface area and porosity, wide framework diversity and controllable window sizes, and thus they have seen much interest in the field of separations, including separating gases such as CO_2/N_2 and CO_2/CH_4, biofuel recovery, water purification and hydrocarbon separations.[150,151]

ZIF-8 ($Zn(MeIM)_2$) is one such ZIF structure comprising of zinc metal centres and 2-methylimidazolate . It possesses a sodalite topology containing cavities connected by small windows with a diameter of diameter 3.4Å as shown in figure 3.2.[148] This diameter is between that of the kinetic diameters of CO_2, 3.30 Å, and of N_2, 3.64 Å, which interpreted simply suggests it could potentially show a molecular sieving behaviour for the CO_2/N_2 separation.[124,152]

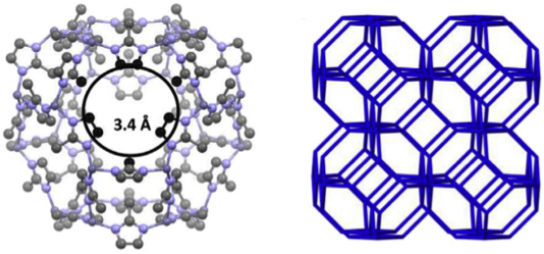

Figure 3.2: Structure showing the window and SOD topology of ZIF-8.[150]

Table 3.1: Synthesis conditions of PEBAX-based membranes and MMMs from literature.

PEBAX Grade	Solvent	Dissolution conditions[1]	Filler mixing conditions	Drying Conditions	Reference
1657	EtOH:H_2O (70:30 wt.%)	80°C, 4 h,[3]	Minimum of 3 hours of ultrasonic mixing, further 6 h of stirring	Ambient, further drying in vacuum oven	[108]
1657	EtOH:H_2O (70:30 wt.%)	3 wt.%, 80°C, 4 h	Stirred overnight, 5 minutes of ultrasound to degas	40°C, 24 h	[142]
1657	EtOH:H_2O (70:30 wt.%)	3 wt.%, stirred at 80°C, 2 h	-[2]	Ambient temperature	[138]
1657	EtOH:H_2O (70:30 wt.%)	70°C, overnight[3]	-[2]	30°C	[145]
1657	EtOH:H_2O (70:30 wt.%)	3 wt.%, 80°C, 2 h	-[2]	30°C, 48 hours	[135]
1657	Acetic acid	Up to 5 wt.%, Stirred at 50°C, 6 h	Ultrasonic treatment for 2 h, stirred for 2 days, further ultrasound for 10 m	60°C, 4 days, then under vacuum at 70°C for 2 days	[146]
1657	1-butanol	1 wt.%, vigorous stirring[5]	-[2]	Using a heating plate, then a vacuum oven[5]	[132]
1657	Propanol:n-butanol (3:1 wt.)	3 wt.%, stirred, 80°C	80°C, filler formed during mixing	Ambient temperature, 2 weeks	[143]
2533	1-butanol	4 wt.%, 80°C,[4]then 70°C overnight	"Mixed"	Ambient temperature, 3-5 days	[147]
2533	Ethanol	3 wt.% 70°C, 3-4 hours	20 - 30 minutes of ultrasound following mixing	Ambient, annealed under vacuum at 70°C	[112]

[1] The concentration refers to PEBAX in the solvent.
[2] No filler was used.
[3] Concentration was not disclosed.
[4] Time was not disclosed.
[5] Temperature(s) not disclosed.

In contrast to any simple behaviour however, several complex effects have been shown to occur that affect the adsorption and transport behaviours of small molecules in ZIF-8. One of the most well observed effects has been the flexibility of the imidazolate linker. Experimental studies have shown molecules distinctly larger than that of the 3.4Å window to be admitted into the cavities.[153–155] A study by Zhang et al. looking at the transport of a range of small molecules (from 3Å to 7Å) showed that the corrected diffusivity decreased by 8 orders of magnitude for molecules between 4 and 5Å suggesting that ZIF-8 may not be size selective for the CO_2/N_2 separation on account of this structural flexibility.[156]

Several studies utilising molecular simulation have attributed this behaviour to the flexible nature of ZIF-8 wherein a structural transition, often referred to as a 'gating effect,' in the imidazolate linkers has been shown to occur.[157–159]This is in concurrence with work carried out by (a different)Zhang et al who pointed out that the stiffness of the linker not only plays a strong role in determining the precise diffusivity values of molecules, but that the flexibility of ZIF-8 is essential to describing the diffusion of gases in ZIF-8.[160] The flexibility of the IM linker has also been observed experimentally by deuterium NMR measurements.[155]

Another interesting facet of diffusion in ZIF-8 is the suggestion of a 'hindering' effect wherein CO_2 molecules can sit in the pore windows and reduce the diffusivities of other guest molecules. Multiple studies have shown evidence to suggest the existence of this effect.[150,160,161] Using molecular simulation both Chmelik et al[161] and Zhang et al.[160] showed that for the diffusion of CO_2/CH_4 mixtures in ZIF-8, CO_2 had a tendency to sit in the pore windows hindering the transport of CH_4, which correlated well with the IRM results obtained by the group of Chmelik et al. While it is speculative, it is logical to think a similar effect may be observed with other CO_2 mixtures. If so this would be an obvious boon for membrane separations involving ZIF-8 and CO_2 as much greater selectivities would be observed than unary permeation data suggests.

Hwang et al. produced hollow ZIF-8 spheres by coating the surface nanosized polystyrene particles with ZIF-8 before removal of the polystyrene template. These ZIF-8 hollow spheres (ZIF-8-HS) were combined with poly(vinyl chloride)-g-poly-(oxyethylene methacrylate) (PVC-g-POEM), an amphiphilic graft polymer, to produce MMMs with remarkably improved separation properties.[162]

3.3 ZIF-8 in Mixed Matrix Membranes

ZIFs have recently been receiving much interest as a filler for MMMs due to its aforementioned potential molecular sieving properties.[71,111,163–165] A range of poly-

mers have been tested including PIMs,[110,166] polyimides,[71,139,151,152,164,165,167–170] polyetherimides,,[111] polyetheramides,[112,163,171] and polysiloxanes.[128]

One of the most common facets within the literature of MMMs containing ZIF-8 is the prevalence of agglomerations. These have been observed in a multitude of studies using a variety of differing polymers, solvent, ZIF-8 particle size and preparation conditions. Aside from the simple distinctions such as differing polymers and solvents, very varied methods of preparation have been utilised, in particular the means by which the particles are mixed and dispersed within the polymer dope solution. It is very common for a 'priming' technique to be used wherein a proportion of the polymer solution (usually less than ten percent of the total) is first added to particles prior to adding the remaining polymer solution.[71,111,168,170,172] It is thought that this improves the subsequent dispersion of nanoparticles, preventing agglomeration, within the polymer-solvent-filler mixture. Mixing methods and length of time of mixing are also dissimilar: techniques involve stirring, blending, direct and indirect ultrasonication and tumbling have been utilised, often in conjunction or alternation, and the times of which can vary from the order of seconds to days. Given the diversity of preparation conditions it is very challenging to draw any conclusions or infer any significant correlations that outline the formation of agglomerations. Seemingly they are present irrespective of polymer or other details of preparation and thus both the mechanisms and factors that dictate their formation are poorly understood.

Amirilargani and Sadatnia also saw clustering of nanosized ZIF-8 in PVA composite membranes for pervaporation of alcohols. They noted no agglomerations at low loadings up to 5 wt.% and saw increases in permeation of up to 500% albeit with a loss in the separation factor. Between 5 and 10 wt.% they saw agglomerations which markedly increased the permeation and decreased the separation factor.[173] Shahid et al.[139] utilised a novel approach to overcome the formation of agglomerations by first functionalising the polymer particles themselves with the imidazole and then growing the ZIF-8 particles in-situ. They noted no agglomerations, even at 40 wt.% loadings.

ZIF-8 has also been included in PEBAX membranes during the time of this work. Nafisi and Hägg[112] looked at the inclusion of ZIF-8 into PEBAX-2533 for various gases including CO_2 and N_2 in both dry and wet conditions. They synthesised dual-layer flat sheet MMMs and reported increases in permeability coefficient of all gases as filler content increased with notable increases in CO_2 permeability which increased from around 350 Barrer to nearly 1300 Barrer at a 35% weight loading. They did however note a slight decrease in CO_2/N_2 selectivity at all non-zero loadings. Clusters were not observed below loadings of 30 wt.% and they noted good interaction between filler and polymer at lower loadings.

Very recently Sutrisna et al. looked at ZIF-8/PEBAX membranes[163] successfully combining ZIF-8 with both flat sheet *and* hollow fibre membranes. They noted a significant effect on the chain packing of the PEBAX phase in flat sheet membranes which resulted in increased permeabilities, almost certainly due to higher free volume. Similar to Nafisi and Hägg, they noted a slight decrease in selectivity which they attributed to non-continuous microscale voids.

Dai et al. looked at MMMs formed from graphene oxide functionalised with imidazole linkers (ImGO) and PEBAX. While these were functionalised with carboimidazole, which differs slightly from the 2-methylimidazole present in ZIF-8, the imidazole ring is the most sterically available moiety in both. Despite their seemingly unsubstantiated assertion that the wrinkles observed in cross-sectional SEM images were due to interface voids, the tensile test and gas permeation results seem to suggest quite the contrary. Although this work was limited to producing membranes only of up to 1 wt.% loadings of ImGO, equivalent to 0.5% by volume, they did observe appreciable losses in permeability and increases in selectivity over the range of loadings explored. Despite this limitation, this particular study does provide some evidence that there is good interaction between PEBAX and the imidazole ring.[142]

3.4 MCM-41

Mobil composition of matter (MCM) are a range of mesoporous structured silicas first developed by Mobil in the early '90s.[174] Similar to ZIFs and zeolites, they have seen a lot of interest for carbon capture applications due to the diversity of potential structures, and high surface area and porosity.

MCM-41 is one such variant of these materials composed of an array of regular hexagonal pores which has seen some interest in gas separation due to its ease of functionalisation, highly tunable pore size, ease of synthesis and high surface area.[175,176] The origin of its ordered structure lies in its typical synthesis which utilises self-assembled surfactant template which the silica then forms around. By varying the size of the template molecules the diameter of the pores can be controlled.[177,178] Much work has been done into the functionalisation of silicas, including MCM-41, with amines demonstrating the improvement in CO_2 sorbent capacities and CO_2-N_2 separation ability.[179,180]

3.5 MCM-41 in Mixed Matrix Membranes

Multiple studies have involved the inclusion of mesoporous silicas to form mixed matrix membranes.[70,143,181–183] Several studies combining MCM-41 with polysulfone have been undertaken with varying results. Reid et al.,[178] in the earliest work found to use MCM-41 as a MMM filler, incorporated micron sized particles into polysulfone noting agglomeration of the filler material and and increase in brittleness in membranes. Several other studies utilising both MCM-41 and polysulfone (PSF) have observed both aggregation of particles as well as voids and taken various steps to avoid this. Kim and Marand compared the inclusion of unmodified MCM-41 with that which had been treated with trimethylsilane and saw reduced agglomeration with the treated particles. They claimed this was due to the decrease of hydrogen bonding interactions between particles.[176] They further noted the adsorption capacities of both CO_2 and N_2 of the highest loading (40 wt.%) membranes were less than the simple additive prediction based upon the pure component isotherms which suggests a degree of pore blockage of the MCM-41 was limiting the accessible volume of the filler particles. Khan et al. achieved similar morphological results, eliminating both the occurrence of agglomerations and small voids surrounding them by utilising a modified PSF and amino-functionalised MCM-41 and then cross-linking the phases.[184] Valero saw minimal clustering which was attributed to the sphericity of the particles limiting the attractive forces between molecules.[76]

Several groups have noted poor MCM-41-filler interactions and taken steps to modify the surface of the MCM-41 to improve interfacial interactions. Khan et al.[184] noted poor adhesion between polysulfone acrylate (PSFa) and amino-functionalised MCM-41. In the unmodified MCM-41-PSFa membranes, as the mass loading of MCM-41 was increased from zero to 30 % they reported increases in CO_2 permeability coefficient of over 100 % from around 5 to over 10 Barrer, but decreases in CO_2/N_2 selectivity from 28 to 18. A large increase in permeability and loss of selectivity can nearly always be associated with voids. By modifying the surface of the MCM-41 using aminopropyltrimethoxysilane (APTMS) to add amino groups of the surface of the MCM-41, which they claim results in covalent linkages between the acrylate and amino moieties of the polymer and filler respectively, they noted much improved adhesion at the interface. This was matched by increases in CO_2/N_2 selectivities compared with the unmodified MCM-41, from 28 to 33.

Zornoza et al.[185] used MCM-41 spheres, as well as Grignard surface functionalised MCM-41 spheres in 6FDA-DAM. The Grignard treatment results in the growth of magnesium hydroxide ($Mg(OH)_2$) "whiskers" on the filler surface, which they claim decrease filler-solvent interactions and improve the interfacial forces between the polymer and filler phases. This produces a rougher surface morphology which is thought to encourage the entanglement of polymer chains in the whisker structures

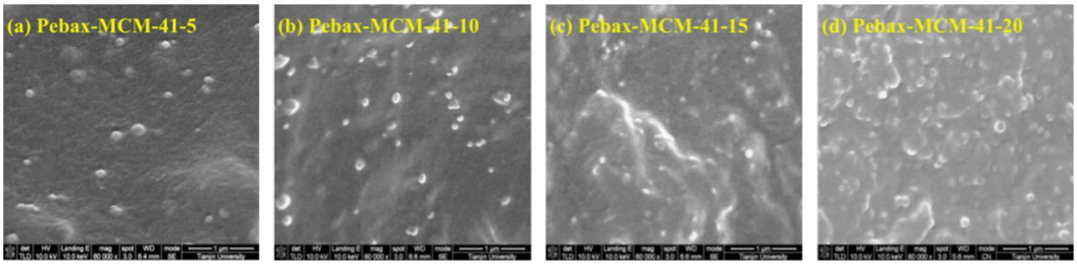

Figure 3.3: SEM images of unmodified MCM-41-PEBAX MH1657 mixed matrix membranes.[56]

by way of minimising the entropy of the chains. TEM images showed good adhesion between both unmodified and treated spheres but the polymer did appear to adhere better to the modified surface. Correspondingly they saw improved gas transport properties over neat 6FDA-DAM with increases in both selectivity and permeability with the treated spheres demonstrating the best properties close to the upper bound.

Several studies have also investigated MCM-41 and PEBAX-based membranes with contrasting observations regarding interfacial adhesion. Tan et al[186] looked at MCM-41-PEBAX 2533 membranes for the pervaporation of butanol from aqueous solutions and noted good interaction between the phases observing no voids nor clustering. Wu et al[56] incorporated both unmodified MCM-41 as well as polyethylenimine-modified MCM-41 into PEBAX MH1657, the particular grade of PEBAX used in this work. They claim the SEM images of the unmodified materials in PEBAX demonstrate poor adhesion between phases. This claim would imply that voids were observed. However these SEM images are reproduced in figure 3.3; no voids nor any features suggesting poor adhesion are clear to the author and instead it is suggested that the contrary is the case and these images demonstrated good adhesion.

Since MCM-41 has a relatively large pore size compared with that of the kinetic diameters of CO_2 and N_2, thus providing virtually zero size selectivity, several groups have tried to functionalise the surface to improve the selectivity by creating facilitated-transport MMMs.[56,187] In facilitated transport membranes a reversible reaction occurs between reactive 'carriers' in the membrane and the desired greater permeating species (CO_2).[78,188] Some of these including the previous work mentioned by Wu et al.[56] have noted great increases in selectivity however facilitated membranes are plagued by issues of long term carrier stability.

The use of MCM-41 as a filler in mixed matrix membranes is limited. One particularly interesting facet of the novel MCM-41 hollow spheres used in this study lies in their geometry. Previous work into other materials in the form of hollow

spheres have highlighted the benefits of hollow fillers. The hollow centre allows molecules to diffuse through the centre rapidly with minimal resistance which can leaded to increased permeability coefficients.[189] If the exterior is selective then the less mobile species must travel around the spheres, increasing the effective path length of these molecules and can increase the selectivity of the overall composite. Roh et al.[190] saw increases in both permeability and selectivity when incorporating mesoporous hollow titanium oxide spheres. In this study, TiO_2 nanospheres with an average diameter of 280 nm, a shell thickness of 30 nm and an average pore size of 18 nm, were added to an amphiphilic graft polymer of poly(vinylchloride) (PVC) with poly(oxyethylene methacrylate) (POEM) side chains (PVC-g-POEM). Similar to PEBAX, PVC-g-POEM is a copolymer that separates in glassy and rubbery domains. The TiO_2 spheres were functionalised using (3-aminopropyl)-trimethoxysilane and poly(ethelene glycol) diglycidyl ether to improve their affinity with CO_2 which was otherwise minimal. At the highest filler loading of 30 % by weight they reported increases in CO_2 permeability from 45 to 85 Barrer, and a modest increase in selectivity from 38 to 43. While these values do not approach the Robeson upper bound, they are a successful demonstration of including hollow particulates in MMMs.

Hwang et al.[162] similarly used PVC-g-POEM but with 700 nm diameter ZIF-8 hollow spheres. The noted a remarkable increase in CO_2 permeability coefficient of nearly 900 % from 70 to 623 Barrer with only a slight loss of selectivity (13.7 to 11.2). An increase in permeability of such proportions could normally only be explained by widespread voids or cracks which would decrease the selectivity drastically. Given the only slight drop in selectivity it further provides evidence for the influence of hollow fillers in mixed matrix membranes.

Chapter 4

Experiments and Techniques

Within this project, numerous mixed matrix membranes (MMMs) were synthesised from PEBAX pellets and various pre-prepared filler particles and subsequently characterised to investigate the interaction of phases and materials. Given the wide range of filler particles available, and the necessity to narrow the scope of the project to feasible limits, the filler particles were prepared externally.

Zeolite 13X, nano-scale ZIF-8 particles and nano-scale MCM-41 hollow spheres were used as fillers and combined with PEBAX grade MH1657 in various loadings. Initially zeolite 13X was used as a filler material as a preliminary means to test the synthesis procedure. Zeolite 13X was chosen for this purpose simply due to the great interest shown in it as an adsorbent for carbon capture combined with its immediate accessibility despite the relatively large particle size. Subsequently, once the synthesis procedure had been refined, nano-sized ZIF-8 particles and variations of novel hollow-sphere MCM-41 particles were incorporated into PEBAX-based MMMs. The loading of filler incorporated into the membranes was varied to investigate the influence of the filler materials and the interaction of phases on the gas transport properties of the composite materials.

The resulting membranes were then characterised using a constant-volume variable-pressure gas permeation technique to determine the permeability and diffusivity. In conjunction with this technique, scanning electron microscopy was utilised to investigate the internal morphology of the membranes to link their physical nature with their gas permeation behaviours.

The follow sections detail the procedure of mixed matrix membrane synthesis and characterisation utilising the constant-volume variable-pressure gas permeation technique and scanning electron microscopy.

4.1 Membrane preparation

As discussed in section 3.1.1, various solvents, dissolution conditions, filler dispersion methods, and casting conditions have previously been carried out in literature. The following procedure to fabricate the mixed matrix membranes from PEBAX was based upon the work of this previously published literature and then refined to promote good dispersion of nanoparticles and membranes sufficiently strong to be tested using permeation techniques described later in this chapter.

4.1.1 Materials

The PEBAX, grade MH1657, was kindly provided by Arkema. PEBAX was chosen as the sole polymer in this work not only due to its aforementioned (in Chapter 3) inherent high selectivity, but its mechanical properties, relatively low cost, ease of accessibility, and good previous performance when used with mixed matrix membranes. The nano-sized ZIF-8 was prepared by collaborators in Deakin University, Victoria, namely Li He, James Wainaina Maina, and Ludovic Dumée. The MCM-41 hollow spheres were prepared primarily by Chris Starkie at Johnson Matthey Technology Centre (JMTC). The zeolite 13X was purchased from Sigma-Aldrich and supplied by Johnson Matthey. The ZIF-8, MCM-41 and zeolite 13X were all stored in dehumidified environments.

Preparation of ZIF-8 and ED-ZIF-8 Nanoparticles

Synthesis and modification of the ZIF-8 nanoparticles was carried out by Li He and James Wainaina Maina at Deakin University in Victoria, Australia.

ZIF-8 nanoparticles were prepared using a colloidal route previously described by Cravillion et al.[191] 1.47 g of zinc nitrate hexahydrate (Zn(NO3)2.6H2O) and 3.25 g of 2-methylimidazole (2-MeIM) were separately dissolved in 100 cm^3 of methanol, following which the zinc nitrate solution was rapidly poured into the 2-MeIM solution, and vigorously stirred for 1 h, at room temperature. The particles were then separated using centrifugation, and subsequently washed three times with deionized water.

The ethylenediamine-modified ZIF-8 (ED-ZIF-8) was also produced by our partners at Deakin University via a high pressure wet impregnation method based on work previously detailed by Zhang et al.[192] The ZIF-8 crystals were produced using the aforementioned procedure. The crystals were then added to a 30% aqueous ethylenediamine solution which was then placed into an autoclave and heated to

416 K for 1 hour and then kept at 381 K for a further 6 hours. The product was washed with deionised water and then dried overnight at 383 K.

Preparation of MCM-41 Hollow Spheres

The MCM-41 hollow spheres were synthesised based on previous work detailed by Qi et al,[193] and Sonwane and Bhatia,[177] outlining the synthesis of hollow spherical particles with mesoporous shells, and the characterisation of MCM-41 materials respectively. The syntheses of the different MCM-41 hollow spheres were carried out by Chris Starkie, formerly of Johnson Matthey Technology Centre.

The MCM-41 hollow spheres were made by forming MCM-41 via hydrothermal synthesis using alkyltrimethylammonium halides as templates for the pores and pre-fabricated polystyrene spheres as a template for the spherical structure. By controlling the length of the alkyl chain of the alkyltrimethylammonium halide, the pore size of the MCM-41 can be controlled.[177]

The polystyrene spherical templates were first produced. 0.88 ml of 2-(acryloyloxy)ethyltrimethylammonium chloride solution was added to a 390 ml of purified water whilst being stirred followed by adding 44 ml of styrene. The solution was heated to 90°C and degassed under nitrogen for 30 minutes. 1g of 2,2-Azobis(2-methyl proprionamidine) dihydrochloride in 10 ml of water was then added. This emulsion was then maintained at 90°C for a further 24 hours under an inert atmosphere. This template mixture of 9.5 wt.% polystyrene was then used without purification for synthesis of the hollow spheres.

To synthesise the MCM-41 hollow spheres 0.80 g of hexadecyltrimethylammonium bromide (CTAB) (for C16-MCM-41-HS) or 0.86 g of octadecyltrimethylammonium bromide (for C18-MCM-41-HS) was dissolved at ambient temperature in a solution of water (29 ml), ethanol (15.2 ml) and ammonium hydroxide (1.0 ml). Following complete dissolution 20.0 g of the freshly made spherical polystyrene template mixture diluted to 4.5 wt.% with water was added to the solution. This light gray mixture was stirred for 30 minutes. 4.29 ml of tetraethyl orthosilicate (TEOS) was then added dropwise to the solution. After 5 minutes the solution started to change to a bright white colour. The solution was then stirred for 48 hours at ambient temperature. Following the synthesis procedure the solids were extracted by centrifugation at 4000 rpm. The solids were washed with absolute ethanol twice and then once more with purified water yielding a bright white powder.

The solid was dried under vacuum for 48 hours to remove any residual solvent. To remove the polystyrene template the solids were then calcined at 600°C for 8 hours with a ramp rate of 3 °C min^{-1}.

During synthesis of the MCM-41-HS the CTAB, which is the template molecule for the MCM-41 pores, arranges itself around the polystyrene template. Due to the steric hindrance of the proximal alkyl chains of the CTAB, the pores formed should all be perpendicular to the surface of the spheres.

4.1.2 Dissolution of polymer

For PEBAX MH1657, the grade that was used in this work, an ethanol:water mixture (70:30 wt.) was most commonly utilised. It was decided to also use this as a solvent due to its low toxicity which provided the flexibility to cast it outwith a fume hood. While most studies in literature used a 3 wt.% PEBAX solution, it was found that utilising a higher concentration solution of 6.7 wt.% were both easier to cast, and produced thicker, stronger membranes.

The casting polymer solution was made by dissolution of PEBAX in an ethanol-water mixture whilst heating and stirring under constant reflux. The mass of polymer was weighed using a Mettler-Toledo semi-microbalance to a precision of 0.1 mg (capable of 0.01 mg). A mass of approximately 1 g of PEBAX was typically used although this was lessened to 0.5 g for the ED-ZIF-8 sample to minimise the usage of the sample material which could only be produced in small batches. The polymer was added to a round bottomed flask with ethanol (EtOH) and purified water (H_2O) to produce a mixture of 1:10.5:4.5 wt. ratio of PEBAX, EtOH and H_2O respectively. Using a stirrer-heater plate, this mixture was heated to 75 °C (± 5 °C) whilst being stirred gently. The solution was then left stirring until complete dissolution of the polymer mixture which would take around 5-6 hours.

4.1.3 Preparation and Addition of Filler Particles

The mass of filler required to produce a membrane of desired loading, θ, was determined and weighed into a glass vial using a Mettler-Toledo semi-microbalance to a precision of 0.1 mg (capable of 0.01 mg).

At filler loadings of less than 6 wt.%, or preliminary higher loading membranes, equation 4.1 could be used to approximate the mass of filler, m_{filler}, required for a desired loading, $\theta_{desired}$ and mass of polymer, $m_{polymer}$. The actual loading could then be determined using equation 4.2. At lower than 6 wt.%, if the mass of filler added was exactly equal to the estimated mass, the deviation of the actual loading from the desired loading is less than 6%, or a difference of less than 0.4% in terms of loading. With the knowledge that this estimation slightly underestimated the mass of filler required by neglecting the mass of filler in the total mass, this could

also be compensated for when weighing the filler, reducing the deviation from the desired loading. This gave a fast, simple way of measuring the required masses, and since the mass of both filler and polymer were accurately known did not reduce the precision of the loading.

$$m_{filler} \approx \theta_{desired} \cdot m_{polymer} \tag{4.1}$$

$$\theta = \frac{m_{filler}}{m_{polymer} + m_{filler}} \tag{4.2}$$

In cases where precise control of the loading value was more desirable, for example when attempting to obtain intermediate loadings to previous experiments, or at loadings of particular interest, the mass of filler was weighed first, and the mass of polymer was subsequently weighed using eq. 4.2 rearranged for the mass of the polymer as this gave greater control over the loading as the polymer far outweighed the filler component. It should be noted that this did not alter the precision of the loading but allowed for more control over the accuracy of the loading. The volume of EtOH:H_2O solution was adjusted to maintain the correct ratio of polymer to solvent.

Prior to the addition of filler particles to the casting solution, the particles were treated with ultrasound to break up any agglomerations of nano-particles that had formed during storage. Immediately following the weighing of the sample, approximately 1 cm^3 of ethanol was added to the test tube containing the filler particles and the particles were lightly ground using a spatula to break up the largest clusters. Then, the top of the tube was sealed with flexible para-film to ensure minimal loss of ethanol whilst allowing for production of vapours and expansion of gases while undergoing ultrasonic (US) treatment. To ensure full break up of any agglomerations the solid particles were treated with ultrasound by placing the samples in an ultrasonic water bath for 6-8 hours. In the case of ZIF-8 which was prone to forming large, difficult to break agglomerations, the solid suspensions were treated for 48 hours. Two water baths were used in the course of this project: first, a Fisher-Scientific Model 15047 ultrasonic water bath, and secondly, a Branson CPXH series ultrasonic water bath details of which are shown in table 4.1. The Fisher Scientific model was used to fabricate all of the ZIF-8-PEBAX membranes, whilst both models were used to synthesise the MCM-41-PEBAX membranes due to equipment logistics.

The use of ultrasound to treat casting solutions and break up filler agglomerations is frequently employed in literature. The use of both probes and baths are utilised. Specifications and power outputs of equipment are frequently not quoted.[183] Times

Table 4.1: Ultrasonic water bath details.

Model	Frequency (kHz)	Volume (litres)	Maximum power (W)
Fisher Scientific 15047	37 kHz[1]	0.8	240 (Peak)
Branson CPXH 1800	40 kHz	1.9	70 (RMS)

[1] Impulse waveform[197]

of ultrasonic treatment vary from a few minutes,[142] to tens of minutes,,[183,194,195] and up to several hours.[146,180,196] Periods of application are also diverse: ultrasound is applied for a fixed period, or in intervals, often interspersed with other mixing techniques such as agitation or simple stirring. Given there was little consensus in literature of a 'best approach' the times used in this study were based on preliminary synthesis procedures using the water bath. It was observed that for ZIF-8, crystalline agglomerations present in the ZIF-8 which were visible with the naked eye until 24 hours of treatment with ultrasound. Given there was little chance of damaging the ZIF-8 structure with ultrasound it was decided that it was better to overestimate the required time and double this time was used. SEM of the initial membranes confirmed successful dispersion and following the procedure was not altered.

Once treatment with ultrasonication was complete, the solid suspension was poured into the polymer mixture whilst still undergoing stirring, and the round bottom flask was immediately transferred to the ultrasonic water bath set at 50 °C and left for 2 hours. Ultrasound was used to ensure good mixing as well as to make sure no agglomerations formed during this time. A temperature of 50 °C was set to allow for a slightly more viscous casting solution to be produced which in turn allowed for thicker, stronger membranes to be formed. The mixture was left for 2 hours to allow time for both good mixing and to give sufficient time for the mixture to reach thermal equilibrium.

4.1.4 Casting and Drying of Membranes

After 2 hours of sonication, the mixture was degassed using ultrasound for 5 minutes and then cast onto clean 15 cm by 15 cm glass slides, themselves placed on top of a levelled surface as seen in figure 4.1. Preliminary tests using neat PEBAX showed that using the casting knife produced higher quality membranes than those cast in a petri dish. A doctor blade set to 130 μm was used to create a uniform surface and the plates were covered with perforated boxes and left to dry at ambient temperature for 24 hours. Following this the membranes were removed from the

glass slides, simply by carefully peeling them off, and evacuated and heated to 110 °C in a vacuum oven to ensure complete removal of any residual solvent.

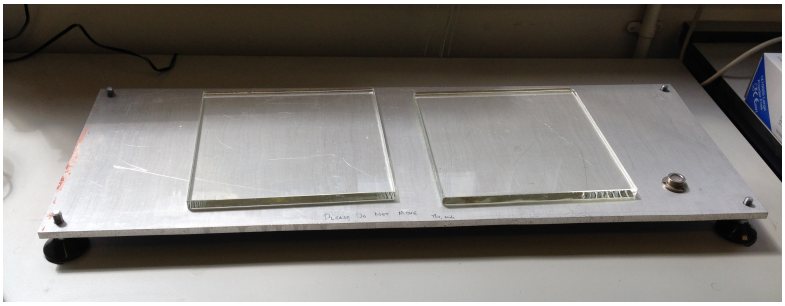

Figure 4.1: Glass plates on levelled aluminium surface with height-adjustable legs

4.1.5 Preparation of the Membrane for Time-Lag Experiments

The thickness of the membranes was measured using a Mitutoya micrometer with a resolution of 1μm.

Initially membranes were cut using a circular punch to be the exact dimensions to fit the membrane cell: 49mm. It was found that using a foil annulus to seal the outer perimeter of the membranes minimised the leaks present in the system and also facilitated the testing of stiffer membranes which were prone to breaking, either due to the pressure from the seals, or from the forces due to the pressure differential. The foil annuli were produced using punches of known dimension, thus the area of the membrane surface exposed was always known. The punches used were either 2.86 cm ($1\frac{1}{8}$ in) or 3.49 cm ($1\frac{3}{8}$ in) in diameter.

4.2 Constant-Volume Variable-Pressure Gas Permeation Method

The constant-volume variable-pressure gas permeation method, also known as the time-lag permeation technique, is a widely used technique to determine the permeability and diffusivity of membranes.[93,142,145,198,199] The time lag technique dates back to the work of Daynes in 1920 and has seen great developments through the further work of Barrer, Rogers et al. and Frisch to name a few who presented solutions to this mass balance in numerous geometries and developed analytical tools which greatly improved its applicability.[199]

It is a simple but powerful technique which allows both a transient component, the time lag, and a steady state component of permeation to be observed. The experiment, in short, involves passing pure gas through a membrane of known thickness into an evacuated volume. By virtue of the fact that the upstream volume is relatively large, and thus the pressure within can be assumed constant, and knowledge of several parameters describing the membrane and the volume of the downstream volume, an approximation of steady state flux can be created from which the permeability and diffusivity can be calculated.

4.2.1 The Theory behind the Time Lag Permeation Method

The mass balance of 1D permeation in a membrane is given by equation 4.3:

$$\frac{\partial C}{\partial t} = -\frac{\partial}{\partial z}\left(D\frac{\partial C}{\partial z}\right) \tag{4.3}$$

where C is the concentration of the permeating species in the membrane, t is time, D is the diffusion coefficient and z is the axis along which transport occurs.

Assuming D to be constant this relationship becomes:

$$\frac{\partial C}{\partial t} = D\frac{\partial^2 C}{\partial z^2} \tag{4.4}$$

At time equal to zero the concentration in the membrane can be assumed to be zero, the upstream concentration is constant throughout, and the downstream surface concentration can be assumed to be negligible. As such the boundary conditions can be defined as follows:

IC: $t = 0$, $C = 0\ \forall z$

BC1: $t > 0$, $z = 0$, $C = C_0$

BC2: $t > 0$, $z = l$, $C \approx 0$

These previous boundary conditions can be achieved by ensuring the initial concentration in the membrane is zero by thorough evacuation to remove penetrant gases, along with using sufficiently large volumes to ensure that the flux of mass through the membrane is insufficient to significantly alter the concentration at either surface.

Via use of either Laplace Transform or separation of variables, the solution of equation 4.4 can be found analytically, as shown by Crank in The Mathematics of Diffusion[200] to be similar to equation 4.5:

$$C = C_0(1 - \frac{d}{l}) + \frac{2C_0}{\pi} \sum_{n=1}^{\infty} \frac{1}{n} \sin \frac{n\pi z}{l} e^{\frac{-Dn^2\pi^2 t}{l^2}} \tag{4.5}$$

This can then be used to describe the total flux through the membrane at any given time which can in turn be used to find a relationship to the downstream pressure. Taking a limit as $t \to \infty$, the pressure in the downstream, P_D caused by the steady state flux can be shown to be:

$$\lim_{t\to\infty} P_D = \frac{P_0 DA}{V_D l} \left(t - \frac{l^2}{6D} \right) \tag{4.6}$$

where P_0 is the upstream pressure, A is the area of the membrane, V is the downstream volume, and l is the thickness of the membrane.

By plotting the downstream pressure versus the time a plot similar to that shown in figure 4.2 can be produced. A steady state region, to which a straight line can be fitted, should be observed. This straight line intercepts the time-axis at what is known as the time lag and is inversely proportional to the diffusivity as given by equation 4.7.

$$t_{lag} = \frac{l^2}{6D} \tag{4.7}$$

4.2.2 Experimental Procedure

Figure 4.3 shows the schematic of the in-house built rig. The experimental procedure is carried out as per the following steps:

- The membrane is placed in the membrane cell as seen in figure 4.4 and fitted in place in the permeation rig.
- The membrane cell and downstream volume are evacuated until removed of all penetrant gases.
- Concurrently or prior, the upstream reservoir is evacuated, flushed and filled with the experimental gas.
- The downstream pressure is recorded to determine the leak into the downstream.
- The valve allowing gas to flow to the membrane is opened and the increase in pressure in the downstream is recorded.

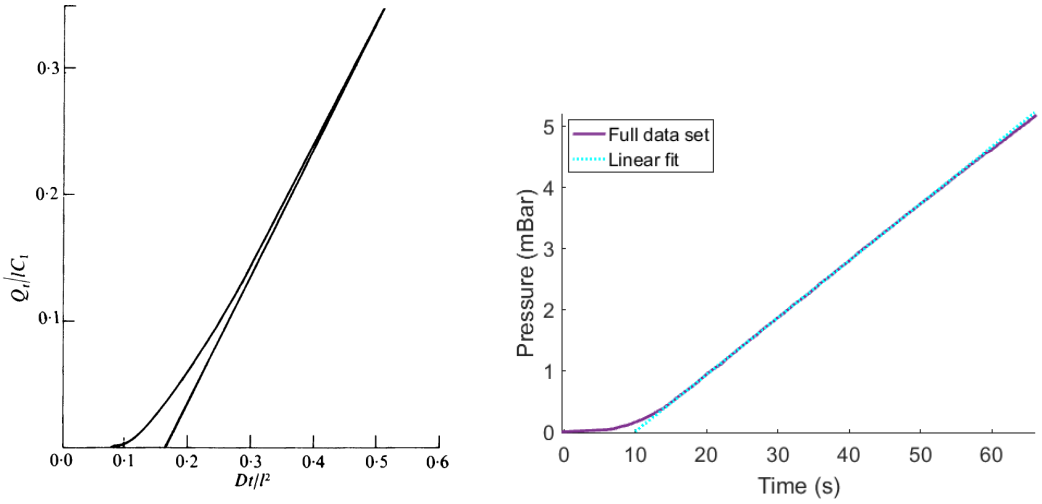

Figure 4.2: The non-dimensionalised approach to steady-state flux through a plane sheet as given by Crank in The Mathematics of Diffusion[200] (left) and typical experimental data showing the approximation of steady state flux and the linear fit to the steady state region

- An approximate steady-state is reached and a straight line is observed. Once sufficient data (see below) are collected, data collection is ceased, and the cell and downstream volume can be evacuated to perform repeat measurements.

A bespoke Labview® code was written and used to interface with the pressure transducer and record the time and pressure data, the block flow diagram and user interface of which can be seen in figure 4.5.

Avoiding a leak of some magnitude into the system is virtually impossible. It is almost always of a small, yet noticeable scale, and thus must be accounted for. To do this some data were always recorded prior to the 'start' of the experiment - the point at which the valve is opened allowing gas to flow from the reservoir to the membrane cell. A straight line was fit to this data as shown in figure 4.6a. Subsequently the data could be corrected using the gradient of this linear fit using equation 4.8. Figure 4.6b shows the difference between the non-adjusted and corrected data.

$$p_{adj} = p_{raw} - \nabla_{leak} t \tag{4.8}$$

where p_{adj} is the adjusted, or corrected, data vector, p_{raw} is the raw data vector, ∇_{leak} is the gradient of the leak, and t is the time data vector.

Once the leak has been adjusted for a straight line can be fit to the steady state region and the gradient and time-lag can be determined graphically as shown in

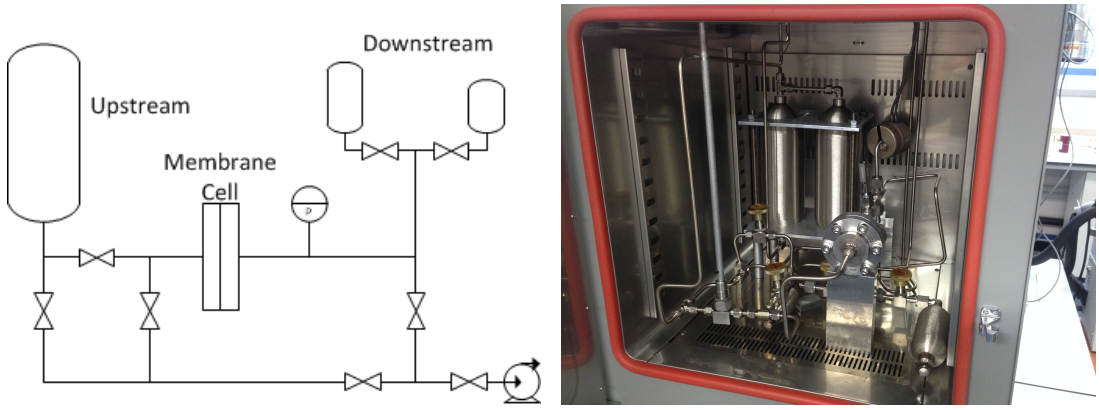

Figure 4.3: Schematic (left) and photograph of the constant-volume variable-pressure apparatus.

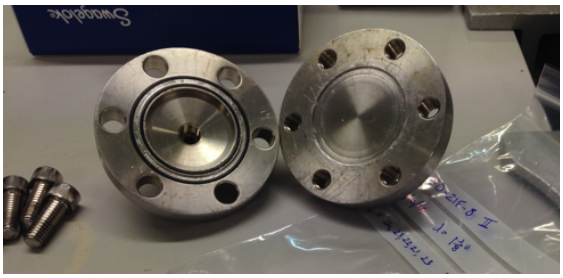

Figure 4.4: The membrane cell

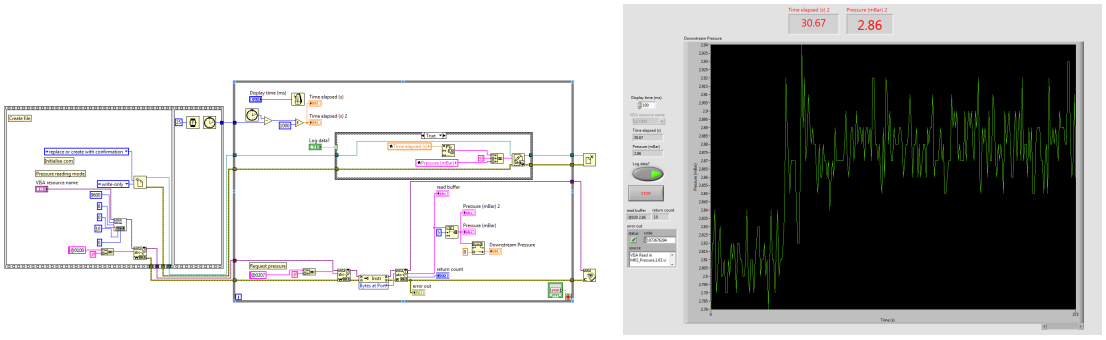

Figure 4.5: The block flow diagram and user interface of the pressure data acquisition code.

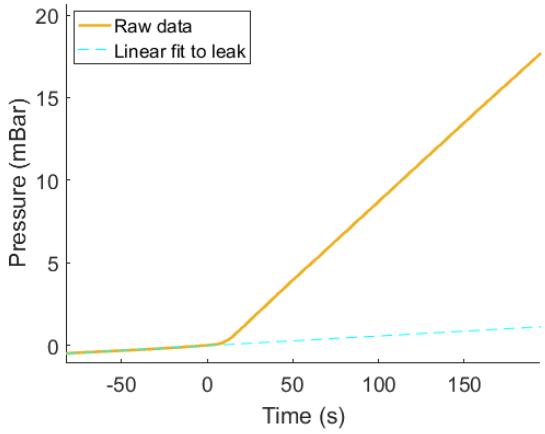

(a)

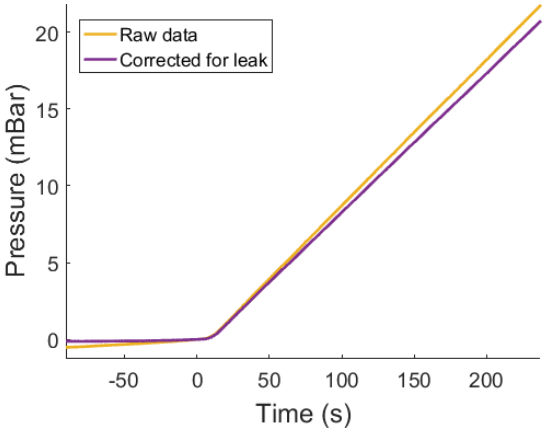

(b)

Figure 4.6: A straight line is fitted to the leak (top) and the difference between the unadjusted and correct pressure signal.

figure 4.7. Thereafter the diffusivity and the permeability can be calculated using equations 4.7 and 4.9 respectively.

$$P = \frac{dp}{dt} V_D \frac{T_{STP}}{P_{STP} \cdot T_{exp}} \frac{l}{A \cdot p_0} \tag{4.9}$$

where P is the permeability, dp/dt is the pressure gradient at steady state, V_D is the volume of the downstream, T_{STP} is the standard temperature, 0 K, P_{STP} is standard pressure, 101325 Pa, T_{exp} is the experimental temperature, l is the thickness, A is the exposed area of the membrane, and p_0 is the upstream pressure.

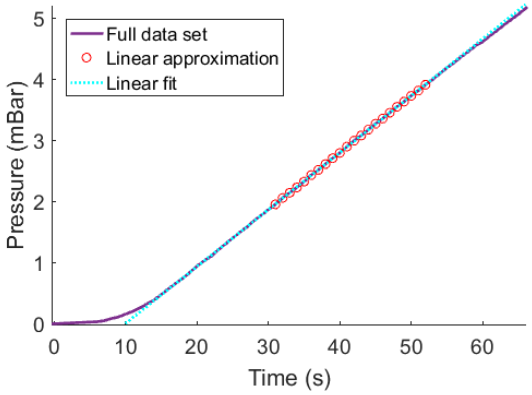

Figure 4.7: A linear fit is used to determine $\frac{dp}{dt}$ and the time-lag (the x-axis intercept).

Careful treatment of the units is required to convert this into Barrer.

This procedure of plotting and correcting the data was simplified by utilising MATLAB ® scripts that can be found in the supplementary electronic files.

4.2.3 A note on some time-lag test results

The system was often affected by noise in the pressure signal during the first few seconds of the experiment. This noise was attributed to vibrations caused by opening a valve creating a spike in the signal from the pressure transducer. This often made it difficult to accurately determine the exact time-lag. Further, particularly for experiments with nitrogen, the time-lag was often insufficiently large. These two points meant that often diffusivity could not be calculated or the uncertainty in the diffusivity value exceeded the value itself. This is why several results are quoted only with permeabilities and not diffusivities.

4.3 Scanning Electron Microscopy

Several scanning electron microscopes, or SEM, were utilised extensively to investigate the internal structure of the synthesised MMMs. SEMs probe a sample with a beam of electrons to gain topographical or compositional information from the sample surface. They generally consist of an electron source, lenses to generate a focussed electron beam, a means of deflecting the beam such that it can be rastered across the sample surface and, often multiple, detectors.[201]

A wide variety of detectors are used for SEM; the detectors used here were variants of secondary electron detectors (SE) and energy selective backscatter detectors (ESB). The incident electron beam causes the ejection of secondary electrons from the surface sample, that is, electrons that were priorly present in the outer orbitals of the sample. Secondary electrons can be distinguished from incident electrons by the fact they have significantly less energy - as such the majority of secondary electrons are ejected from very close to the sample surface and so are very useful for obtaining topographical information. Backscattered electrons are the result of the deflection of the incident electrons through an angle of greater than 90°, such that they exit the sample surface. The degree of prevalence of backscattered electrons is heavily influenced by the atomic number of the sample nuclei and so is often utilised to obtain information on the composition of the sample.[202,203]

The membranes had to be prepared prior to coating and imaging. To view the internal cross-section of the membranes, small MMM samples were immersed in liquid nitrogen, which made them brittle, and then fractured to produce a clean edge free from stretching. These samples were then mounted vertically on to SEM stubs. To view the surface of the membranes, a small section of sample was cut and placed horizontally onto a stub.

To prepare the nanoparticles for imaging, a dilute suspension of the particles was made in ethanol and ultrasonicated for 48 hours. A small drop of the suspension was placed onto a clean silicon slide. The ethanol quickly evaporated leaving a thin layer of particles on the surface. The silicon slide was then affixed to an SEM stub.

Samples were either carbon- or gold-coated using the conventional sputtering method to prevent charging, a phenomenon where the surface of a non-conductive sample becomes charged while undergoing electron bombardment and subsequently saturates the detectors. While the PEBAX was often easily damaged by the electron beam, even at low accelerating voltages, it was obvious where the damaged sections were and they did not impair the visibility of the observable structures.

The following three SEM facilities were utilised in the course of this project: University of Edinburgh (UoE) Molecular Plant Sciences SEM facility ('Biology SEM'), UoE School of Geosciences SEM facility ('Geology SEM'), and the Johnson Matthey Technology Centre Analytical Department SEM (JMTC SEM). Details of these SEMs and the settings used to capture the images are found in table 4.2. Both the School of Geology SEM and JMTC SEM possessed in-lens secondary electron detectors. This particular detector picks up more backscatter and thus is often used to provide a high contrast topographical image highlighting variation in sample density and elemental composition.

Table 4.2: SEM facilities and conditions of imaging.

Facility	Model	Detectors	Aperture (μm)	Working Distance (mm)	Accelerating voltage (kV)	Resolution (nm)
Biology SEM	Hitachi 4700 II cold Field Emission SEM	Secondary Electron	30	4 to 5	5 to 15	1000
Geology SEM	Carl Zeiss SIGMA HD VP Field Emission SEM	Everhart-Thornley and In-lens secondary electron	30	4 to 6	5	1nm (15kV) to 1.9nm (1kV)
JMTC SEM	Zeiss Ultra 55 Field Emission electron microscope	ESB	30 to 60	7 to 8	20	1nm
		Secondary electron and In-lens secondary electron	20 to 30	2 to 3	1.6	1nm

4.4 Thermogravimetric Analysis

Thermogravimetric analysis (TGA) was used to determine CO_2 isotherms on both the modified and unmodified ZIF-8. TGA is a useful tool to accurately investigate small changes in the weight of samples and measure tiny heat flows as a function of temperature or time.[204] Isotherms were produced by increasing the partial pressure of CO_2 in a mixed gas stream up to 1 bar and recording the mass uptake. Heat flows were also measured for each uptake step and the heat of adsorption subsequently determined.

Approximately 30 mg of sample was added to the sample crucible and precisely weighed using a Mettler-Toledo semi-microbalance, whilst an equivalent mass (to within 1 mg) of lead balls was added to the reference crucible to counteract any buoyancy effects due to change in the density of the gas mixture when the composition was changed. Samples were regenerated at 200°C under 20 $cm^3\ min^{-1}$ helium flow for 2 hours and then left at 20°C under the same flow rate of helium for a further 2 hours. Following this the CO_2 concentration was increased in 10% steps with He as the carrier gas up to 100% CO_2 flow every 1.5 hours maintaining the same total flow rate. Gases were well mixed in a volume prior to the sample chamber. Samples were regenerated at 200 °C and the experiment repeated once.

The step changes in mass and integrals of the heat flow curves were calculated using the Setaram analysis software. The heats of adsorption, ΔH, could then be calculated using equation 4.10 for each step change.

$$\Delta H = \frac{\int_{t_1}^{t_2} Q dt}{m_{t_2} - m_{t_2}} \tag{4.10}$$

where Q is the heat flow, t_1 and t_2 are the times at the start and end of the step, and m_{t1} and m_{t2} are the total sample masses at the start and end of the step.

Chapter 5

Nano-scale ZIF-8 particles in PEBAX

ZIF-8, as discussed previously in Chapter 2, is of notable interest for carbon capture and other gas separation applications, particularly due to its pore size which is in the range such that it may act as a molecular sieve for the CO_2/N_2 separation and the hindering effects that may limit transport of other species in the presence of carbon dioxide.

The aforementioned procedure in Chapter 3 was implemented to successfully create membranes containing ZIF-8 up to 10 wt.% loading. The 10 wt.% ZIF-8 membranes were, however, fragile and did not possess sufficient tensile strength to be tested using the gas permeation rig. MMMs of 7 differing loadings from 1.1 to 7.0 percent were tested with both CO_2 and N_2, with 4 of the membranes also being tested with He.

As will be discussed at greater length later in this chapter, large clusters were observed at loadings above 5 wt.% loadings. As a possible means to better disperse the particles, functionalisation of the ZIF-8 surface was carried out in collaboration with our partners at Deakin University. Thus, in an attempt to improve the dispersion of ZIF-8 in the MMMs and reduce clustering, the ZIF-8 nanoparticles made via an identical procedure were modified post-synthesis using a high pressure, wet impregnation method with ethylenediamine. The idea behind this was to improve interaction between the ZIF-8 particles and PEBAX, by adding strong polar groups which would interact favourably with the polar groups present in PEBAX. Subsequently, an identical fabrication procedure was carried out to successfully produce ethylenediamine-modified ZIF-8 (ED-ZIF-8) MMMs with PEBAX of up to 12.5 wt.% loadings.

5.1 Estimations of composite properties

Prior to experimentation, it was possible to make predictions using ideal models discussed in section 2.4 of the properties of the PEBAX-ZIF-8 mixed matrix membranes based on the individual properties of PEBAX and ZIF-8. As previously described, these ideal models only require the permeability coefficients of a species in the combining materials to determine the composite permeability coefficient for given volumetric loadings. While the permeability of PEBAX can be simply determined, or easily found in literature, permeability coefficients for particulate fillers such as ZIF-8 are less easily found. One method of approximating the permeability of filler materials is by using the relationship between the permeability coefficient and the diffusivity and solubility coefficients given by equation 2.6, $P = DS$.

Values from literature for both the diffusion and solubility coefficients for ZIF-8 were found, a summary of which can be found in tables 5.1 and 5.2. Equation 5.1 is a reformulation of equation 2.6 accounting for the conversion of mmol g^{-1} and cm^2s^{-1} to Barrer:

$$P_e = 10^{10} D \cdot S \cdot \rho_{\text{ZIF-8}} \cdot \frac{V_{\text{M,STP}}}{75} \tag{5.1}$$

where P_e is the effective permeability in Barrer, D is the diffusivity in cm^2s^{-1}, S is the solubility coefficient in mmol g^{-1} bar^{-1}, $\rho_{\text{ZIF-8}}$ is the density of ZIF-8, taken to be 0.950 g cm^{-3}, and $V_{\text{M,STP}}$ is the molar volume in litres per mole at standard temperature and pressure.

Using equation 5.1 and values of diffusivity and solubility coefficient for each gas, effective permeabilities of ZIF-8 could then be estimated. The diffusivities of ZIF-8 from literature span nearly 3 orders of magnitude. Due to this span, the range of effective permeability coefficients ZIF-8 could have for CO_2 ranges from around 500 to 20000 Barrer. To cover the range of values of predicted permeabilities this could create, three cases were envisaged: case 1, in which the ZIF-8 had the highest diffusivity and solubility coefficients reported in tables 5.1 and 5.2 for CO_2 and the lowest for N_2; case 2, in which intermediate values were chosen for both gases; and case 3, in which each gas was assigned the lowest values possible; essentially case 1 being the best case scenario, and case 3 being the worst. Case 1 assumes that the potential gating mechanism discussed in section 3.2 in which CO_2 hinders the transport of N_2 is occurring. Table 5.3 summarises the solubility and diffusivity coefficients chosen for each, and the subsequent effective permeability coefficient and selectivities for each case. Choosing intermediate values from tables 5.1 and 5.2, equation 5.1 could be used to calculate the effective permeability of ZIF-8.

Table 5.1: Diffusivity coefficient values of ZIF-8 from literature.

Reference	Method	Type of diffusion	Gas	Diffusion coefficient ($cm^2\ s^{-1}$)
Chmelik et al.[161]	Molecular simulation	Effective Fickian	CO_2	$1.5 - 6 \times 10^{-6}$
Chmelik et al.[150]	Molecular simulation	Transport	CO_2	$1 - 7 \times 10^{-6}$
Chokbunpiam et al.[158]	Molecular simulation	Self	N_2	$3 - 10 \times 10^{-6}$
Pantatosaki et al.[205]	Isobaric- isothermal molecular dynamics	Transport	CO_2	$3 - 10 \times 10^{-7}$
	Infrared microscopy	Transport	CO_2	$1 - 7 \times 10^{-6}$
Zhang et al.[160]	Molecular simulation	Self	CO_2	$5 - 9 \times 10^{-6}$

Table 5.2: Sorption or solubility values of ZIF-8 from literature.

Reference	Method	Gas	Temperature (K)	Solubility coefficient[1] ($mmol\ g^{-1}$)
Huang et al.[206]	Autosorb	CO_2	298	0.7
		N_2	298	0.01
McEwan et al.[207]	Gravimetric analysis	CO_2	298	0.8
		N_2	298	< 0.1
Pérez-Pellitero et al.[208]	Magnetic balance	CO_2	303	0.6
		N_2	303	< 0.1
Zhang et al.[192]	Magnetic balance	CO_2	298	1
		N_2	298	<1
This work	Gravimetric analysis	CO_2	293	0.7

[1] Reported at 1 bar.

Table 5.3: Details of the 3 cases for the effective permeability coefficients of ZIF-8 based on adsorption and diffusivity data from literature.

Case	Gas	D (cm^2 s^-1)	S (mmol g^{-1})	P (Barrer)
1	CO_2	9 $\times 10^{-6}$	0.8	20000
	N_2	1 $\times 10^{-6}$	0.05	140.00
				(α= 140)
2	CO_2	1×10^{-6}	0.7	2000
	N_2	1×10^{-6}	0.05	140
				(α= 14)
3	CO_2	3×10^{-7}	0.6	510
	N_2	3×10^{-7}	0.05	43
				(α= 1.2)

Using a value of 1 $\times 10^{-6}$ $cm^2 s^{-1}$ for the diffusivity coefficient of both species, and 0.7 and 0.05 mmol g^{-1} for the CO_2 and N_2 solubility coefficients respectively gives effective permeabilities of roughly 2000 and 200 Barrer.

Using these values, and values of volumetric loading from 0 to 20 %, predictions of the PEBAX-ZIF-8 MMM properties can be made using the Maxwell and Bruggeman models for the three cases. Figure 5.1 shows both the predicted permeabilities and selectivities of the composite materials of all three cases on a Robeson plot. It can be seen that the expected values differ greatly for each case but are similar for each model as is expected. Case 1 clearly represents the most optimistic outcome, with increases in permeability and a slight increase in selectivity. In cases 2 and 3 a slight decrease in selectivity is expected with increased loading since the selectivity of the ZIF-8 in these cases is predicted to be less than that of PEBAX. It is interesting to note that the maximum CO_2 permeability predicted for the overall composite membranes in cases 1 and 2 are not greatly different, despite the order of magnitude difference between the calculated effective permeability of the ZIF-8 filler phase.

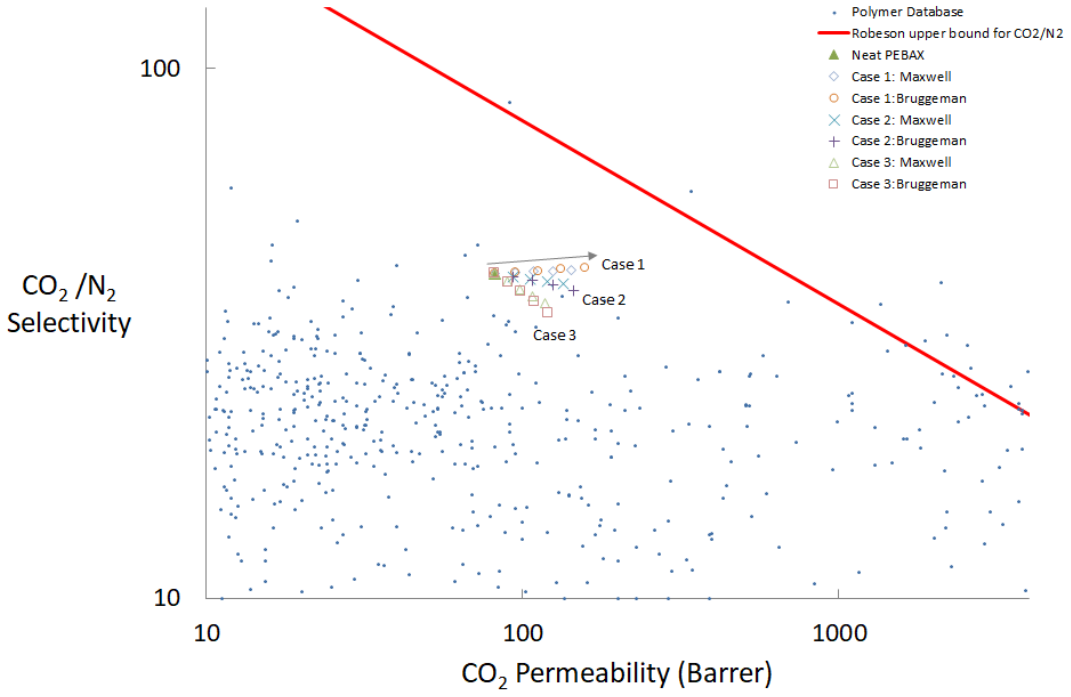

Figure 5.1: Robeson plot showing neat PEBAX and the predictions using the Maxwell and Bruggeman models of PEBAX-ZIF-8 mixed matrix membranes. Both models are plotted using 5 % loading increments in the direction of the arrows up to a maximum loading of 20 %.

5.2 ZIF-8 and ED-ZIF-8 Nanoparticles

5.2.1 Characterisation of ZIF-8 and ED-ZIF-8 Nanoparticles

Several tests were run on the samples to characterise the ZIF-8 and ED-ZIF-8 nanoparticles. X-ray diffraction (XRD) and Fourier transform infrared spectroscopy (FTIR) were performed post-synthesis by our collaborators at Deakin University and SEM of the unmodified particles and TGA of both samples were undertaken here at the University of Edinburgh.

Scanning electron microscopy analysis was carried out on the unmodified ZIF-8 sample. Figure 5.2 shows a summary of the observed images on a increasing scale. The large white crystalline structures are agglomerated ZIF-8 particles. At high magnification the individual ZIF-8 nanoparticles can be observed within these crystals. In the two highest magnification images (the bottom two) discrete particles are observed (the duller greyer area). This demonstrates the tendency of the nanoparticles to agglomerate into a variety of cluster sizes from sub-micron sized to several microns containing thousands of particles.

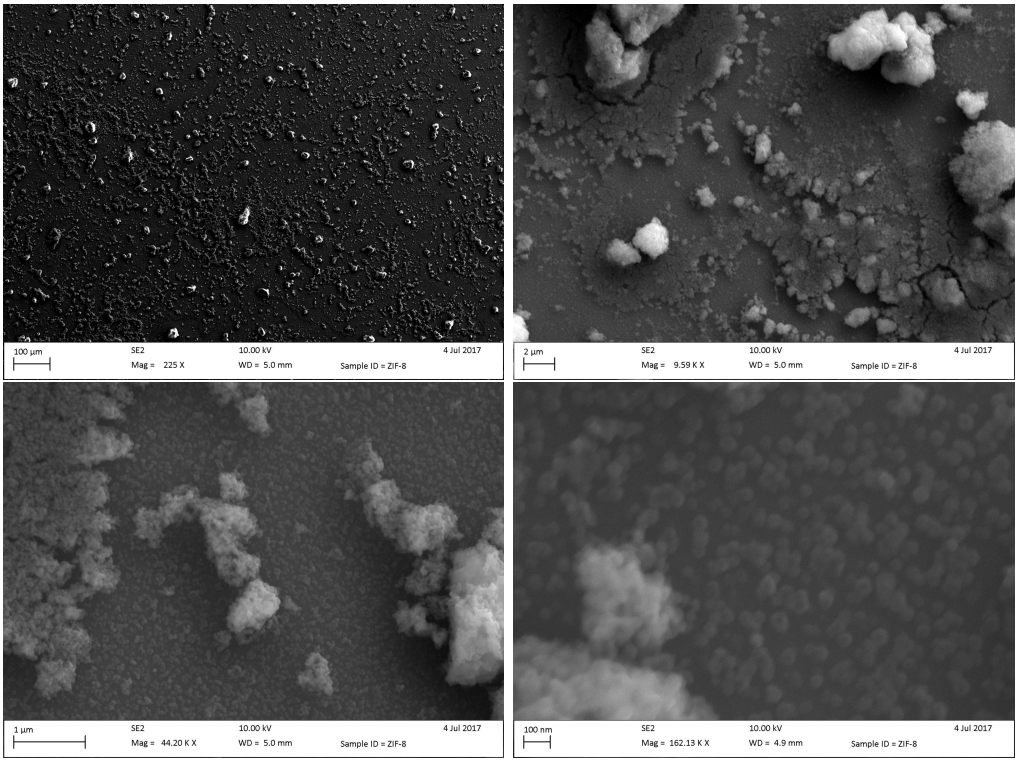

Figure 5.2: Images of nanoscale ZIF-8 particles treated with ultrasound for 48 hours.

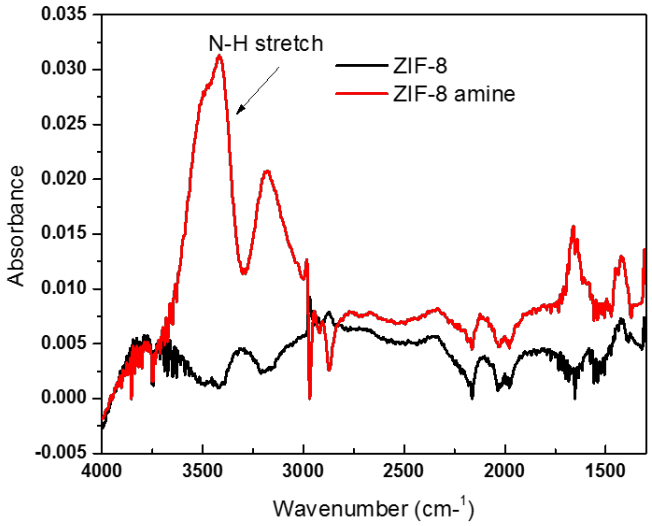

Figure 5.3: FTIR spectra of the modified ZIF-8 showing the peaks associated by the uptake of amine groups.

The uptake of ethylenediamine (ED) was confirmed by FTIR as can be seen in figure 5.3 showing the peaks associated by the N-H bond stretch in the ED. It is expected that a coordination bond between the zinc metal centres and the ED is formed.

The results of the XRD tests can be seen in figure 5.4. Despite the discrepancy in the baselines, they share the same peaks suggesting the crystal structure remains the same after modification with ethylenediamine as was expected.

The TGA was used to investigate the adsorption of CO_2 on both ZIF-8 and ED-ZIF-8 samples as per the method elucidated in chapter 4. The mass of the ED-ZIF-8 was unstable due to unknown reasons and as such both the uptake and heats of adsorption are corrected for this loss in the mass of sample during the experiment. Figure 5.5 shows the CO_2 isotherms of both samples. Linear isotherms were observed for the unmodified ZIF-8 and an average uptake of 0.7 mmol g^{-1} at 1 bar CO_2 partial pressure which was similar to literature findings as can be seen in table 5.2.[206–208] The heat of adsorption for each step change in partial pressure was determined. The uptake at 1 bar and mean heat of adsorption for each run can be found in table 5.4. The uptake and isotherms for the ED-ZIF-8 differed between runs and the capacity observed in the second run was higher, almost as if a sample had not fully regenerated. This deviation could however be due to the unstable mass of the sample and merely be an artefact of this phenomenon.

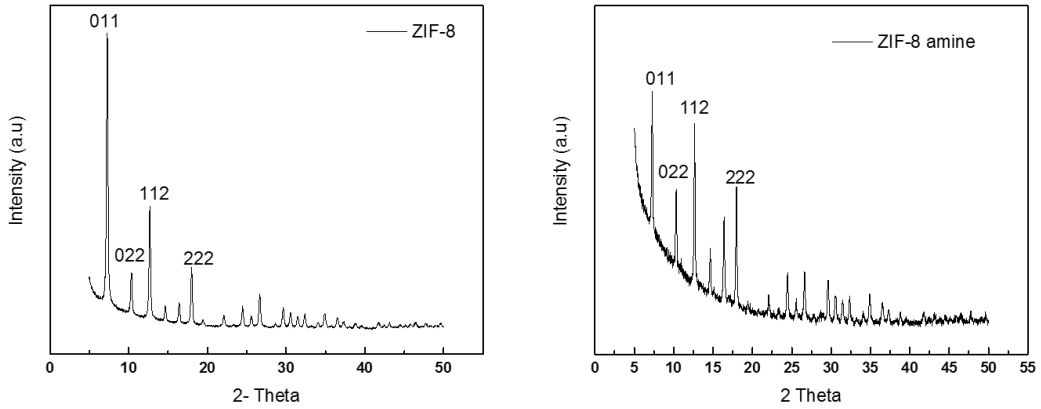

(a) ZIF-8 (b) ED-ZIF-8

Figure 5.4: XRD analysis of the ZIF-8 and ED-ZIF-8.

Table 5.4: Uptake and average heats of adsorption of CO_2 on ZIF-8 and ED-ZIF-8 at 20°C.

Sample	Run	Uptake at 1 bar (mmol g^{-1})	Mean heat of adsorption (kJ mol^{-1})
ZIF-8	1	0.71 ± 0.02	-16.7 ± 0.8
	2	0.70 ± 0.02	-17.2 ± 0.9
ED-ZIF-8	1	0.37 ± 0.09	-12.8 ± 2.0
	2	0.54 ± 0.07	-12.5 ± 0.9

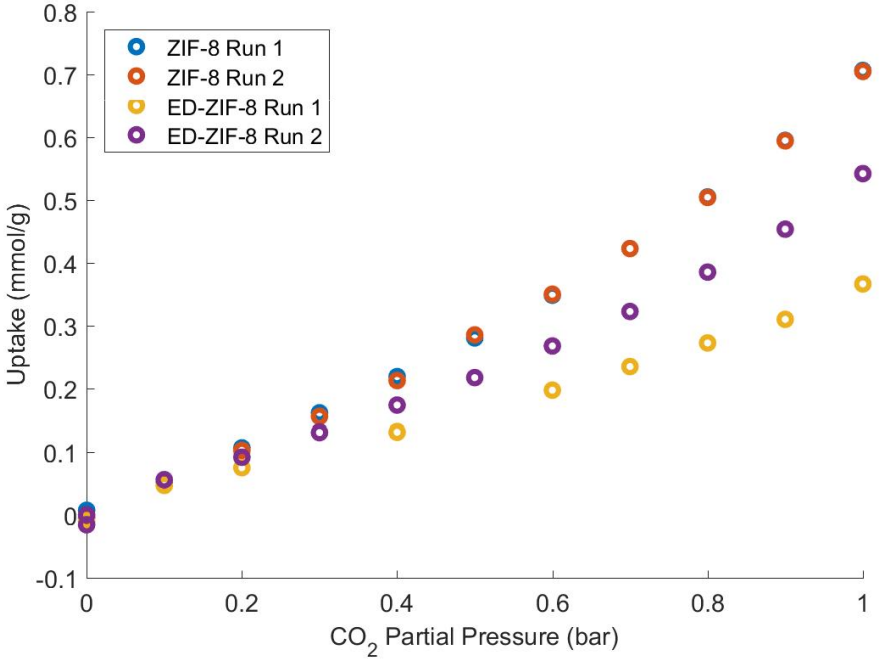

Figure 5.5: CO_2 isotherms of CO_2 on ZIF-8 and ED-ZIF-8 at 20°C

5.3 Results

5.3.1 ZIF-8-PEBAX Membranes

The unmodified ZIF-8 was initially used to create MMMs with PEBAX with loadings by weight in roughly 2 wt.% increments of approximately 1, 3, 5 and 7 wt.%. Following this MMMs with intermediate loadings of approximately 2, 4 and 6 wt.% were produced from a second batch of ZIF-8 produced via an identical synthesis procedure. Table 5.5 shows a full list of membranes that were produced.

Table 5.5: List of details of the unmodified ZIF-8-PEBAX MMMs produced.

Loading (wt.%)	Mass of PEBAX (g)	Mass of ZIF-8 (g)	Thickness (µm)
1.1	1.0053	0.0112	21
2.2[1]	1.0044	0.0222	25
3.0	1.0066	0.0306	16
4.4[1]	1.0028	0.0464	46
5.1	2.0047	0.1076	30
5.6[1]	1.0322	0.0618	45
7.0	1.0185	0.0762	47

[1] Produced with the second batch of ZIF-8.

There is also a moderate positive correlation between the loading and the thickness of the resulting membranes (Pearson correlation coefficient = 0.80) suggesting that the presence of solids in the mixture could play a role in the thickness of the membranes, potentially via causing an increase in viscosity.

Figure 5.6 shows a photo of the first 3 ZIF-8-PEBAX MMMs produced ranging from 3 to 7 wt.% loadings. Under close observation of this image striations or repeating patterns can be seen that are more pronounced at higher loadings. Large clusters, visible with the naked eye, were observed in the 7.0 wt.% membranes. These can clearly be seen in figure 5.7 which shows images of the 7.0 wt.% ZIF-8-PEBAX MMMs taken with both a DSLR (digital single-lens reflex) camera and a low-power optical microscope which highlighted the linearity and order present in the macroscopic scale distribution of these particles.

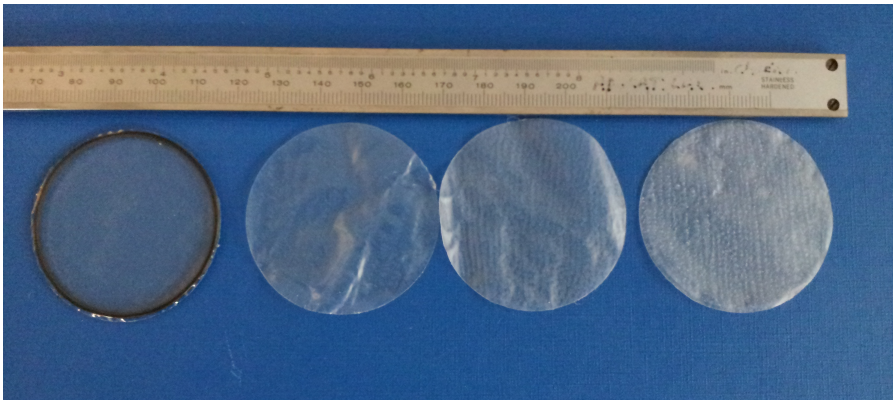

Figure 5.6: Neat PEBAX, and 3.0, 5.1 and 7.0 wt.% ZIF-8-PEBAX MMMs (left to right).

SEM Analysis

The images in this section were taken with two different instruments as discussed in section 4.3. The first 4 membranes produced, 1.1, 3.0, 5.1 and 7.0 wt.%, were imaged using the School of Biology SEM facilities while the rest imaged using the JMTC SEM facilities. Details of these instruments and the settings used to take them can be found in table 4.2. As per all the SEM analysis, further images can be found in the electronic material.

Figure 5.8 shows a cross section of neat PEBAX for reference. The left image was taken with a secondary electron detector which gives a clear image. The vertical striations in this image are artefacts from being cut as opposed to being snapped in liquid nitrogen. The image on the right was taken with an ESB detector which gives high contrast images, highlighting differences in elemental composition. The lack of contrast in the cross section is representative for a pristine membrane.

Figure 5.9 shows representative cross-sections of the mixed matrix membranes produced from PEBAX and ZIF-8. In figure 5.9a, the 1.1 wt.% membrane looks similar to that of neat PEBAX. For the most part the membrane is smooth and nothing on the scale of the ZIF-8 particles can be observed. The raised, slightly lighter sections are deformations from the cracking of the membrane. In figure 5.9c in the 3.0 wt.% membranes, small white dots in the left image can be seen. These are very possibly nanoparticles, however the limit of the resolution was similar to that of the scale of the particles. Thus it is impossible to say with certainty that these were the ZIF-8 nanoparticles. In the right image of the 3 wt.% membranes, what appears to be an agglomeration of these particles was observed. It should be noticed this was the only potential cluster seen, but beyond that no other evidence of clusters in the 3 wt.% sample was found.

In the 5.1 wt.% membranes (figure 5.9c) multiple clusters were observed, all of

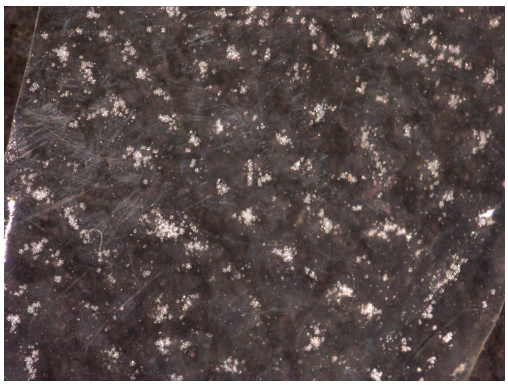

(a)

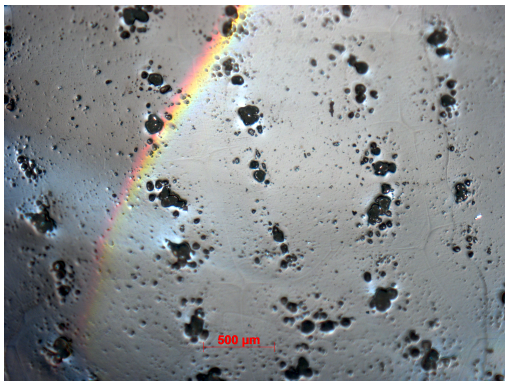

(b)

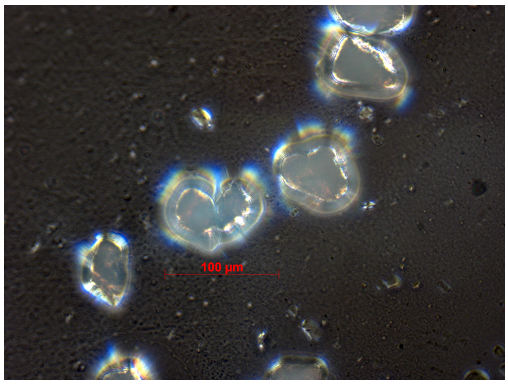

(c)

Figure 5.7: Images of 7.0 wt.% ZIF-8 MMMs taken with (a) a DSLR with a 200mm lens, and (b) and (c) an optical microscope at 2.5x and 20x magnification respectively.

the scale of several microns. These are the large light structures in the images. Likewise in the 7.0 wt.% membranes agglomerations were also observed but they were noticeably more prevalent and larger. Similar to the 3 wt.% membranes, what could be well distributed particles were seen throughout the bulk of the membrane.

Some surface images were also taken using the School of Biology SEM facilities shown in figure 5.10. The neat PEBAX showed a relatively uniform surface with some slight irregularities, most likely contamination. Similar to the cross sections the 1.1 wt.% showed minimal differences from the neat PEBAX. There were however two notable features that differed from the neat PEBAX surface in both the 3.0 and 7.0 wt.% samples. In these lighter, circular regions were seen. When viewed under higher magnification these appeared to be hair-like structures protruding from the surface. They are much too large to be polymer chains themselves, nor are they particulate as is the ZIF-8. It is not clear what they were or what caused them, the circular drop like pattern suggests some form of contamination during the casting stage.

To investigate the morphology of the clusters in the higher weight percentage membranes the cross-sections were imaged using the JMTC SEM facilities with the aid of an analytical technician present. A summary of these images are seen in figure 5.11 showing the cross sections of the 5.1, 7.0 and 10 wt.% membranes.

Figure 5.11a shows the 5.1 wt.% membranes: well dispersed particles were clearly seen throughout the membrane. These are the small white dots seen throughout. In these membranes no clusters were observed despite their noticeable presence when imaged with the other SEM (in figure 5.9c) suggesting the clusters were only few in this sample.

In the 7.0 wt.% membranes, seen in figures 5.11b and 5.11c, agglomerations, again on the scale of microns, were rife within the membrane and could be seen with incredible detail. The first two images highlight the scale of the clusters - showing the same large white object in the centre of the membrane. With the ESB detector in the second image (top right) a smaller cluster can be seen on the left (highlighted). Similar clusters can be seen in the third (bottom left) image. In the final image a cluster can be seen in the lower portion of the image interestingly surrounded by well dispersed particles. Overleaf in figure 5.11c this same cluster can be seen under much higher magnification. The cluster was clearly made up of smaller ZIF-8 particles. Voids were clearly visible within the cluster, although at the interface between the polymer and the cluster, good adhesion was present. The top right image of the same figure shows a similar scenario of an agglomeration of ZIF-8 particles (the white cube-like shape on the right) surrounded by otherwise well distributed particles. The final images highlight how excluding the agglomerations the ZIF-8 particles were well homogeneously distributed throughout the remainder

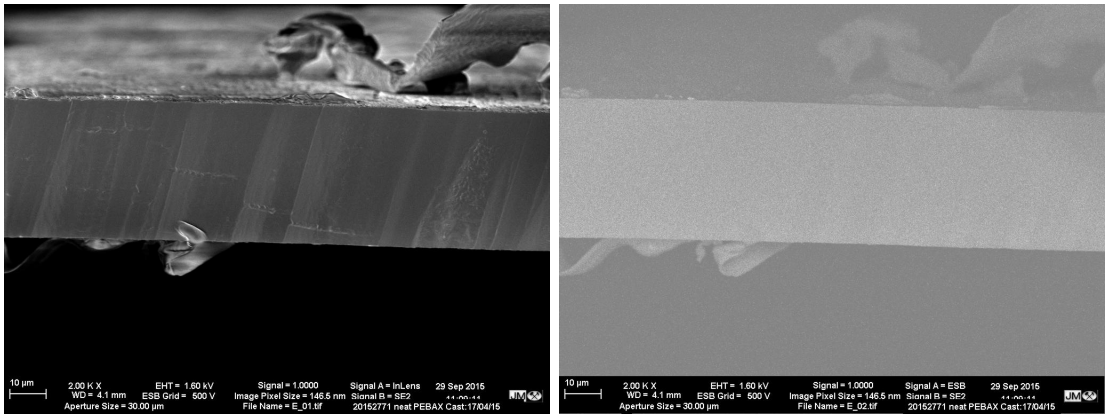

Figure 5.8: Neat PEBAX taken with JMTC SEM facilities. The left image was taken with an inlens secondary electron detector; the right image was taken with an energy selective backscatter (ESB) detector.

of the membrane.

In the 10 wt.% membrane (figure 5.11d) similar clusters were observed. Shown here is the edge of the membrane formed when casting. At the far right of the first two images a cluster can be seen. Interestingly, seen in the third and forth images, parallel striations of nanoparticles were seen just beyond the edge of a cluster, parallel to its edge, which almost looked as if the particles were flowing at one point.

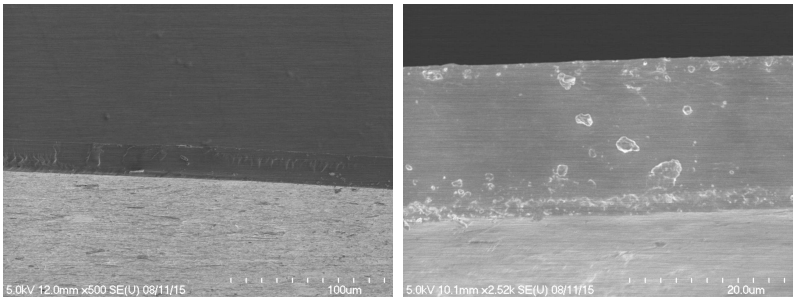

(a) 1.1 wt.%

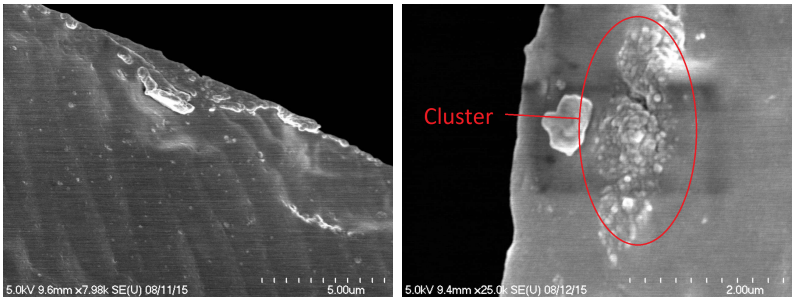

(b) 3.0 wt.%

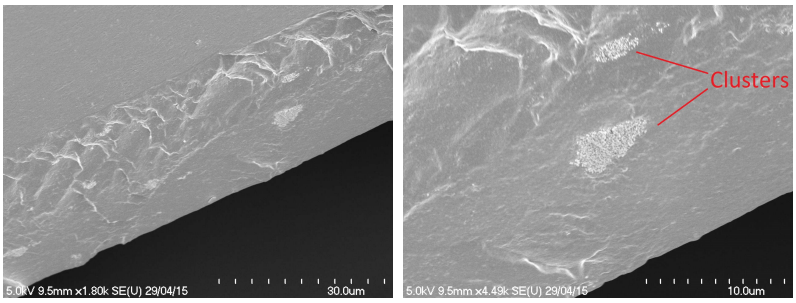

(c) 5.1 wt.%

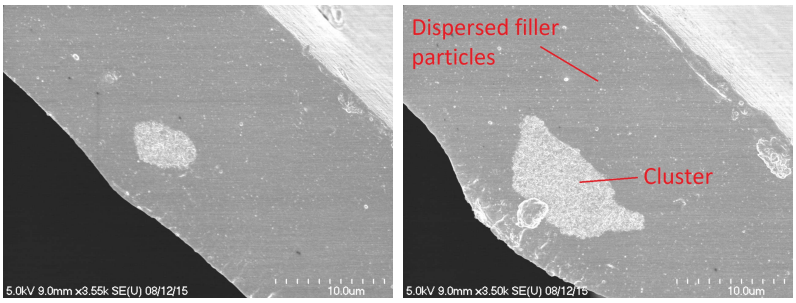

(d) 7.0 wt.%

Figure 5.9: Cross-section of ZIF-8-PEBAX membranes taken with the School of Biology SEM facilities.

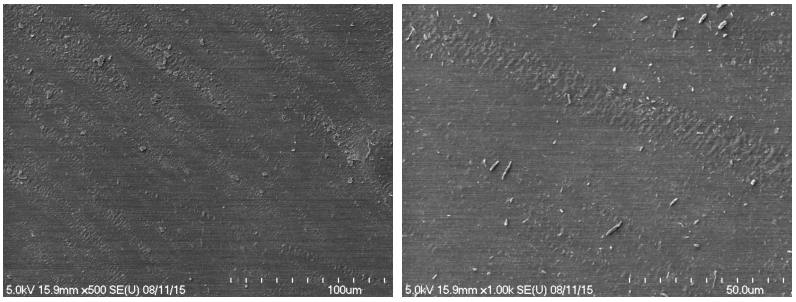

(a) Surface of Neat PEBAX

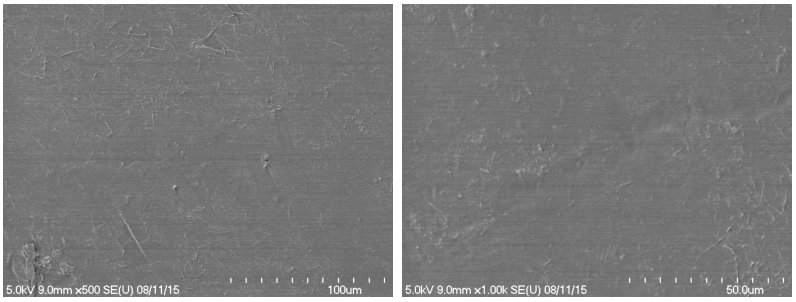

(b) Surface of 1.1 wt.% ZIF-8

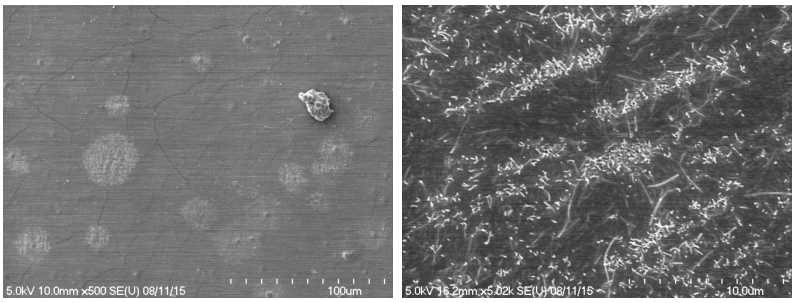

(c) Surface of 3.0 wt.% ZIF-8

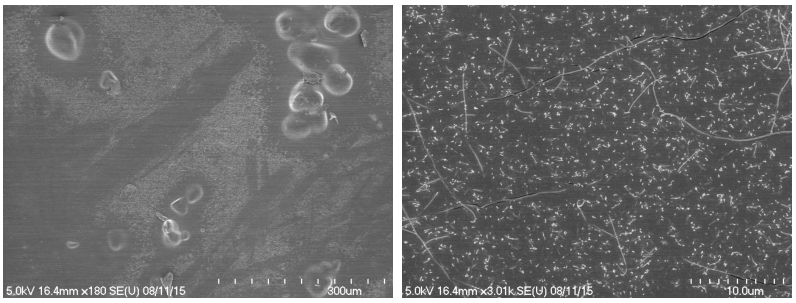

(d) Surface of 7.0 wt.% ZIF-8

Figure 5.10: Surface images of ZIF-8 membranes.

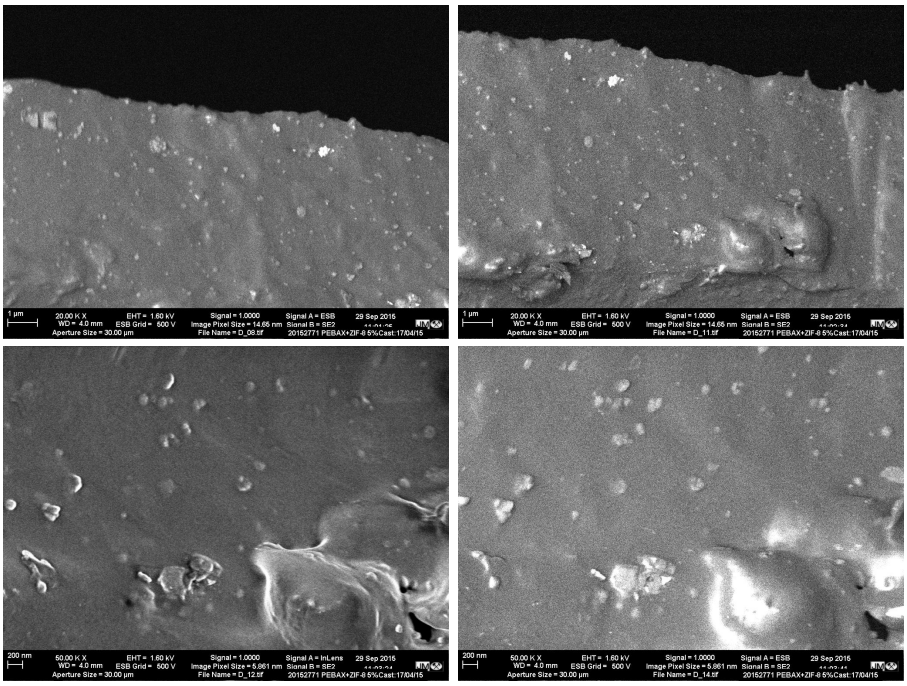

(a) 5.1 wt.%

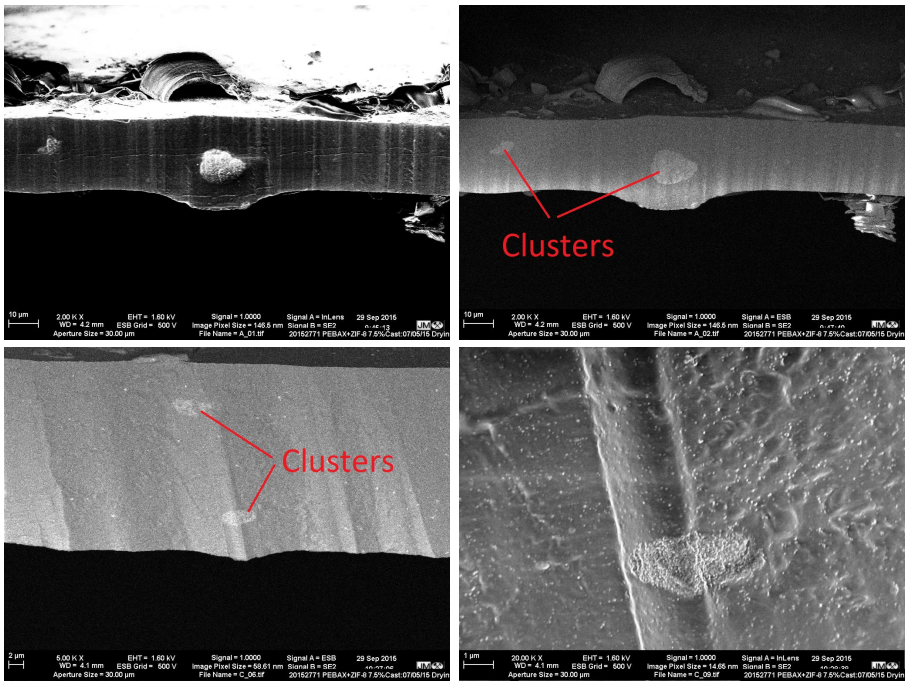

(b) 7.0 wt.%

Figure 5.11: SEM of ZIF-8 membranes taken with the SEM at JMTC analytical facilities.

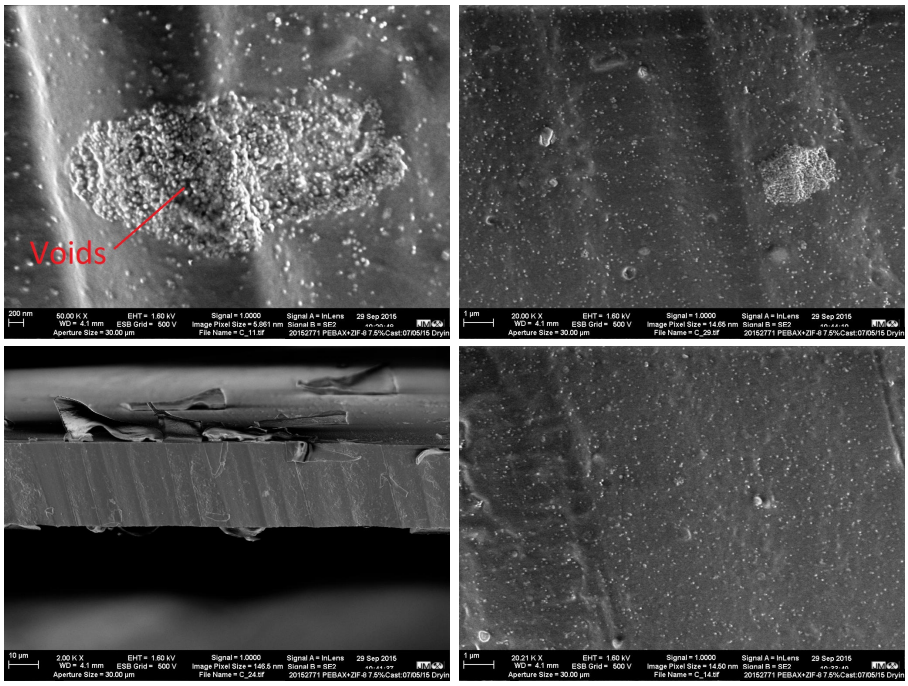

(c) 7.0 wt.% (cont.)

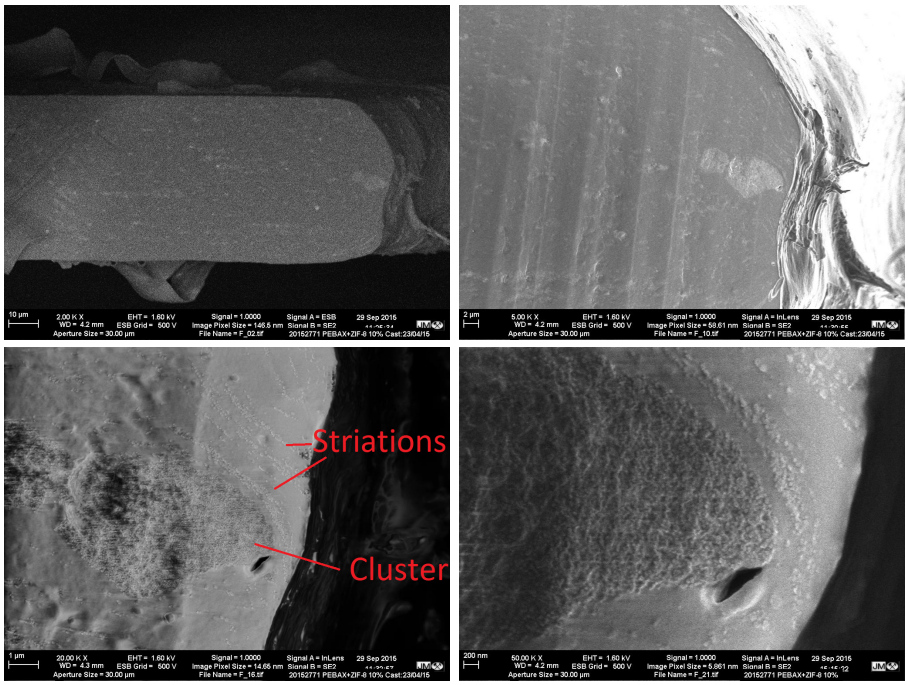

(d) 10 wt.%

Figure 5.11: SEM of ZIF-8 membranes taken with the SEM at JMTC analytical facilities.

Time-lag Permeation Results

Time-lag experiments were run on all the samples produced bar ones that possessed insufficient mechanical strength. Experiments were often carried out in duplicate or triplicate to confirm reproducibility. The repeat runs showed that the experiments were highly reproducible. Due to the aforementioned effects in the pressure signal previously discussed in section 4.2.3 some experiments are not presented with diffusivity data. Figure 5.12 shows some of the normalized raw data of the experiments that displayed the expected theoretical pressure trend but a full presentation of the raw experimental data is superfluous to elucidate the main features of the data.

A complete list of the successful permeation tests is presented in table 5.6. Figure 5.13 shows a summary of the time-lag permeation tests. Figure 5.13a shows the averaged results of the permeability coefficients for helium, nitrogen and carbon dioxide. It can be seen that the permeability coefficient for each gas roughly follow the same trend, however there were slight differences in behaviour. For all of the gases the trend above and below 5 wt.% loading is markedly different. Up to 5 wt.% all the gases only show slight deviation, up to 20 % difference, from neat PEBAX, but above this large increases in permeability of over 200 % are seen. The carbon dioxide permeability coefficients shown are slightly elevated over neat PEBAX in the 1.1 and 2.2 wt.% membranes, but the 3.0 and 4.4 wt.% membranes show permeabilities similar to that of the neat PEBAX. In the same range however the nitrogen permeability coefficient decreases steadily with increased loading, lending to the idea that the ZIF-8 could hinder the transport of nitrogen in the presence of carbon dioxide. Above 5 wt.% the permeability coefficients of all three gases rise remarkably.

Figure 5.13b shows the permeability coefficients of CO_2 and N_2 normalised to the values of neat PEBAX. In this plot the decrease in N_2 permeability up to 5 wt.% loadings is much clearer, showing a minimum nearly 40 % lower than the pristine PEBAX value. While the trends of both gases are similar, the relative CO_2 permeabilities are all, except for the 7.5 wt.% sample, higher than that of N_2 which relates to an improvement in selectivity and the ZIF-8 clearly favouring the transport of carbon dioxide.

Figure 5.13c shows the same CO_2 permeability coefficients but plotted with the selectivity. The effect of the decrease in nitrogen permeability in membranes below 4 wt.% loadings results in modest increases in selectivity. The low nitrogen permeability coefficient found for the 4.4 wt.% sample equates to an ideal selectivity of well over 100. Above 5 wt.% the trend in selectivity is less clear. The 5.1 and 5.6 wt.% samples shown have an ideal selectivity closer to the low loading samples. At the highest loading tested, 7.5 wt.%, the selectivity is virtually identical to that of neat PEBAX.

The large increases in permeability coefficients and loss of selectivity above 5wt.% loadings overlap with the onset of agglomerations within the particles. It is highly likely this loss of selectivity can be attributed to voids within and around the clusters.

The results are plotted on a Robeson plot in figure 5.14. A clear trend is not immediately clear on these axes. The arrows give a rough indication as to what could be considered showing an increase in selectivity up to a maximum and then a subsequent decrease coinciding with the occurrence of voids. Interestingly the 4.4 wt.% is above the upper bound.

Table 5.6: Results of the time-lag experiments for the ZIF-8-PEBAX membranes. All experiments were run with 1 bar upstream pressure at 30 °C except where noted.

Loading (wt.%)	Permeability Coefficient (Barrer)			Diffusivity Coefficient ($\times 10^{-8}$ cm^2 s^{-1})		
	He	N_2	CO_2	He	N_2	CO_2
0		2.0 ± 0.2	80 ± 10		17 ± 3	15 ± 2
		1.9 ± 0.2	80 ± 10		17 ± 3	17 ± 2
1.1	7.1 ± 0.8	1.8 ± 0.2	100 ± 10	13 ± 3	11 ± 5	11 ± 2
	6.8 ± 0.7	1.8 ± 0.2	90 ± 10	-	-	12 ± 3
2.2		1.6 ± 0.2	90 ± 10		-	12 ± 2
			100 ± 10			12 ± 4
3.0	5.8 ± 0.6	1.6 ± 0.2	80 ± 10	9 ± 2	-	6 ± 2
	5.8 ± 0.6	1.6 ± 0.2	90 ± 10	6 ± 2	-	7 ± 1
4.4		1.3 ± 0.1[2]	80 ± 10[2]		8 ± 4[2]	16 ± 3[2]
		0.2 ± 0.1	90 ± 10			29 ± 6
			90 ± 10			31 ± 6
5.1	8.2 ± 0.9	2.4 ± 0.3	130 ± 10	-	-	23 ± 5
	9 ± 1	2.5 ± 0.3	130 ± 10	140 ± 30	-	23 ± 5
		2.4 ± 0.3	130 ± 10		-	22 ± 4
5.6		2.0 ± 0.3[1]	140 ± 20		-	38 ± 8
7.0	16 ± 2	5.9 ± 0.6	210 ± 20	50 ± 20	150 ± 60	130 ± 20
	18 ± 2	4.8 ± 0.5	230 ± 20	50 ± 30	100 ± 40	60 ± 10

[1] Run at 25 °C.
[2] Run at 28 °C.
- Dashed denote where an experiment was run but a value was not determined.

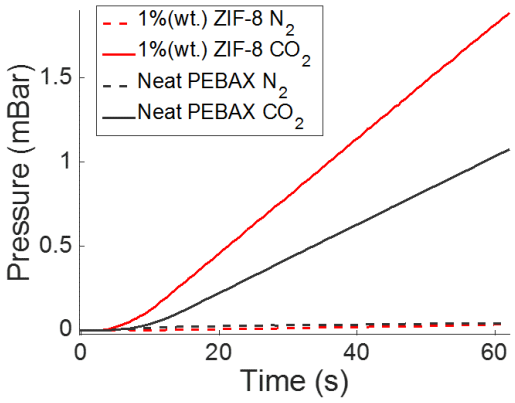

(a)

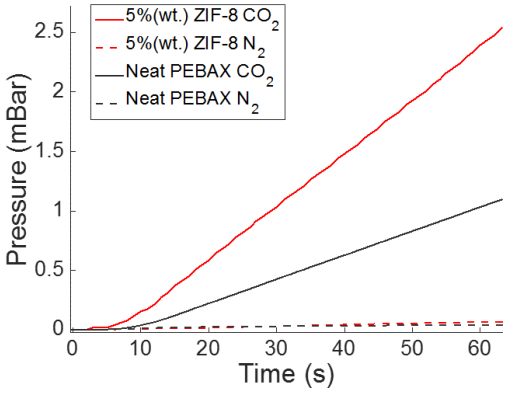

(b)

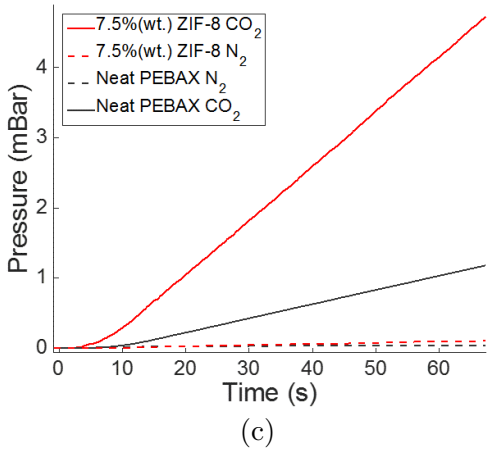

(c)

Figure 5.12: Normalised time-lag results for 1.1, 5.1, and 7.0 wt.% loadings.

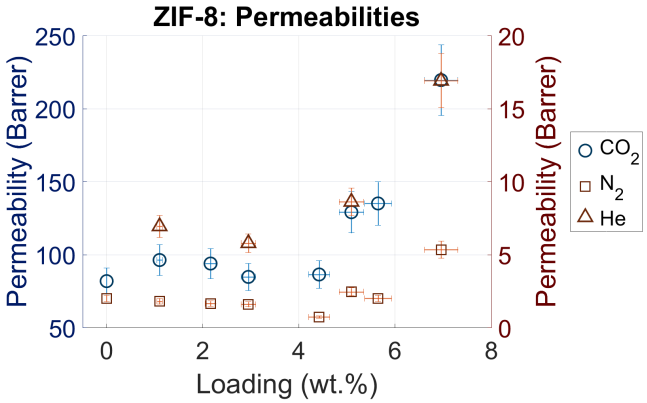

(a) CO_2, N_2 and He Permeabilities.

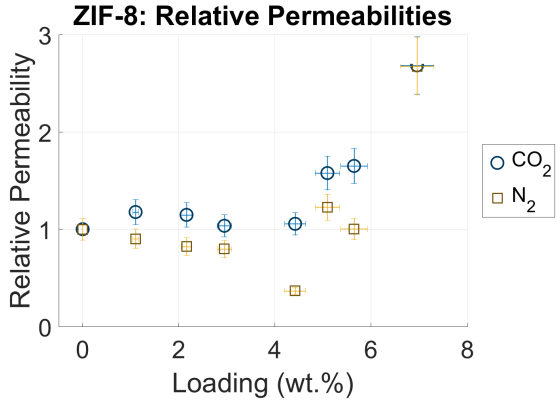

(b) Permeabilities of CO_2 and N_2 relative to that of neat PEBAX.

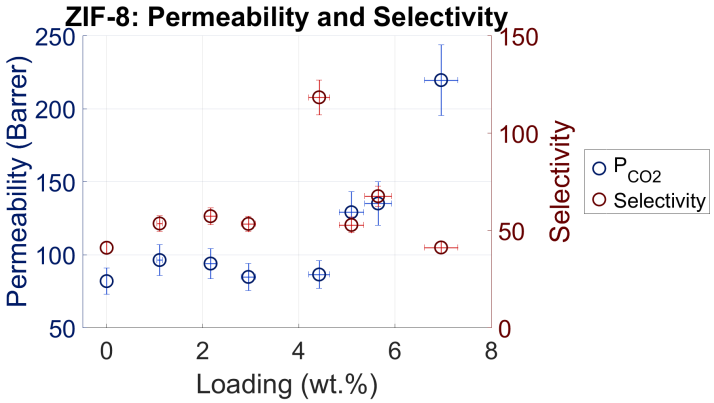

(c) CO_2 permeability and ideal CO_2/N_2 selectivity.

Figure 5.13: Summarised results of the time-lag experiments.

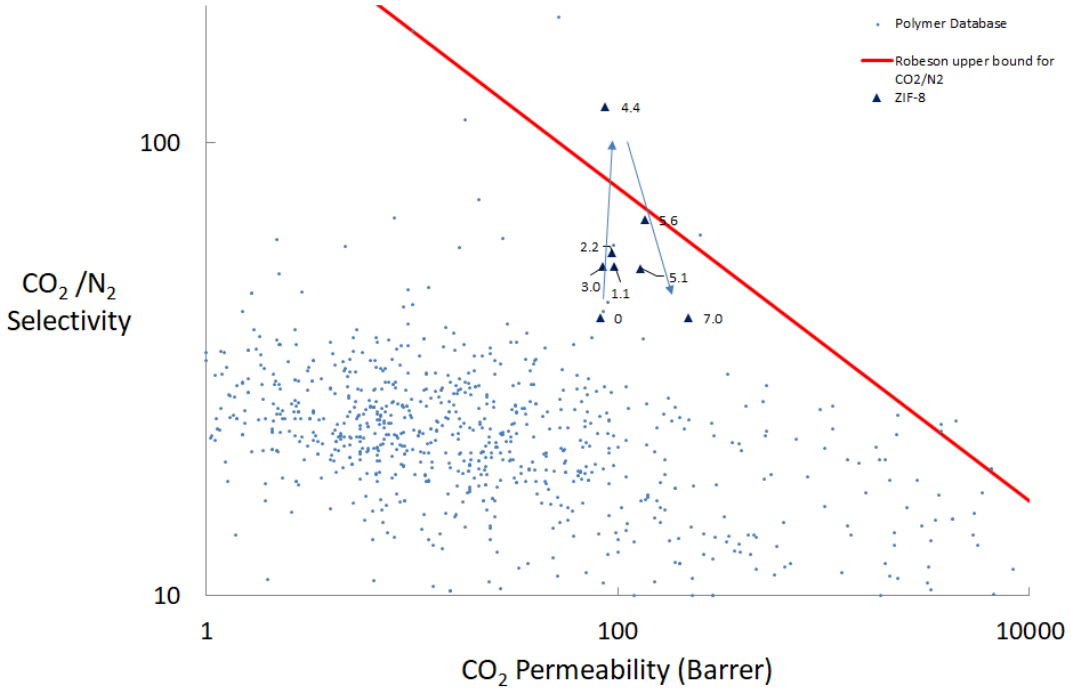

Figure 5.14: The experimental permeation test data for ZIF-8-PEBAX membranes. The data labels are the loading by weight of the filler in each membrane. The blue arrows show a rough trend of the data in which the selectivity greatly increases and then falls at higher loadings.

Comparison of ZIF-8 Experimental Data with Ideal Models

The CO_2 and N_2 permeability coefficients were compared with the previous predictions of the composite material using the ideal Maxwell and Bruggeman models in section5.1. Figure 5.15 shows the individual gas predictions plotted with the experimental data. In figure 5.15a, the experimental CO_2 permeability coefficients below 5 wt.% are similar to that of the ideal models suggesting an 'ideal' morphology with minimal defects. Above 5 wt.% the experimental data clearly deviates from the models. This makes sense given that both agglomerations and voids were seen in the SEM images differing from the morphology of the ideal models.

The experimental nitrogen coefficients clearly deviate from the predicted properties as is seen in figure 5.15b. The models both predict a small increase in permeability but a steady decrease is observed. A further limiting case is plotted to represent a nitrogen permeability coefficient of zero in the discrete filler phase. Even when modelling the filler as totally impermeable to nitrogen, this decrease cannot be accounted for.

At the range of loadings used, both models only predict slight deviations in composite permeability for the three separate cases, in spite of the order of magnitude difference between the estimated CO_2 permeability coefficients in ZIF-8 (510 to 20000 Barrer). This is one of the reasons why back-calculating the properties of a filler in an MMM is so challenging.

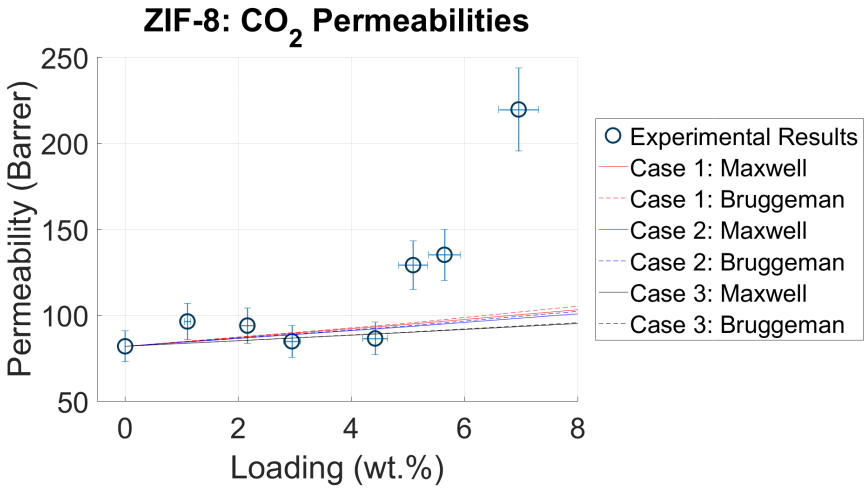

(a) CO_2

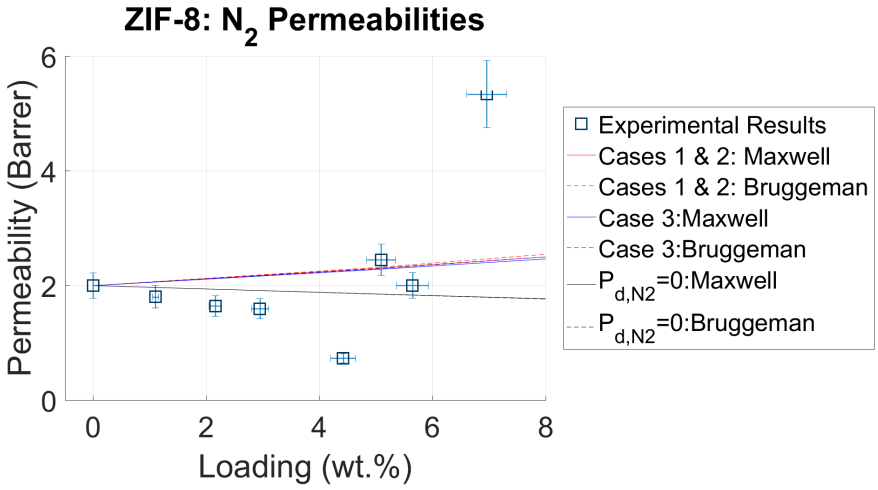

(b) N_2

Figure 5.15: Permeability coefficients of CO_2 and N_2 in ZIF-8-PEBAX MMMs with predictions using the Maxwell and Bruggeman models.

5.3.2 ED-ZIF-8-PEBAX Membranes

Four membranes were successfully produced with the modified ED-ZIF-8 sample up to loadings of 12.5 wt.% Given the limited mass of the ED-ZIF-8 available, the membrane fabrication procedure was modified slightly by reducing the mass of polymer to around 5 g and thus reducing the mass of filler material required.

Table 5.7: List of details of the ED-ZIF-8-PEBAX MMMs produced.

Loading (wt.%)	Mass of PEBAX (g)	Mass of ED-ZIF-8 (g)	Thickness (µm)
2.4	1.0116	0.02485	42
5.4	0.5810	0.03300	79
7.0	0.3665	0.02752	51
12.5	0.4985	0.07130	23

SEM Analysis

The images in this section were all taken with the School of Geosciences SEM. Images of the 2.4, 5.4, 7.0, and 12.5 wt.% ED-ZIF-8-PEBAX membranes were taken and can be found in figures 5.16 to 5.19. Similar images were taken of the same materials using the JMTC facilities, however these samples were contaminated with other substances such as gold and aluminium during sample preparation and, although similar features were seen in both images sets, some details in the JMTC set are not as clear. For conciseness only representative images are presented here and further images can be found in the additional electronic material.

Figure 5.16 shows images of the 2.4 wt.% ED-ZIF-8-PEBAX membranes. As can be seen from this set of images clusters were seen throughout the membranes, although interestingly the clusters seemed to exist close to one another with some areas showing multiple agglomerations and some areas very few. The first image shows a single small cluster, which can be seen at higher magnification in the second image. In this second image the particles show good interaction with the polymer phase. The third image (numbered from left to right, then top to bottom) highlights the cracks that were observed in parts of the membrane. These cracks were only seen in some sections of the membrane and it is not clear what led to them. The fourth image (right, middle) highlights the prevalence of clusters that were observed in some areas. In this image, no less than eight clusters can be seen in close proximity to one another. A large void in the form of the crack can be

seen within one of the clusters near to the upper surface of the membrane. In the fifth image (bottom left) the discrete filler nanoparticles are clearly observed within the agglomeration. Similar to the unmodified ZIF-8 PEBAX membranes in which clusters were seen, there are well dispersed filler particles in the bulk polymer phase immediately outwith the cluster. In the sixth image (bottom right) three clusters (labelled) are further observed in close proximity to one another.

Figure 5.17 shows representative images of the 5.4 wt.% ED-ZIF-8-PEBAX mixed matrix membranes. The two left images show several clusters throughout the membrane of up to 10 µm in diameter. The right images show insets of each of these images. In the top right image distinct cracks can be seen within the cluster. At the edge of the cluster at the interface between phases, there are no voids demonstrating good interaction with the polymer phase. The bottom left image shows in detail the scale of the clusters.

Figure 5.18 shows the 7.0 wt.% membranes. Strata in the polymer structure running perpendicular to the surface in one half of the membrane along with several small voids, separate from any clusters, were seen. These strata can be seen in the top two images. The bottom image shows the good interaction between the nanoparticles and the polymer. Several clusters were also observed but showed significantly higher voidage and were much more loosely packed than in the 2.4 and 5.4 wt.% ED-ZIF-8 membranes. One of these clusters can be seen in the bottom right image in this figure. Strangely the opposite surface from the agglomeration was raised.

Figure 5.19 shows the phenomenon present in the 12.5 wt.% ED-ZIF-8-PEBAX sample. Similar to the other samples both well dispersed particles with good polymer-filler adhesion as well as numerous large clusters were observed. The top four images show the well dispersed nanoparticles with a few clusters present which was representative of a large portion of the membrane. The fifth image (left, third from top) shows a cluster at the surface in which good adhesion between the phases is observed. The sixth image shows a large ellipsoid-shaped agglomeration with significant voids within it. The final two images show an area found containing huge clusters, one of which penetrated half the thickness of the membrane. Significant cracks could be seen around the agglomerations which are clearer in the bottom right image at higher magnification.

In general, the membranes were of noticeably lower quality than the unmodified ZIF-8-PEBAX membranes: cracks were seen in part of the 2.4 wt.% membranes; the 5.4 wt.% membranes possessed many clusters with cracks within them; and in the 7.0 wt.% membranes, strange strata in the polymer structure were observed. In the 12.5 wt.% membrane, agglomerations came close to penetrating the entire thickness of the membrane. The agglomerations in question were only slightly

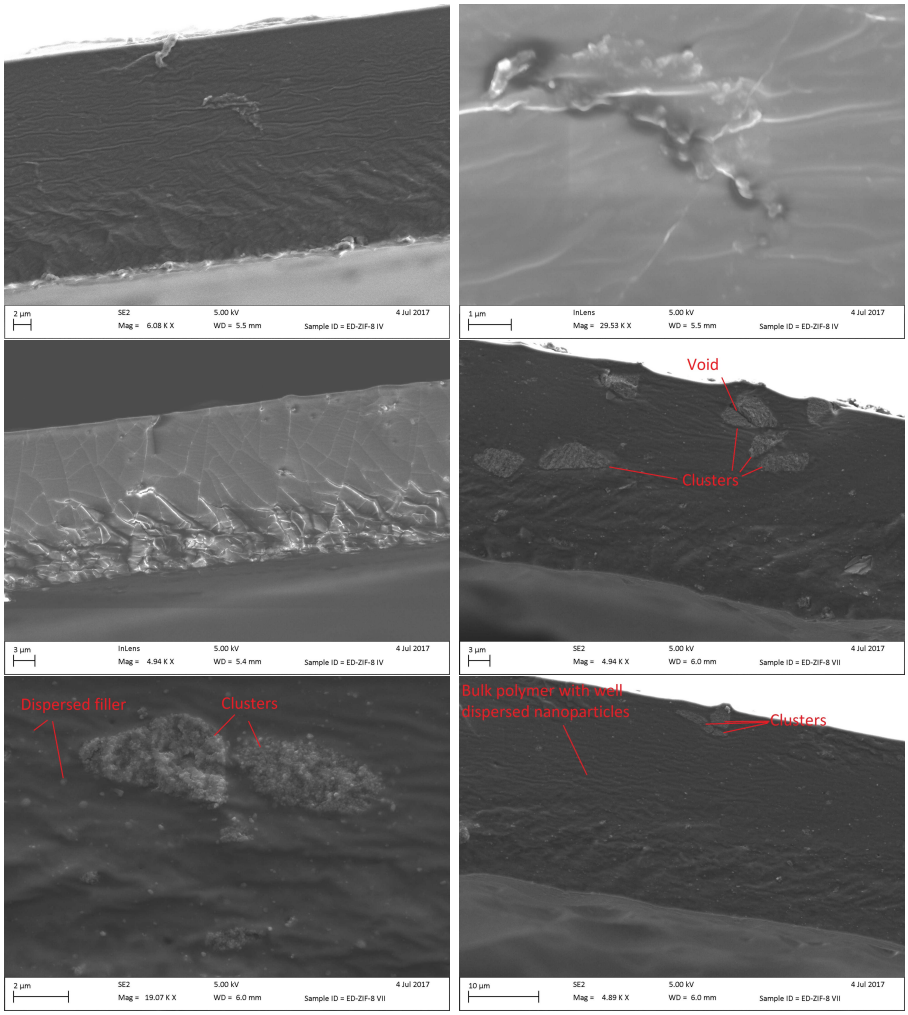

Figure 5.16: 2.4 wt.% ED-ZIF-8-PEBAX MMMs

larger than typically seen but the 12.5 wt.% membrane was by far the thinnest of the ED-ZIF-8 membranes, measured at 23 µm with the micrometer, and 12 µm using the SEM. This discrepancy in thickness is discussed later in the chapter.

Agglomerations were seen in all of the ED-ZIF-8-PEBAX samples. The clusters were highly numerous, much more so than in the unmodified ZIF-8-PEBAX samples. In the 5.4, 6.9, and 12.5 wt.% membranes voids and cracks were clear in, and in the immediate vicinity of, the clusters, however the majority of the clusters seen showed good interaction with the polymer. Similar to in the unmodified ZIF-8 membranes the clusters were surrounded by well dispersed nanoparticles which also displayed good adhesion with the polymer.

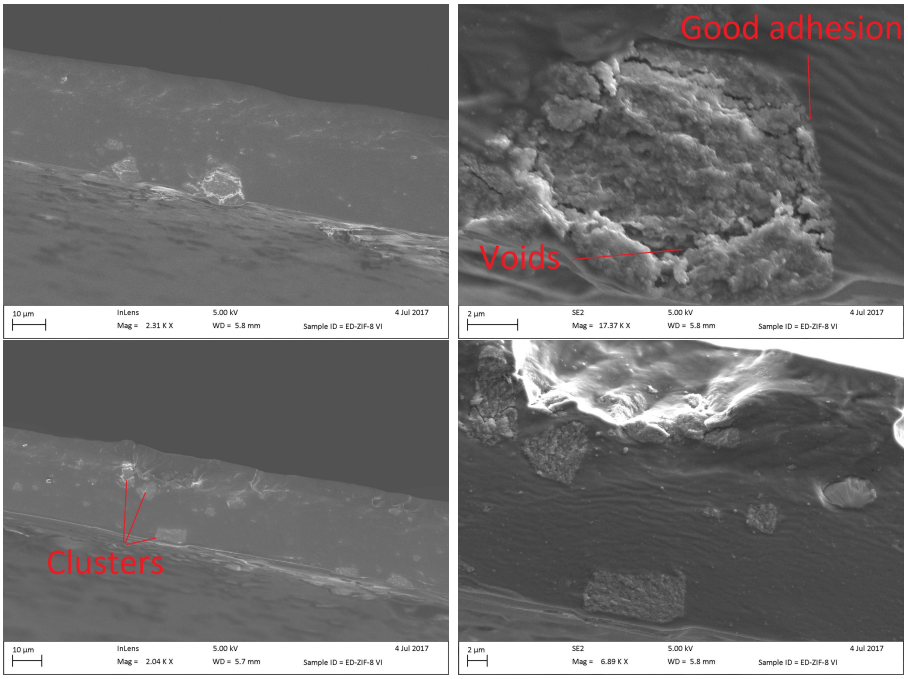

Figure 5.17: 5.4 wt.% ED-ZIF-8-PEBAX MMMs.

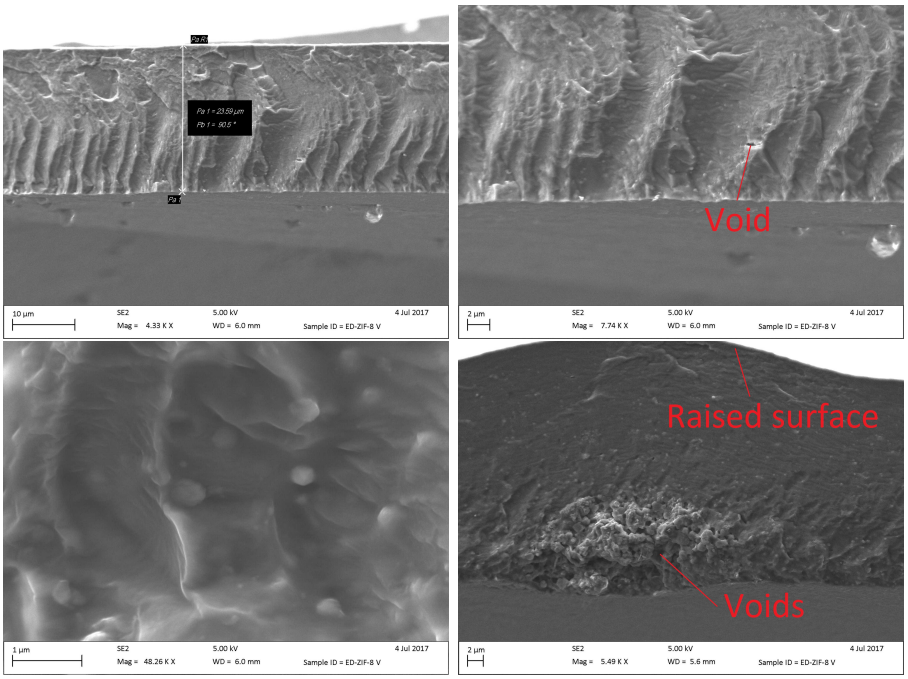

Figure 5.18: 7.0 wt.% ED-ZIF-8-PEBAX MMMs.

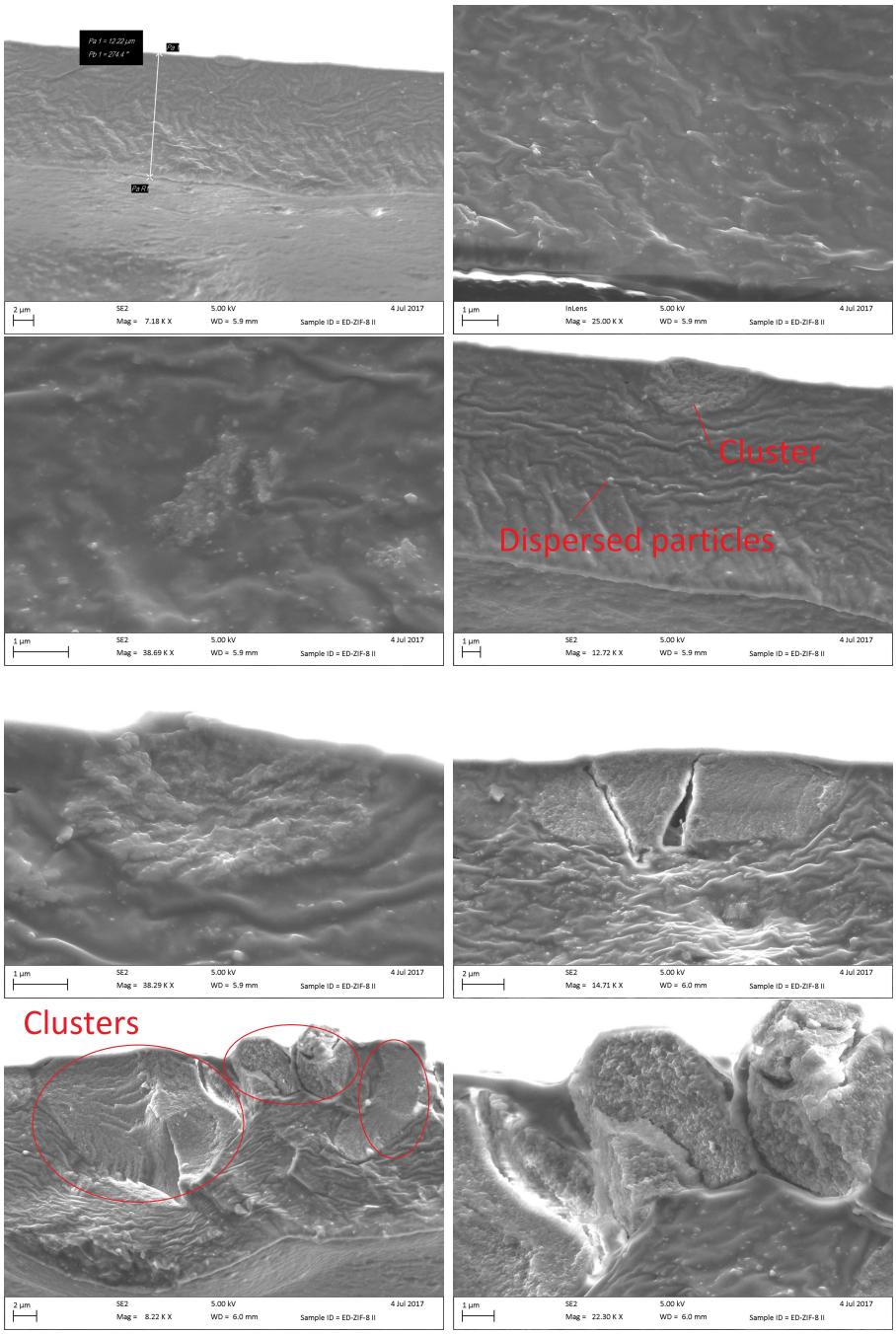

Figure 5.19: 12.5 wt.% ED-ZIF-8-PEBAX MMMs.

Time-lag Permeation Results

Time lag experiments were successfully run on all of the ED-ZIF-8 PEBAX samples produced. Table 5.8 contains a full list of all of the permeation tests. As discussed in section 4.2.3 several of the results are presented without diffusivity data. Figure 5.20 shows the summarised results of these permeation experiments for the ED-ZIF-8-PEBAX membranes. It should be noted due to the extremely high permeability and low selectivity of the 12.5 wt.% sample, it was deemed to be effectively non-selective and omitted from the plots.

Table 5.8: Results of the time-lag experiments for the ED-ZIF-8-PEBAX membranes. All experiments were run with 1 bar upstream pressure at 25 °C.

Loading (wt.%)	Permeability Coefficient (Barrer)		Diffusivity Coefficient ($\times 10^{-8}$ cm^2 s^{-1})	
	N_2	CO_2	N_2	CO_2
0	2.0 ± 0.2	80 ± 10	17 ± 3	15 ± 2
	1.9 ± 0.2	80 ± 10	17 ± 3	17 ± 2
2.4	5.5 ± 0.9	160 ± 20	-	150 ± 20
	4.3 ± 0.8	150 ± 20	-	170 ± 20
5.3	12 ± 1	250 ± 30	-	360 ± 40
7.0	61 ± 7	230 ± 30	-	130 ± 10
	58 ± 6	220 ± 20	400 ± 100	200 ± 20
12.5	700 ± 80	860 ± 80	260 ± 80	-
	660 ± 70	-	780 ± 70	

Figure 5.20a shows the average permeability coefficients of carbon dioxide and nitrogen for neat PEBAX and the 2.4, 4.4 and 7.0 wt.% samples. All three samples show much higher permeabilities compared with neat PEBAX. The general trend is that an increased loading results in increased permeabilities of both gases. The 2.4 wt.% sample shows increases of 200 % and 250 % in carbon dioxide and nitrogen permeability coefficients respectively compared with neat PEBAX; the 5.3 wt.% sample shows increases of 300 and 600 %. The 7.0 wt.% membrane breaks from the trend and has a lower CO_2 permeability coefficient than the 5.3 wt.% sample.

The permeability coefficients normalised to neat PEBAX values in figure 5.20b highlight the drastic increase in the permeability coefficient of nitrogen, especially when compared to that of CO_2. This mirrors what is clearly seen in figure 5.20c: the clear decreasing selectivity as loading of ED-ZIF-8 is increased. This is highlighted

by the 12.5 wt.% omitted from the plots which had a selectivity of only 1.2 despite showing a increase in CO_2 permeability of over 1000 %.

The increases in permeability are much greater than compared with the unmodified ZIF-8 membranes. Even at the low loadings the permeabilities are greatly increased over neat PEBAX. The selectivity, however, rapidly declines with the increasing loading of filler material. This can likely be attributed to the cracks and voids seen throughout the SEM of these materials.

Plotting the gas permeation results on a Robeson plot as in figure 5.21 further emphasises the large gains in permeability and loss of selectivity as the loading of ED-ZIF-8 is incorporated into the filler matrix.

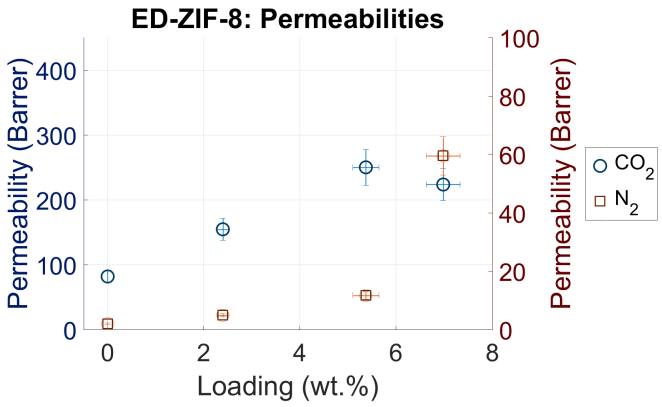

(a) CO_2 and N_2

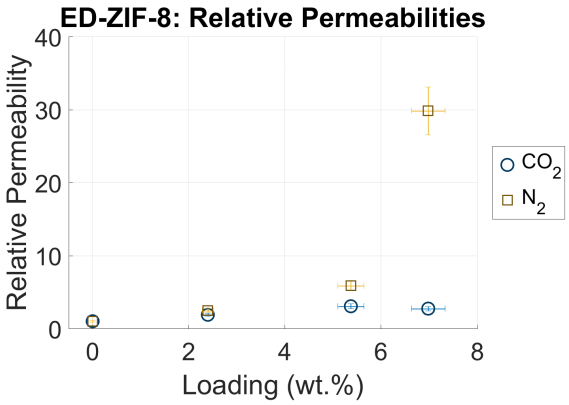

(b) Permeabilities relative to that of neat PEBAX.

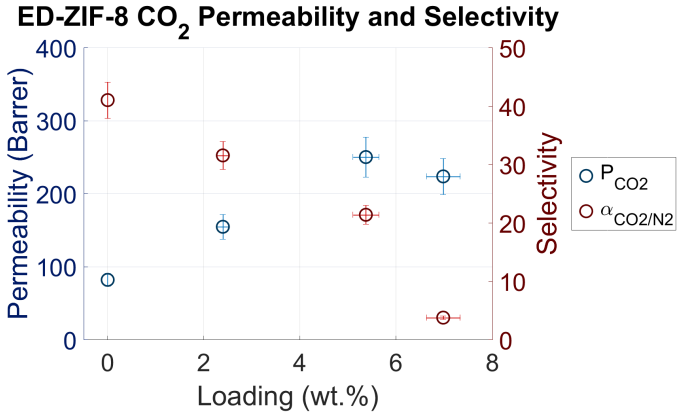

(c) CO_2 Permeability and Ideal Selectivity

Figure 5.20: Summarised results of the time-lag experiments

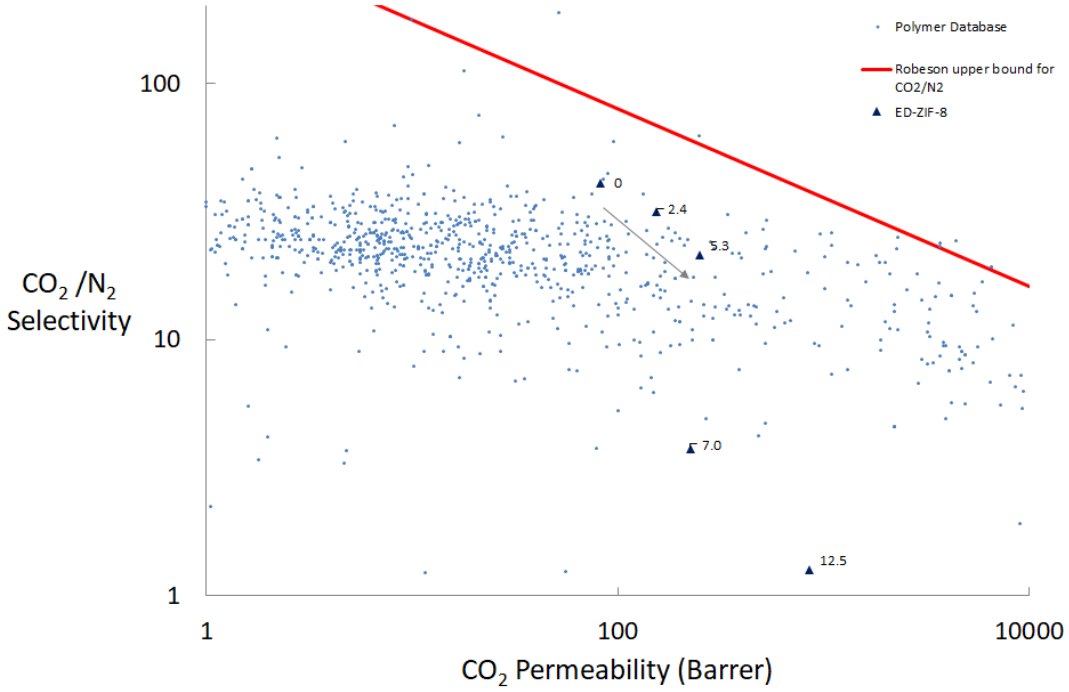

Figure 5.21: The experimental permeation test data for the ED-ZIF-8-PEBAX membranes. The data labels are the loading by weight of the filler in each membrane. The grey line illuminates the trend in the low loading data points.

5.4 Discussion

Mixed matrix membranes with both ZIF-8 and ethylenediamine-modified ZIF-8 in PEBAX MH1657 were successfully produced using the methods detailed in section 4.1. The synthesis methods were, however, not one hundred percent reliable. On some occasions membranes were produced that were too fragile to be tested in the gas permeation apparatus, such as the 10 wt.% ZIF-8 sample.

It was also noted that the measured thicknesses of the membranes produced were far from consistent (see table 5.5). It is thought both inaccuracies in measuring the thickness as well as variation in the thicknesses of the membranes are the cause of this. These variations in thickness suggest the preparation and casting conditions were not controlled sufficiently for fully reproducible synthesis. It is likely a number of factors play a role in this such as accurate control of the viscosity and drying times of the casting mixture. Given the membranes were dried at ambient temperature, variation in temperatures and humidity levels changing the rate of solvent evaporation may well have been contributing factors. It is vital for future work that a dependable fabrication procedure for producing repeatedly similar membranes is established. A better understanding of the rheology of polymer casting solutions and research into the fluid mechanics in mixed matrix membrane formation could well lead to insights in controlling and improving the dispersion of filler particles.

Given the micrometer used measures the thickness over an area of greater than 1 cm^2, any local variation in thickness would not allow for a representative thickness to be determined. Such variation was noted in the 7.0 wt.% ZIF-8-PEBAX membranes, in which SEM images showed an increase in the local thickness in the immediate vicinity of a large cluster (see figures 5.11b and 5.18). In such an instance, the micrometer would only be able to measure the thickness of the widest point of the membrane.

It is speculated the increased thickness and curvature of the membrane above the cluster in figures 5.11b and 5.18 is due to the displacement of polymer solution during the drying phase. As the casting solution dries, it effectively 'contracts' as the solvent dissipates. Thus above and below the cluster, there is simply less solution around the cluster and thus remains thicker. Figure 5.22 effectively illustrates this point. This mechanism would also rely on the casting solution being sufficiently viscous so as not to flow and render the surface level.

The thickness was also the largest source of error in calculating the permeabilities. The thickness was measured by taking five individual measurements using the micrometer to cover the whole of the membrane. Even in a 5 cm^2 area of polymer, these five individual measurements could vary by up to 20 microns. This

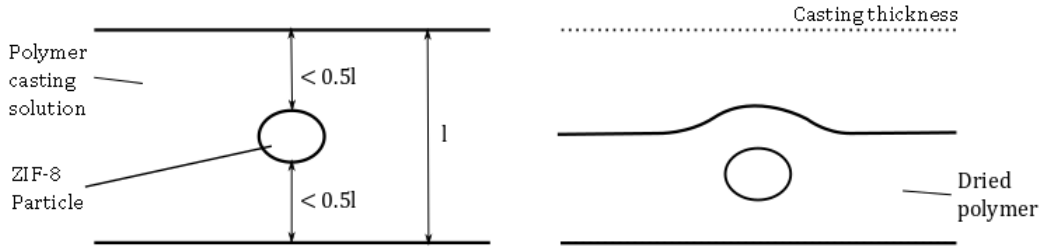

Figure 5.22: Sketch illustrating the mechanism by which the membrane remains thicker around the cluster when drying.

resulted in a high variance and uncertainty in the thickness in a number of the membranes, typically the higher loading ones. This could well be attributed to the aforementioned effect of clusters on the local thickness and their more frequent occurrence at higher loadings. The use of the micrometer to measure the thickness of materials mostly composed of an elastic material (PEBAX) is also potentially flawed. When comparing the thicknesses as measured by the micrometer and the SEM there was also a clear difference, further leading to a lack of confidence in the values. The values determined using the micrometer were higher than the thicknesses of the same membranes measured using the SEM. This could well be due to the micrometer measuring local maximums as seen in figures 5.11b and 5.18. The SEM analysis may well be a more accurate tool to determine the thickness of these membranes in future.

The densities of the membranes produced were not reported in this work. This could have been a simple way to verify the loadings of filler in the membranes. Initially the densities of the membrane samples *were* measured by weighing a small area (approximately 5 cm^2) of the membrane samples produced. Due to the combined uncertainty from the sample masses and the uncertainty in the measurements of the thickness of the membranes which propagate to the uncertainty in the estimated volume, it was calculated that the error in the density was approximately 30 %. Given the low loadings of ZIF-8 in PEBAX and the not dissimilar densities (0.950 and 1.130 g cm^{-3} for ZIF-8 and PEBAX respectively) of the two phases it was calculated that at a maximum loading of 10 wt.%, a change of less than 2 % in density was expected to be observed. Given that all of the initial density measurements overlapped with the expected values due to the high uncertainty

they were mistakenly deemed to be uninformative. However this data should still have been recorded and reported. This was a notable omission that would be carried out in future work.

Scanning electron microscopy was utilised to great effect to investigate the morphology of the mixed matrix membranes. The most notable feature of the ZIF-8-PEBAX mixed matrix membranes seen in the SEM images was the prevalence of ZIF-8 agglomerations in the membranes with loadings above 5 wt.%. Even on a macroscopic scale large clusters could be seen with the naked eye as shown in figures 5.6 and 5.7. These large clusters were on the scale of 100 µm, so large that they would almost certainly have been visible had they been present in the casting solution, although given the semi-opaque nature of the casting solution it is possible they could not be seen. Since they were not observed, it leads to the strong implication that these clusters formed while the casting solution was drying, or that they were too small to observe when cast. For the clusters to have formed during the drying phase the particles *must* be mobile. Thus given these observations it is hypothesised that the particles are mobile during the drying phase.

A further observation of figures 5.7a and 5.7b shows that the particles appeared to arrange themselves in a linear, semi-ordered arrangement. It is impossible that this order in the clusters stems from the chance arrangement during pouring and casting of the solution. While this organisation could possibly be related to dragging the casting knife over the surface, this would not explain the regular distances between the clusters. This organisation could be explained by the documented hydrophobic nature of ZIF-8. Given this hydrophobicity of ZIF-8, the particles could have a tendency to minimise the interfacial contact with the aqueous casting solution. Regardless of whether the clusters were present in the casting solution or formed when drying, this level of organization would seem to be near proof of the mobility of the particles during the drying phase.

Macroscopic-scale patterns were often seen in the membranes such as in figure 5.6. This seems to be further evidence of the mobility of nanoparticles during the drying phase, and that these patterns are caused by effects such as local recirculation of the casting mixture affecting the local concentration of solids on a small scale. It is predicted these patterns are formed by effects not dissimilar in nature to the deposition of solids at the edge of drying drops known as the 'coffee stain' effect.[209] In the coffee stain effect recirculation is caused by minute thermal gradients which form by the evaporation of solvent at the surface cooling the local mixture. Further evidence for recirculation type behaviours in the drying solution was present in the SEM images of the 10 wt.% membrane. Figure 5.11d shows SEM images taken near the edge of a membrane where striations around a cluster can be clearly seen. It is speculated that these striations could be attributed to the entrainment of ZIF-8 particles in the casting fluid, where the fluid is recirculating due to drying

near an edge. The deposition and pattern-formation of nanoparticles undergoing solvent dewetting is a complex field in its own right - and so the dewetting of a ternary polymeric-nanoparticle-solvent system intrinsically even more so.[116,210–212] It is highly likely this is the cause of the patterns seen in the membrane.

To summarise, it is hypothesised that the nanoparticles are mobile during the drying phase. Further it is thought that once cast, due to thermal gradients that form due to evaporation of solvent from the surface, recirculation occurs in the polymer-solvent-nanoparticle mixture. Then, given that the fluid mixture is in motion, if the ZIF-8 nanoparticles have a tendency to agglomerate to minimise interfacial surface area with the aqueous casting solution it is highly plausible that an Ostwald type process, in which a dispersed phase spontaneously coalesces over time to minimise surface area, combined with the motion of nanoparticles could lead to such agglomerations.

There is evidence both to this ideas credit and dismissal in the SEM images. Under close inspection of the SEM images of the agglomerations, voids can be seen within the clusters, the size of which appears to be of a similar magnitude to that of the particles. Looking closely at figure 5.11b, both voids towards the left of the cluster can be seen, as well as a region in which polymer is interspersed on the right. If the polymer is indeed interspersed within the cluster it would support the idea that the clusters form during drying because the polymer is mixed within the cluster. The contrary position is that the cluster never broke up during sonication and thus the polymer could not have penetrated into the cluster. Thus this appears to be supporting evidence that the clusters formed during drying, after the nanoparticles had been well mixed with the polymer solution.

Another interesting point drawn from these images was the lack of any intermediate sized clusters. The particles seemed to be in binary states - either within a large cluster greater than 1 µm in diameter, containing hundreds if not thousands of nanoparticles, or were well dispersed single particles that only appeared proximal to each other due to random placement. This could well be evidence to the contrary of the above hypothesis. It arguably implies that these clusters were always present, and never broke up during treatment with ultrasound. However the fact that no clusters were seen at low loadings suggests the ultrasonic treatment was successful.

Some consideration must be taken into account on viewing the SEM images and trying to interpret the degree of clustering. Largely due to the often limited availability of SEM facilities, often only one cross-section of a few millimetres in length could be imaged for each membrane sample. Given that the area of each membrane cast was approximately 2×40 cm^2 the imaged sections may not be representative of the entire membrane. The difference between the 5 wt.% ZIF-8-PEBAX samples imaged with the School of Biology and JMTC SEMs highlight this:

in one, several clusters were seen and in the other, no clusters were seen. Further is the prospect that when there are multiple clusters present there is possibility that many more agglomerations are observed than are truly representative due to the membrane fracturing at these polymer-filler interfaces which may be structurally weaker. Or if the agglomerations are regular and periodic in nature as may be suggested by the images in figure 5.7 and the membranes fracture randomly either many would be seen or very few.

The gas permeation results of the ZIF-8-PEBAX membranes showed that the CO_2 permeability coefficients were similar to the predictions using ideal models at loadings up to 5 wt.%. This agreed with the morphologies that were observed - a well dispersed homogeneous phase in which only a few clusters were seen. The N_2 permeability coefficients however did not agree with the ideal models over the same range of loadings. Below 5 wt.%, even modelling the ZIF-8 as impermeable to nitrogen could not explain the observed decline in nitrogen permeability. Above 5 wt.% the permeability coefficients of both carbon dioxide and nitrogen clearly deviate from the predicted solutions. The large increases in permeability and loss of selectivity that were observed can nearly always be attributed to voids within a membrane. The SEM showed that in this range of loadings that agglomerations of nanoparticles were frequent and that there were voids within the clusters. Thus the clear explanation of the sharp increase in permeability and loss of selectivity is the presence of non-selective voids within the clusters.

When the permeation data was plotted on a Robeson plot, it was seen that the 4.4 wt.% ZIF-8-PEBAX sample crossed the upper bound but at higher loadings the selectivity was lost due to voids within clusters. If the dispersion of ZIF-8 nanoparticles could be controlled at higher loadings, it could possibly lead to even higher selectivities.

The purpose of the surface modification of the ZIF-8 with ethylenediamine was to improve the dispersion of nanoparticles within the membranes by providing some electrostatic stability to the particles, and improving the interaction with the aqueous casting solution given their typical hydrophobicity. Agglomerations were seen in even the lowest loading ED-ZIF-8-PEBAX membranes, and were much more prevalent across the range of loadings than compared with the unmodified ZIF counterparts. Thus in the simplest terms, this procedure was not successful in its goal.

The permeability coefficients and ideal selectivities of the ED-ZIF-8 membranes clearly relate to the observed morphologies. The large increases in permeability and loss of selectivity can almost certainly be related to the voids and cracks observed within the membranes. The permeation data plotted on the Robeson bound highlights the poor performance of these samples.

Figure 5.23 shows the CO_2 permeabilities of the two different sample sets. The CO_2 permeabilities of all of the ED-ZIF-8-PEBAX membranes were all much higher than that of the unmodified ZIF-8-PEBAX membranes with the exception of the 7 wt.% membranes which effectively shared the same value. Given the degree of clustering observed it seems very likely that as in the ZIF-8-PEBAX membranes, the origin of these high permeabilities are due to voidage within the clusters and defects such as cracks in and around the agglomerations. This would also agree with the observed decline in selectivity with increasing loading.

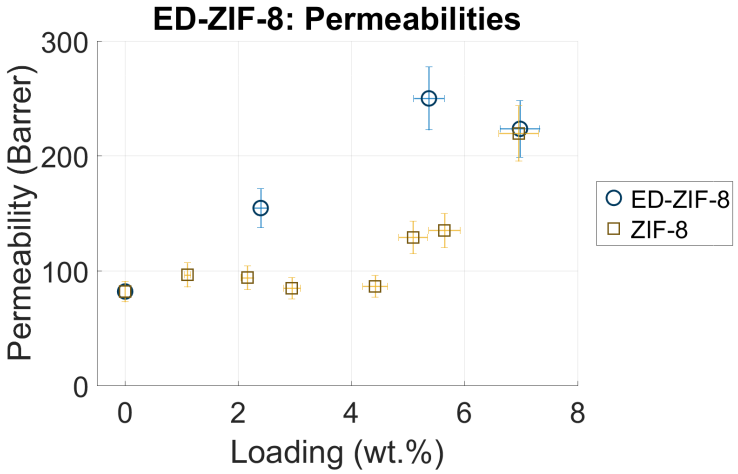

Figure 5.23: Comparison of ZIF-8-PEBAX and ED-ZIF-8-PEBAX CO_2 permeabilities.

5.5 Conclusions and Future Work

- Nanoscale ZIF-8 was successfully combined with PEBAX to form mixed matrix membranes via the method previously described in Chapter 4.
- SEM images showed agglomerations in the ZIF-8 nanoparticles still remained after treating with ultrasound for 48 hours.
- The thicknesses of the membranes produced were inconsistent and some membranes fabricated displayed low mechanical strength. Unknown elements affecting the synthesis procedure, such as precise casting temperature and the filler affecting the viscosity, were the suspected cause of these inconsistencies.
- Patterns seen in the membranes show there was inhomogeneous macroscopic scale dispersion of the nanoparticles.
- The dispersion of ZIF-8 was strongly influenced by the loading. Multiple clusters were seen in the cross-section using SEM in the unmodified ZIF-8-PEBAX membranes in the 5.1, 7.0 and 10 wt.% samples.
- Voids could be clearly seen within some of the clusters.
- Individual ZIF-8 nanoparticles showed good interaction with PEBAX with no signs of separation, or 'sieve-in-a-cage' or morphology, and with the exception of the clusters showed good dispersion on a microscopic scale.
- At loadings of ZIF-8 less than 5 wt.% there was no significant change to the CO_2 permeability compared with pure PEBAX. Above 5 wt.% a significant increase in permeability was seen as the loading increased up to 7.0 wt.%.
- Predictions using the ideal Maxwell and Bruggeman models were made, and matched part of the CO_2 permeation data. However they could not explain the overall transport behaviour which made sense given the non-ideal morphologies such as voids and clusters observed with SEM.
- Four mixed matrix membranes were produced from ethylenediamine-functionalised ZIF-8 and PEBAX up to 12 wt.% using the aforementioned method described in Chapter 4.
- The surface modification of the ZIF-8 with ethylenediamine was not successful in improving the dispersion and reducing the clusters present in the ZIF-8-PEBAX membranes. SEM images show significant agglomerations in all the ED-ZIF-8-PEBAX MMMs produced.
- All of the ED-ZIF-8-PEBAX membranes showed higher permeabilities than neat PEBAX and the ZIF-8-PEBAX membranes, with the exception of the 6.9 and 7.0 wt.% (ED-ZIF-8-PEBAX and ZIF-8-PEBAX membranes respectively) which showed significantly similar carbon dioxide permeabilities.

- It is speculated the increases in permeability of both samples compared with neat PEBAX can mainly be attributed to the occurrence of clusters and voids within the clusters.

There are numerous future avenues which would be both enlightening and worthwhile to pursue. The rheology of polymer gel solutions and the process by which they undergo solvent dewetting are no doubt integral to the fluid motions when drying and likely impact heavily on the both macroscopic and microscopic distribution of nanoparticles. The field of nanoparticle-solvent dewetting is a complex field in its own right and further understanding of how the particle, polymer and solvent move and interact when drying could lead to advancements in the fabrication of mixed matrix membranes.

Although the modification of ZIF-8 in this instance was not successful in improving the dispersion, other modifications could be undertaken to try and achieve a similar goal. The linker of ligand of the ZIF could also be changed such that more amine groups could be accommodated. Or, arguably more simply, the origin of the clusters could be explored by examining the impact of ultrasonication on the occurrence of clusters in the powder itself. This topic has actually formed part of the basis of continuing work undertaken by students at the University of Edinburgh.

As outlined in chapter 2, there is a great demand for new membrane materials if carbon capture using membranes is to compete economically with the current frontrunners of carbon capture technology. These materials must operate above or close to the Robeson upper bound. It was promising to note in the unmodified ZIF-8-PEBAX membranes when the ZIF-8 particles were well dispersed at loadings below 5 wt.% that a trend of increasing selectivity was observed and one membrane possessed transport properties above that of the upper bound. Thus it would be of great interest to attempt to improve the dispersion of ZIF-8 in PEBAX at higher loadings than observed here.

Chapter 6

Nano-scale MCM-41 Hollow Spheres in PEBAX

MCM-41 has seen interest for numerous separation purposes due to its high surface area, tunable porosity and the ease with which it can be functionalised. Novel hollow spheres of MCM-41 were used to fabricate mixed matrix membranes with PEBAX as the continuous phase. While both MCM-41[56,183,184] and hollow spheres of other porous materials[70,162,190] have previously been used to produce mixed matrix membranes for gas separation, no reports in literature of such hollow spheres produced from MCM-41 being used to produce MMMs were found and it is thought that this is the first work to do so.

Three different MCM-41 hollow sphere (MCM-41-HS) samples were utilised in this project: 160 nm C18-MCM-41-HS, 160 nm C16-MCM-41-HS and 450 nm C18-MCM-41-HS, where C16 and C18 refers to the length of the alkyl chain which determines the pore size of the spheres. The C16 and C18 samples should have pore sizes of 3.8 and 4.4 nm respectively.[177] The length in nanometres refers to an estimated external diameter of the particles based upon the polystyrene template.

The methods detailed in Chapter 4 were used to successful synthesise and characterise multiple membranes up to 10 wt.% for both the 160 nm C16 and C18 samples. Three membranes were produced using the 450 nm C18 hollow spheres, however only one of these showed any selectivity for the CO_2/N_2 separation.

6.1 MCM-41 Hollow Spheres: STEM Analysis

The 160 nm C16- and C18-MCM-41-HS were submitted to Johnson Matthey's analytical department for analysis with scanning transmission electron microscopy (STEM).

In preparation for STEM analysis the samples were ground between two glass slides and dusted onto a holey carbon coated copper TEM grid. The samples were examined using a JEM 2800 (Scanning) Transmission Electron Microscope. The accelerating voltage was set to 200 kV, the C2 aperture was 40 and 70 μm, and the dark-field (Z-contrast) was in scanning mode using an off-axis annular detector. The secondary electron (SE) signal was acquired simultaneously with the other STEM images to provide topological information.

Images from the STEM analysis can be seen in figure 6.1 highlighting the hollow nature of the spheres. The main results of the STEM particles size analysis are summarized in table 6.1. The similarity of the mean internal diameter of the shells of both samples is to be expected given the samples were synthesised using the same polystyrene template mixture. The small discrepancy in internal diameter and mean particle size means the shell thickness differs by 10 nm (35 nm for C16 and 45 nm for C18). It was not possible to determine the pore sizes of the samples with this technique.

Table 6.1: STEM Analysis Results

Sample	Mean particle size (nm)	Particle size std. dev. (nm)	Mean shell internal diameter (nm)	Shell thickness std. dev. (nm)
C16	162	18	127	10
C18	170	15	125	9

Figure 6.2 shows images of the surface of similar MCM-41 hollow spheres made via an identical procedure prior to this project. Both the hollow nature of the spheres can be clearly seen, as well as the porous nature of the spheres.

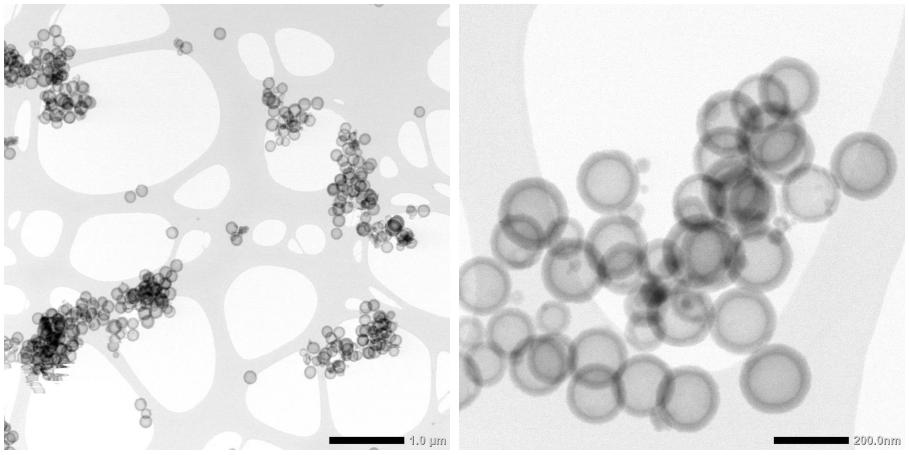

(a) C18

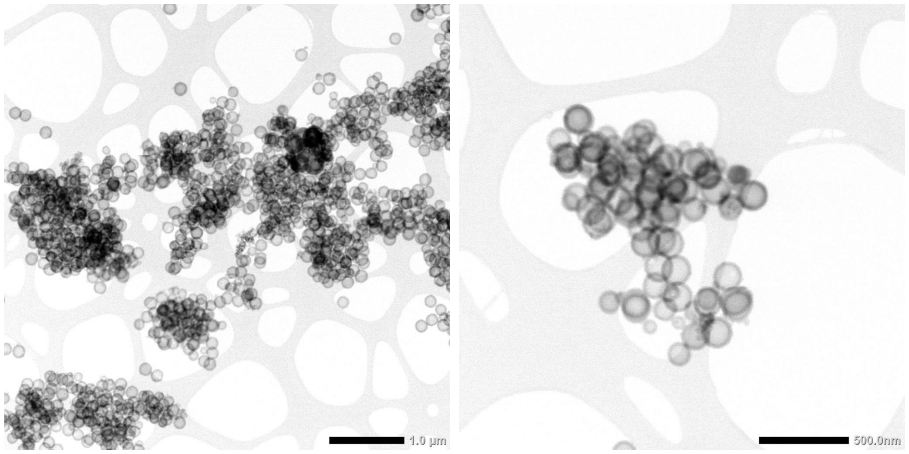

(b) C16

Figure 6.1: Images from the STEM analysis of MCM-41 hollow spheres.

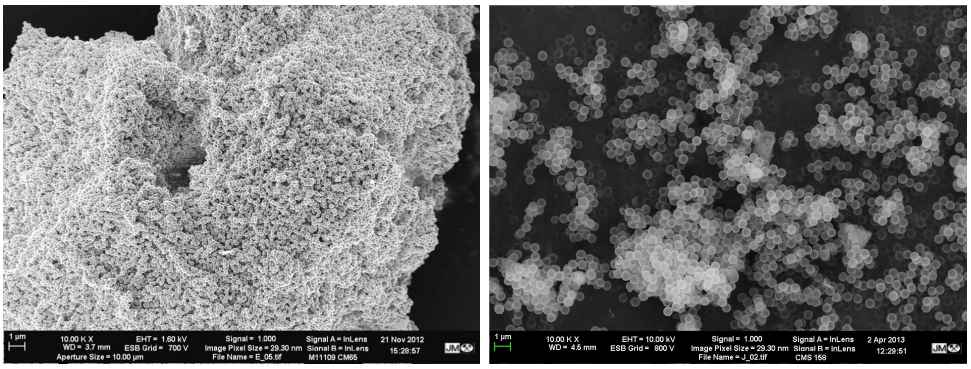

(a) SEM

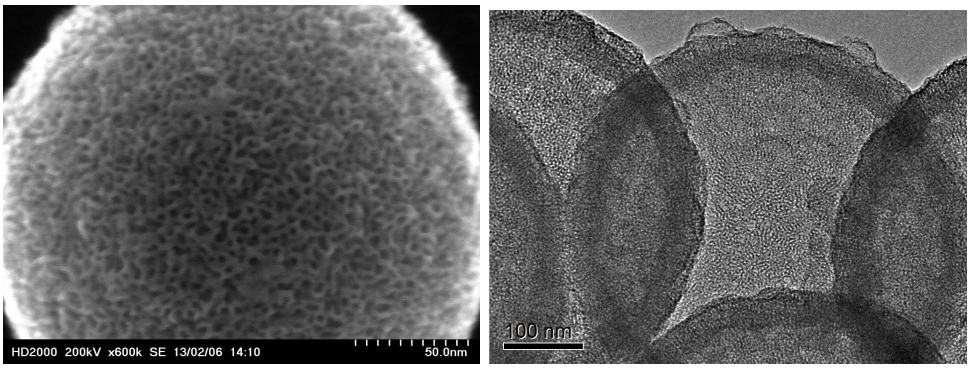

(b) STEM

Figure 6.2: SEM/STEM images of larger MCM-41 hollow spheres made via an identical procedure highlighting the sphericity and porous nature of the particles.

6.2 Results

The 160nm C16- and C18-MCM-41 hollow spheres were incorporated with PEBAX MH1657 to create a multitude of membranes. Tables 6.2 and 6.3 show the full list of membranes that were produced with the C18 and C16 samples respectively. Three membranes were also produced with the 450nm C18-MCM-41-HS sample. Table 6.4 shows the details of these membranes. The thicknesses were determined using the Mitutoya micrometer as discussed in chapter 4. These were compared with the thicknesses of the samples observed with the SEM. These values were either determined using the analytical software of the SEM or subsequently in post-processing of the images using the open source Fiji ImageJ software.[213,214] Where blank these images were not analysed using SEM.

As mentioned in section 4.1.3, two water baths were used to produced the MCM-41 hollow sphere-PEBAX membranes. This was necessary due to limitations of equipment availability. The water bath that was used to produce each membrane is noted in each table. Despite the differences in the models, no attributable distinctions were seen in the membranes produced by each one as is discussed later in section 6.3.

Table 6.2: List of details of the 160nm C18-MCM-41-PEBAX MMMs produced.

Loading		Mass of	Mass of	Thickness (μm)	
(wt.%)	(vol.%)[1]	PEBAX (g)	MCM-41 (g)	Micrometer	SEM
1.4	3.2	1.0010	0.0143	30	-
1.7	3.8	1.0070	0.0176	35	-
2.5	5.5	1.0065	0.0254	31	-
3.2	7.3	1.0114	0.0338	43	42
4.5	10	1.0084	0.0474	25	26
6.1	14	0.9980	0.0653	-	46
6.7	15	1.0014	0.0718	71	33
8.0[2]	18	0.9899	0.0866	42	-
10.0[2]	22.5	0.8870	0.0986	26	-

[1] Rough estimates based on the STEM analysis shell diameters and thicknesses and a shell density of 0.97 g cm^{-3}.[215]

[2] Produced using the Branson CPXH 1800 ultrasonic water bath. All other membranes were produced using the Fisher Scientific model as discussed in section 4.1.3.

Table 6.3: List of details of the 160nm C16-MCM-41-PEBAX MMMs produced.

Loading (wt.%)	Loading (vol.%)[1]	Mass of PEBAX (g)	Mass of MCM-41 (g)	Thickness (μm) Micrometer	Thickness (μm) SEM
2.0	5.5	1.1015	0.0230	35	40
3.5	9.4	1.0110	0.0368	34	28
3.8	10	1.0146	0.0396	34	-
3.9[2]	11	0.9951	0.0405	31	21
5.5	14.7	0.9926	0.0579	47	28
6.9[2]	18	1.0136	0.0750	95	33
7.8	21	1.0163	0.0861	32	37
9.9	26	1.0026	0.1100	19, 40[3]	22

[1] Rough estimates based on the STEM analysis shell diameters and thicknesses and a shell density of 0.97 g cm^{-3}.[215]

[2] Produced using the Branson CPXH 1800 ultrasonic water bath. All other membranes were produced using the Fisher Scientific model as discussed in section 4.1.3.

[3] The 9.9 wt.% sample showed a large variation in thickness between two regions and as such the regions were treated as separate samples and tested separately with the time-lag apparatus.

Table 6.4: List of details of the 450nm C18-MCM-41-PEBAX MMMs produced. All membranes were produced using the Fisher Scientific model.

Loading (wt.%)	Mass of PEBAX (g)	Mass of MCM-41 (g)	Thickness (μm) Micrometer	Thickness (μm) SEM
1.4	1.0037	0.0140	29	32
3.0[1]	1.0044	0.0312	56	-
3.1[1]	1.0160	0.0323	49	30-

[1] Membrane showed no selectivity in permeation tests.

6.2.1 SEM Analysis

The cross sections of several of the three different MCM-41-HS-PEBAX membrane types were imaged using SEM such that a range of loadings could be investigated. SEM analysis was performed on the 3.2, 4.5, 6.1, and 6.7 wt.% 160nm C18-MCM-41-HS-PEBAX membranes, the 2.0, 3.5, 3.9, 5.5, 6.9, 7.8 and 9.9 wt.% 160nm C16-MCM-41-HS-PEBAX membranes, and the 1.4 and 3.0 wt.% 450 nm C18-MCM-41-HS-PEBAX membranes. The 160 and 450 nm C18-MCM-41-HS-PEBAX membranes were imaged using the JMTC SEM facilities. Unlike all the other cross-sections in this work, these membranes were prepared by coating them in a resin, and then grinding and polishing the surface. Only small sections of the samples were imaged with the JMTC SEM and thus it is uncertain if these images are completely representative of the materials produced. The 160nm C16-MCM-41-HS-PEBAX membranes were imaged using the School of Geosciences SEM facilities and were prepared via immersion and fracturing in liquid nitrogen as per the procedure elucidated in section 4.3. These images can be found in figures 6.3, 6.4, and 6.5. Details of the SEM conditions can be found in table 4.2. Similar to the previous chapter, a small selection of representative images has been included here and further images can be found in the additional electronic material.

The SEM images of the 160nm C18 membranes can be seen in figure 6.3. The left images of each sub-figure show a cross section of a particular loading and the right images are insets of the left image. Generally good dispersion of the MCM-41 hollow spheres was observed at all loadings. In figure 6.7a, the spheres can clearly be observed homogeneously dispersed across the cross-section with no signs of agglomeration or other defects. In the higher magnification image on the right there appears to be no separation between the polymer and filler particles demonstrating good adhesion between the PEBAX and MCM-41. The 4.5 wt.% membranes seen in figure 6.7b show a similar morphology. At the external surfaces of the membrane there appears to be some deformation. It is possible that this was damage caused by the resin coating and grinding method used to prepare these cross sections for SEM. In figure 6.7c the left image shows small voids similar in scale to the nanoparticles throughout the cross section. These dispersed voids were unique to this sample and it is not clear what caused them. Their distribution almost makes them look slightly aerated. The voids seem to be located mainly around the filler particles, similar to the 'sieve-in-a-cage' morphology. Also the nanoparticles can be seen forming many small agglomerations of a few particles. The 6.7 wt.% C18 membranes seen in 6.3d displayed an asymmetric distribution of filler particles with many more particles accumulating close to one surface of the membrane. These can clearly be seen on the right side of the membrane in both images. In the bulk of the membrane outwith this high particle density region numerous small clusters of up

to approximately ten particles were seen in addition to many well dispersed singular spheres similar to what was observed in the other C18 membranes. In the high particle density region close to one surface the particles seemed to form connected networks. It was also noted that a large cluster of several hundred particles could be seen in the uppermost extremity of one image, figure 6.3d; unfortunately no higher magnification images of this area were taken. No voids could be seen and all of the filler particles showed good adhesion with the polymer.

Figure 6.4 shows the images of the 160 nm C16-MCM-41-HS-PEBAX membranes. The images of the C16 membranes were taken with the School of Geosciences. In these images the contrast between the MCM-41 hollow spheres and the polymer was much less than in the images taken with the JMTC SEM and the hollow spheres, while clear, are not as immediately discernible. Generally at low loadings the particles could be seen to be well dispersed whilst at higher loadings clusters were observed. While faint, in figures 6.4a, 6.4b and 6.4c the hollow spheres could be seen in the membranes with less than 5 wt.% loading and showed homogeneous distribution of single particles and good adhesion with the PEBAX.

In figure 6.4d, some small clusters of less than ten particles could be seen in the 5.5 wt.% membranes but the majority of spheres were singularly dispersed. Interestingly the hollow nature of the spheres could be seen due to the sensitivity to backscattered electrons of this detector. Again the MCM-41 showed very good adhesion with the PEBAX and no voids were seen.

Like the 6.7 wt.% 160 nm C18 membrane, the 6.9 wt.% C16 membranes were highly asymmetric as seen in figure 6.4e, showing much higher particle density near one surface. This is clearly seen in the top left image. The top right image of figure 6.4e is an inset of the top left image showing this high particle density region at higher magnification. Despite the accumulation of particles, the polymer is well dispersed throughout the majority of this region. Some small voids were seen which are highlighted. The bottom left image shows the scale of these voids of around 0.3 by 1.5 µm. The bottom right image shows a large agglomerations with a high aspect ratio made up of hundreds of filler particles. Similar to the ZIF-8 materials well dispersed particles were seen surround the cluster.

In both the 7.8 wt.% 160 nm C18 membranes, no clusters were seen and the particles were well dispersed. In the four images in figure 6.4f, the hollow nanoparticles can clearly be seen throughout. In the higher magnification images, good adhesion between the phases is clear. In the left images some deformity in half of the cross section can be seen. This was likely caused by stretching during the snapping of the membrane. In figure 6.4g similarly well dispersed particles and good adhesion were noted. The bottom right image shows one cluster-like feature that was seen in the 9.9 wt.% membranes but with close inspection of this agglomeration, it is

clearly not composed of hollow spheres and is likely to be some contamination.

Figure 6.5 shows the SEM images of the 450 nm C18-MCM-41-PEBAX membranes taken using the JMTC SEM. Numerous clusters were seen in the 1.4 wt.% 450 nm C18 membranes. Darker areas around the clusters seemed to highlight some separation from the polymer although this could be an artefact of the grinding and polishing in preparation distorting the polymer around the clusters.

Strange groups of hollow spheres were seen in the 3.0 wt.% 450 nm C18 membranes. As well as the small clusters seen in the other membranes, ring-like structures were seen which looked as if small particles were arranged in rings around a void. STEM analysis was not performed on these larger filler particles but visual inspection of the particles within the membrane seems to suggest a large variance in the particle size distribution. It is not clear if the annulus-like clusters are rings of smaller particles or large hollow spheres damaged by the grinding process. Drawing from Occam's razor the latter case would appear to be the most likely.

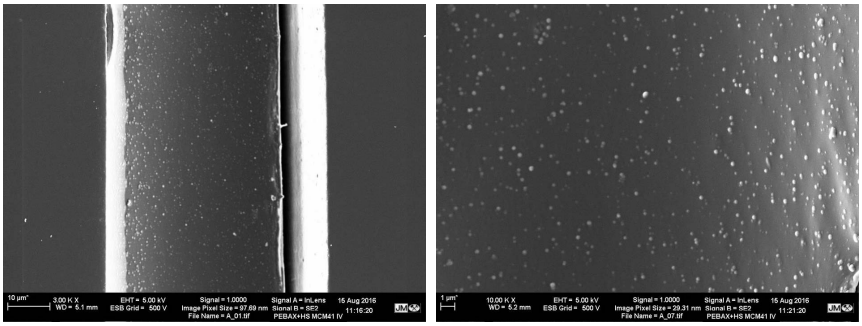

(a) 3.2 wt.%

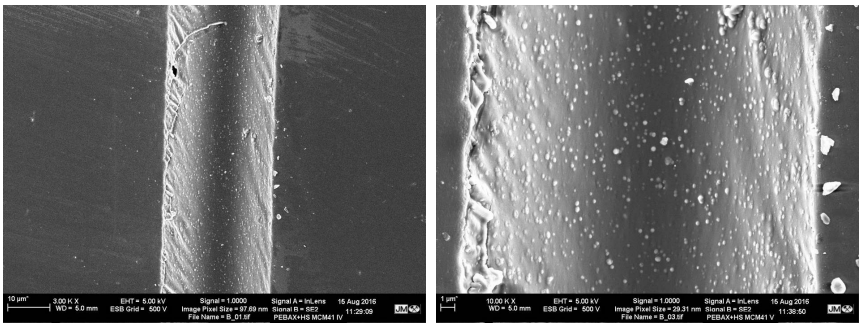

(b) 4.5 wt.%

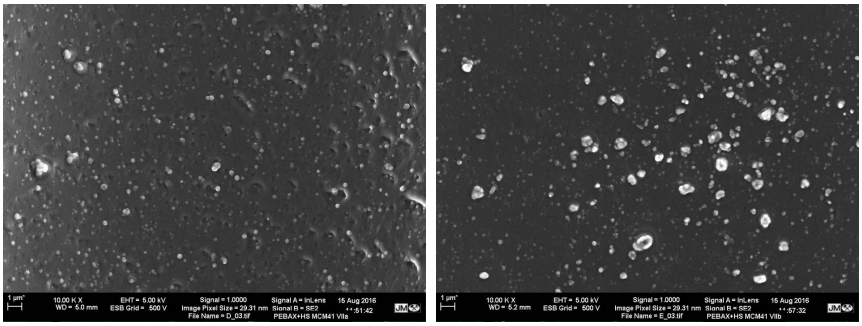

(c) 6.1 wt.%

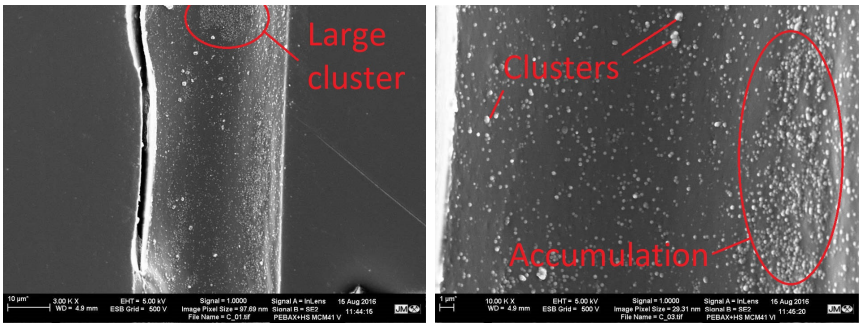

(d) 6.7 wt.%

Figure 6.3: SEM images of the 160nm C18-MCM-41-HS-PEBAX membranes.

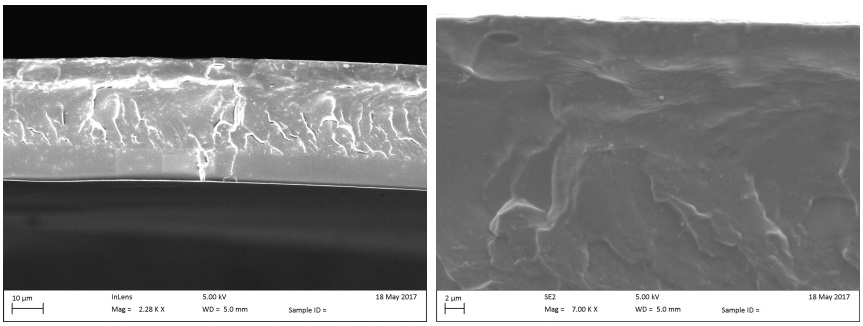

(a) 2.0 wt.%

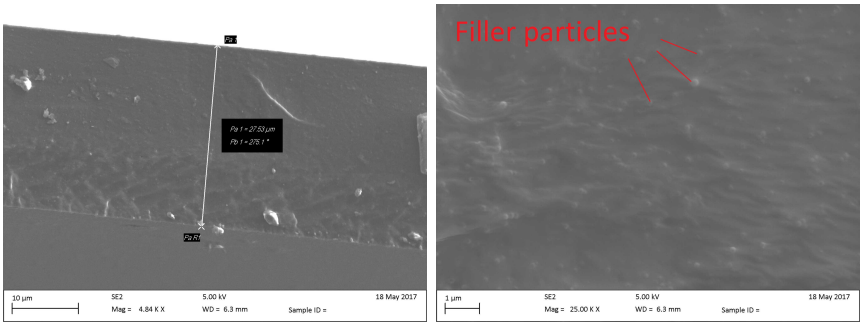

(b) 3.5 wt.%

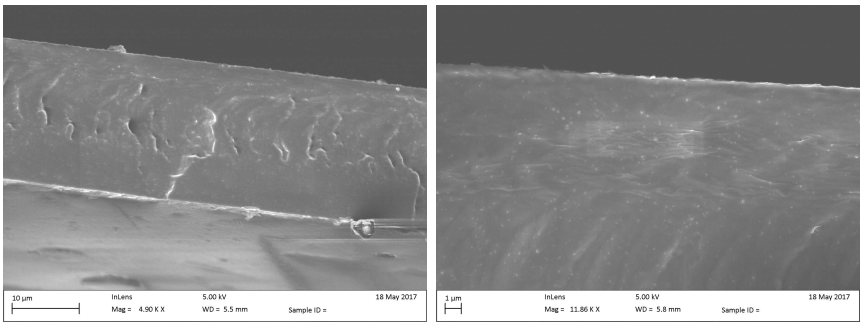

(c) 3.9 wt.%

Figure 6.4: SEM images of the 160 nm C16-MCM-41-HS-PEBAX membranes.

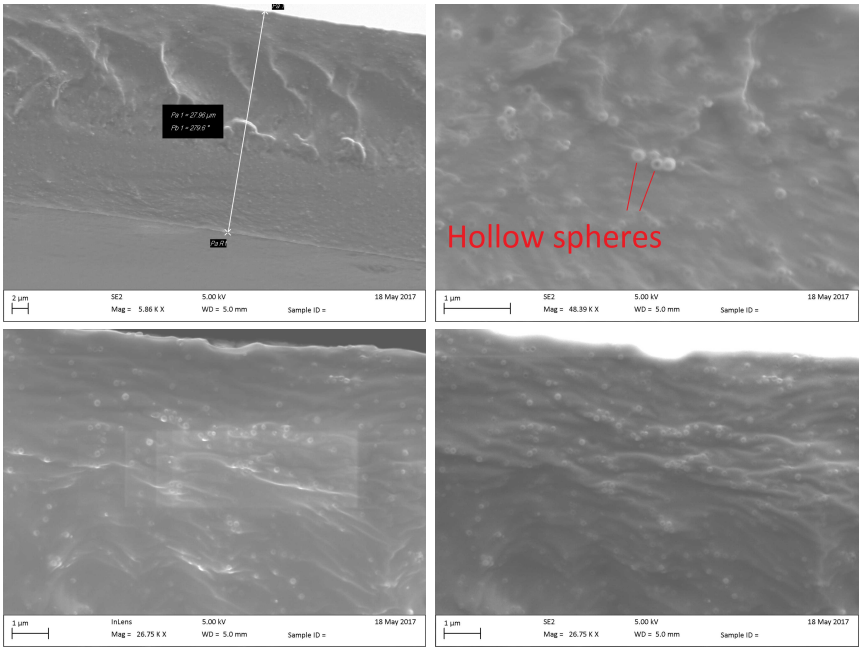

(d) 5.5 wt.%

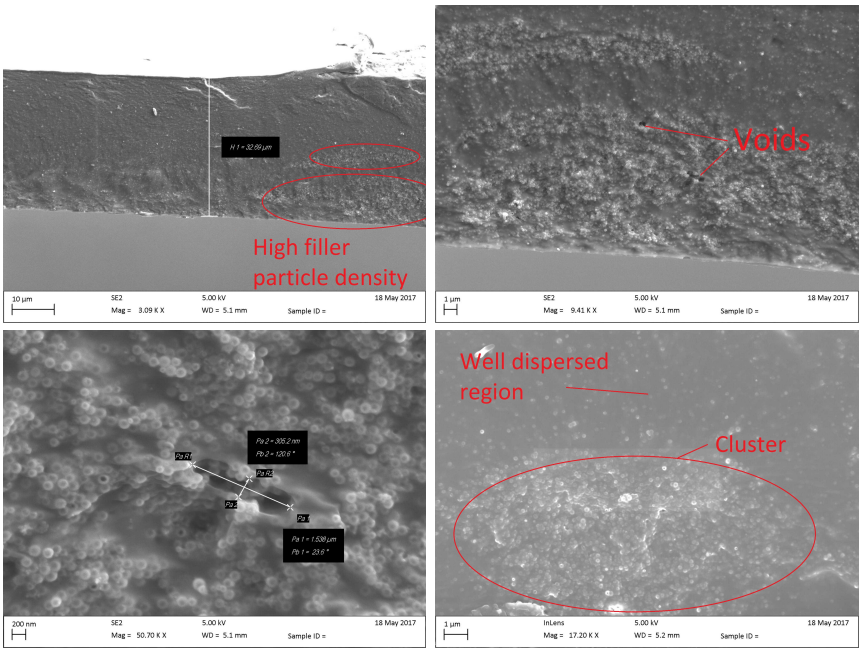

(e) 6.9 wt.%

Figure 6.4: SEM images of the 160nm C16-MCM-41-HS-PEBAX membranes.

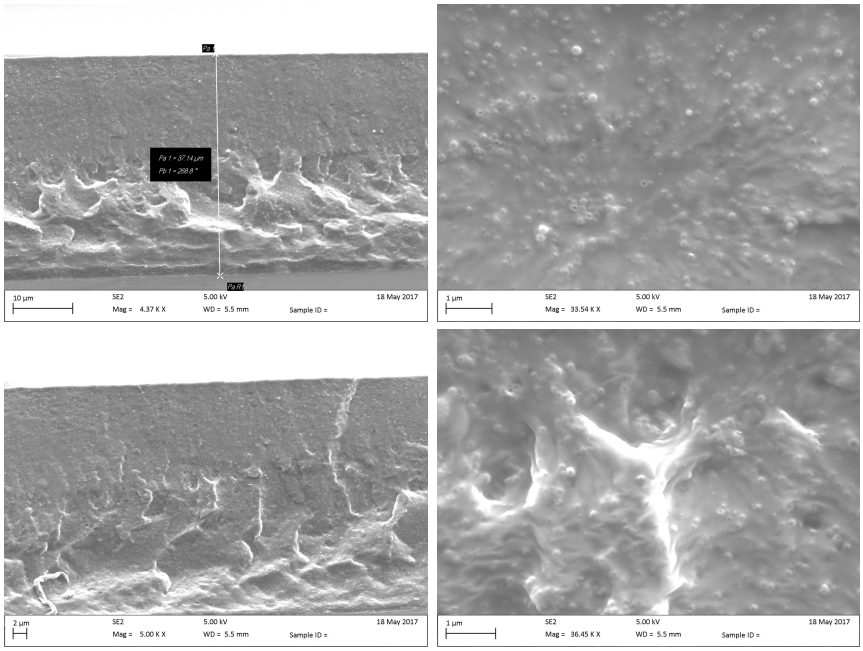

(f) 7.8 wt.% C16

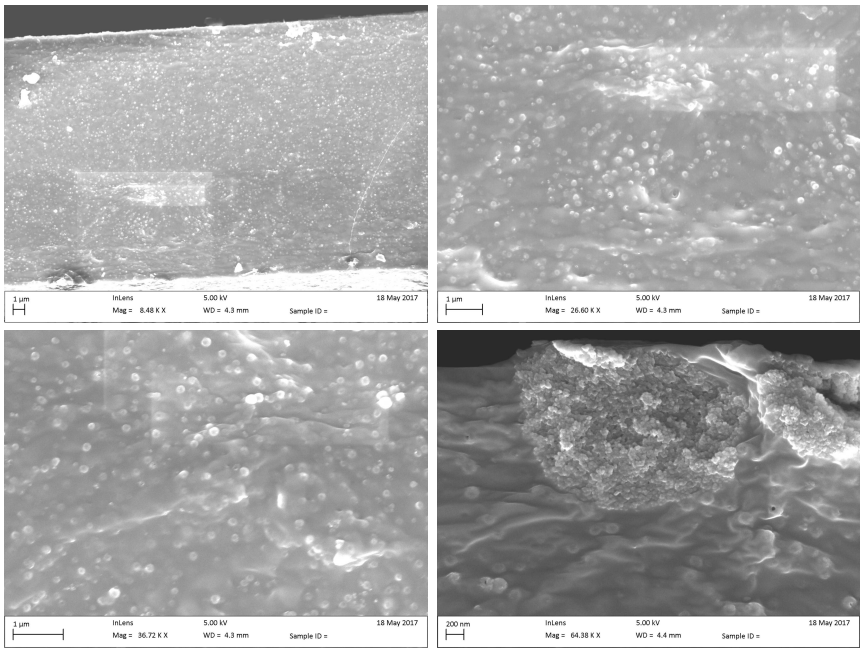

(g) 9.9 wt.% C16

Figure 6.4: SEM images of the 160nm C16-MCM-41-HS-PEBAX membranes.

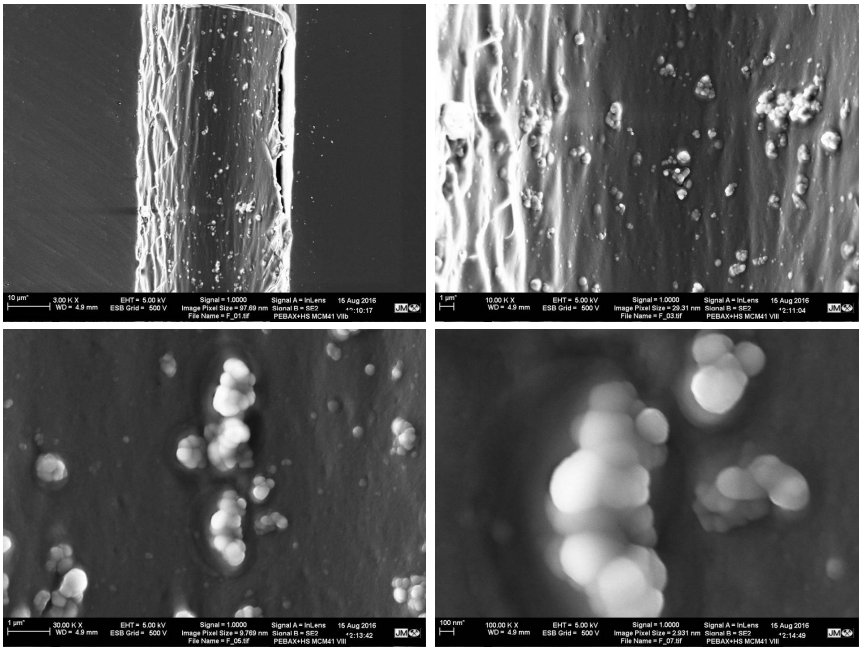

(a) 1.4 wt.%

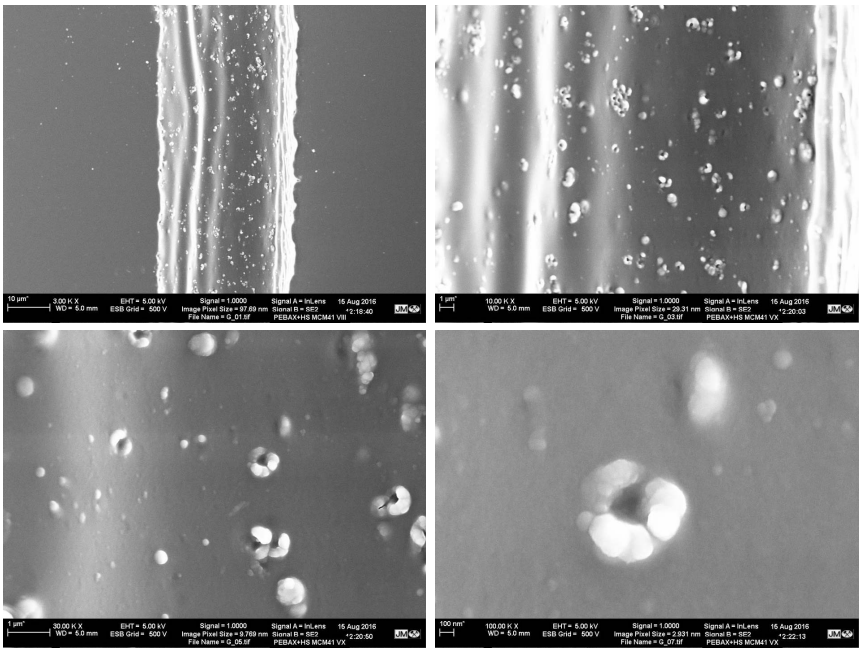

(b) 3.0 wt.%

Figure 6.5: SEM images of the 450 nm C18-MCM-41-HS-PEBAX membranes.

6.2.2 Time-lag Permeation Results

Time-lag permeation tests were carried out according the procedure detailed in section 4.2.2 on all the membranes produced, often in duplicate or triplicate for reproducibility. All of the experiments were carried out at 1 bar upstream pressure. A complete list the successful permeation tests run is presented in tables 6.5, 6.6 and 6.7 for the 160 nm C18-MCM-41-HS-PEBAX membranes, the 160 nm C16-MCM-41-HS-PEBAX membranes, and the 450 nm C18-MCM-41-SH-PEBAX membranes respectively. Due to the aforementioned adverse effects of noise in the pressure signal distorting the trend as mentioned in section 4.2.3, some of these results were invalidated and thus why only one experiment for each gas of some of the membranes is listed. The repeat runs demonstrated the reliable reproducibility of the tests. For nitrogen the time-lag was often imperceptibly small and close to the origin that a fit of the steady state flux gave a negative time-lag value and thus a realistic diffusivity could not be calculated.

The average relative uncertainty in the permeability coefficient values was 14%. The average relative uncertainty in the diffusivity coefficient was 46%. The high uncertainty in the diffusivity coefficient values was attributed either a short time lag or high variance in the thickness of the membranes or both. No trends or reasonable conclusions could be drawn from the diffusivity data.

Figure 6.6 shows the averaged CO_2 and N_2 permeability coefficients of all the membranes successfully tested in totality on single plots for each gas. In figure 6.6a a clear maximum in the CO_2 permeability can be seen in the 160 nm C16- and C18-MCM-41-PEBAX membranes. Over the zero to 5 wt.% loading range both the 160 nm hollow spheres show slightly higher permeabilities over that of neat PEBAX, but above 5 wt.% show a sharp increase in permeability followed by a sharp decrease in CO_2 permeability in the membranes with approximately 8 and 10 wt.% loadings.

Figure 6.6b shows the N_2 permeability coefficients for the three sample sets. There is a notable outlier in the 160 nm C18-MCM-41-HS data in the 3.2 wt.% sample where the N_2 permeability coefficient is 3 times that of neat PEBAX. Looking at the data sets as one it appears there is a small maxima in N_2 permeability coefficient around 5 wt.% loadings.

Figures 6.7 and 6.8 show the results of the permeation experiments for the 160 nm C18- and C16-MCM-41-HS-PEBAX membranes respectively in greater detail with the pure gas results, the ideal selectivities and the permeabilities normalised to that of neat PEBAX.

In figure 6.7a the single gas permeability coefficients for both carbon dioxide and nitrogen in the 160 nm C18-MCM-41-HS can be seen in greater detail. The 1.4,

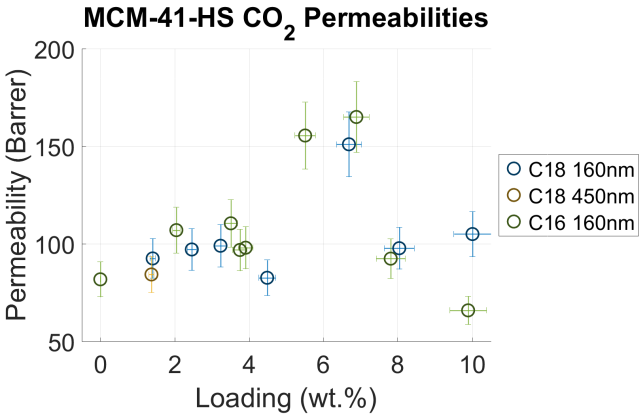

(a) CO_2

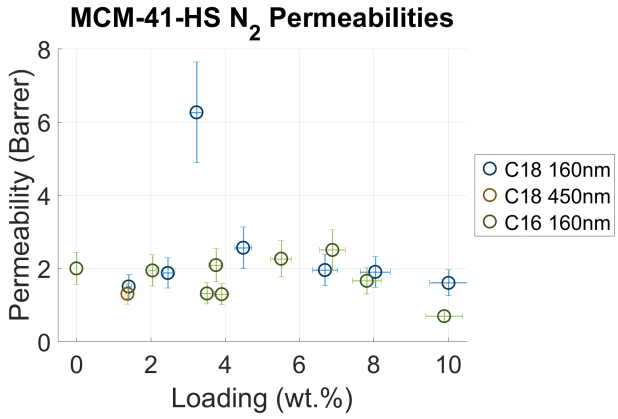

(b) N_2

Figure 6.6: Full CO_2 and N_2 permeability coefficients for the MCM-41-HS-PEBAX membranes.

2.5 and 3.2 wt.% membranes compared with the neat PEBAX show a monotonic increase in CO_2 permeability with increasing loading while the N_2 permeability coefficient for these samples are lower than that of neat PEBAX (excluding the N_2 value for 3.2 wt.% as an outlier). The 4.5 wt.% membrane shows a CO_2 permeability similar to that of neat PEBAX but the 6.7 wt.% had a much higher permeability coefficient for CO_2, 150 Barrer, nearly double that of the unloaded polymer. This particular sample showed a highly asymmetric particle distribution in SEM images. In the highest loading membranes both the CO_2 and nitrogen permeabilities were similar to that of the three low loading (less than 4 wt.%) samples. The 6.1 wt.% membrane, in which voids were seen distributed throughout the membrane showed next to no tensile strength and could not be tested with the time-lag apparatus.

Figure 6.7b shows the same CO_2 permeability coefficients plotted alongside the selectivity data. It is difficult to discern a trend in the selectivity. The 6.7 wt.% 160 nm C18 membrane which had a much higher CO_2 permeability coefficient than all the other samples, also possessed the highest ideal selectivity in this set of fillers. The highly asymmetric distribution of particles seen in the SEM images of this sample could be the reason for both the high CO_2 permeability and the high selectivity. As discussed in section 3.5 if the hollow spheres selectively allow CO_2 to permeate through their centres while the N_2 has to deviate around the spheres, their inclusion in the polymer matrix could translate to increases in both selectivity and CO_2 permeability. It is possible that this highly asymmetric distribution which leads to an area near the packing limit of spheres further exaggerates the influence on the permeability of both gases.

Figure 6.8 shows the gas permeation results for the 160 nm C16-MCM-41-PEBAX membranes. In figure 6.8a a clear maximum in CO_2 permeability coefficient at around 6 to 7 wt.% loading is observed. Both the 5.5 and 6.9 wt.% membranes had high CO_2 permeabilities of over 150 Barrer, while the N_2 permeability coefficients remained similar to that of neat PEBAX. These two samples were notably the only membranes in this set in which clusters or agglomerations were observed. The 5.5 wt.% sample was the lowest loading sample of the C16 membranes in which clusters, albeit of only a few filler particles, were observed. The 6.9 wt.% samples displayed numerous large agglomerations of hundreds of filler particles. The samples with intermediate loadings between zero and 5 wt.%, in behaviour similar to the 160 nm C18- samples, had CO_2 permeabilities higher than that of neat PEBAX around 100 Barrer and N_2 permeabilities less than that of neat PEBAX. The 7.8 and 9.9 wt.% membranes had similar permeability coefficients to the membranes with less than 5 wt.% filler particles. In the 160cn C16- samples the nitrogen permeability coefficient similarly rises to a maximum in the 6.9 wt.% membrane. In the 7.8 and 9.9 wt.% samples the nitrogen permeability drops significantly below that of neat PEBAX, by around 20 and 60 % respectively seen clearly in figure 6.8c.

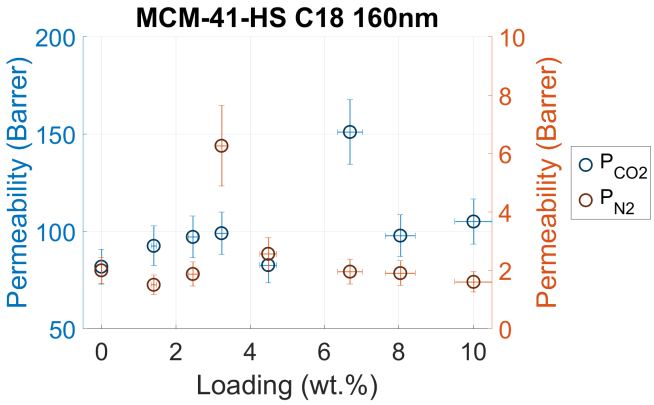

(a)

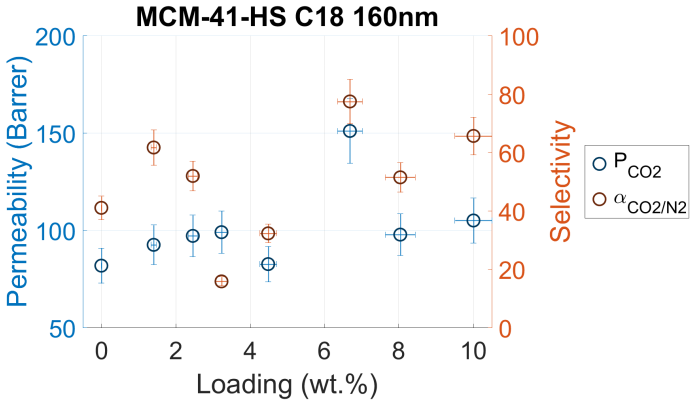

(b)

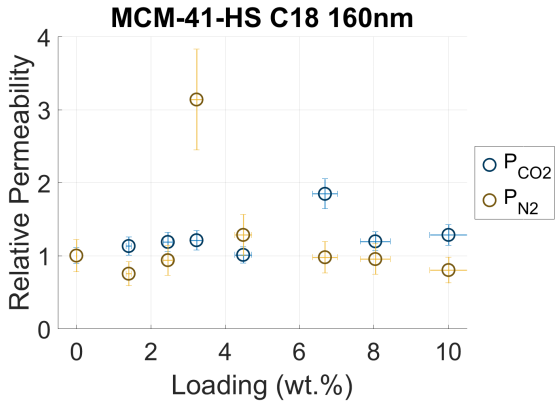

(c)

Figure 6.7: (a) The CO_2 and N_2 permeabilities, (b) The CO_2 permeability with the ideal selectivity, and (c) the permeabilities of CO_2 and N_2 normalised to the values for neat PEBAX, for the 160 nm C18-MCM-41-HS-PEBAX membranes.

Figure 6.8b shows the selectivities of the C16-MCM-41 MMMs. There appears to be a local maximum at around 4 wt.% loading above which the selectivity monotonically drops with the exception of the highest loading, 9.9 wt.% which shows the highest selectivity of all of the MCM-41-HS-PEBAX samples. This sample also shows the lowest CO_2 permeability of all of the C16-MCM-41-PEBAX samples. Thus its high selectivity can be attributed to its barrier-like behaviour to nitrogen flux.

Generally in the membranes of both 160 nm C16-MCM-41 and 160 nm C18-MCM-41 in which asymmetric loading of nanoparticles was observed, large increases in CO_2 permeability coefficient were observed.

Figure 6.9 shows a comparison of the CO_2 data with work carried out by Wu et al.[56] who also looked at mixed matrix membranes formed from MCM-41 and PEBAX MH1657. To allow for a fairer comparison given the MCM-41 in this work was not hollow, estimates of the volumetric loading were determined for both. Using a literature value for the density of MCM-41 the effective density of the hollow spheres could be approximated using equation 6.1:

$$\theta_{vol} = \frac{\theta_{mass} \cdot v_{sphere}}{\rho_{\text{MCM-41}} \cdot v_{shell}} = \frac{\theta_{mass} \cdot d_{sphere}^3}{\rho_{\text{MCM-41}} \cdot (d_{sphere}^3 - d_{centre}^3)} \tag{6.1}$$

where θ_{vol} and θ_{mass} are the volumetric and mass loadings respectively, v_{sphere} and v_{shell} are the mean volumes of the spheres and shells respectively, d_{sphere} is the external diameter of the sphere, d_{centre} is the diameter of the hollow centre, and $\rho_{\text{MCM-41}}$ is the density of MCM-41. The volumes of the sphere and shell were determined using the STEM data from table 6.1 and the density of MCM-41 was taken to be 0.97 g cm^{-3}.[215] Due to the slight differences in sphere diameter and thickness, the density of the C16- and C18-MCM-41 samples differed: they estimated values were 0.37 and 0.45 g cm^{-3} for C16 and C18 respectively. Due to the difference in pore diameter it is unlikely the shell density for each is identical, nor that the density of MCM-41 in the work by Wu et al. also shared the value used and thus figure 6.9 must be viewed with these approximations in mind. Consideration must also be given to the fact the materials differ in pore size and structure. The pore sizes of the MCM-41 in Wu's study were calculated to be 27 Å, while the C16 and C18 pore sizes should be around 38 and 44 Å respectively.

The values from literature overlap with the currently presented data in regards to range but it is obvious that the reported data does not correlate with the literature values. Taking into account that clusters were seen in the membranes displaying the highest permeability coefficient values of each of the C16 and C18 datasets, it could be argued the data disagrees due these morphological distinctions.

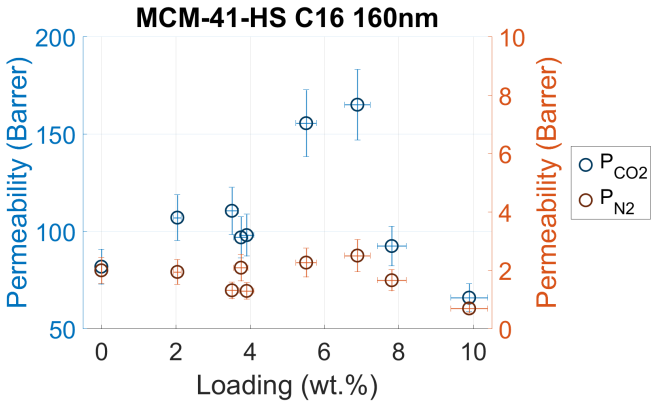

(a)

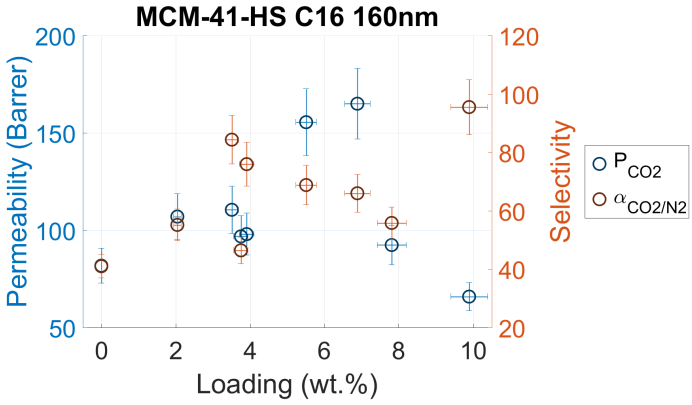

(b)

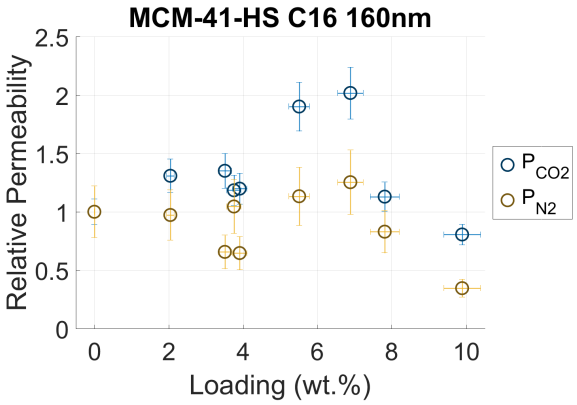

(c)

Figure 6.8: (a) The CO_2 and N_2 permeabilities, (b) The CO_2 permeability with the ideal selectivity, and (c) the permeabilities of CO_2 and N_2 normalised to the values for neat PEBAX, for the 160 nm C16-MCM-41-HS-PEBAX membranes.

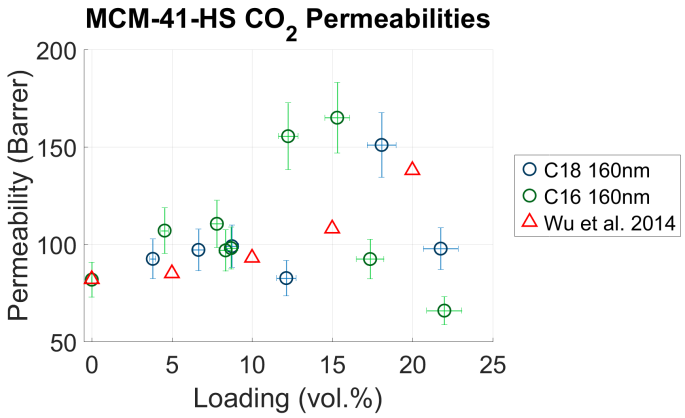

Figure 6.9: CO_2 permeability coefficient data and literature values.[56]

Plotting the permeation data on Robeson plots yields some interesting points. Figure 6.10 displays the permeation data for both the 160 nm and 450 nm C18-MCM-41-PEBAX membranes. The single 450 nm C18 sample that was successfully tested resulted in a large increase in selectivity compared with PEBAX. While the direct impact of the loading on the morphology or the gas transport behaviour was not clear from this plot, it is interesting to note that the 6.7 wt.% sample which possessed the highly asymmetric particle distribution crossed the upper bound. This is evidence to suggest the the high MCM-41 particle density seen in this membrane creates a barrier to nitrogen while allowing CO_2 to selectively pass through the spheres.

Figure 6.11 shows the data of the C16 MMM samples. All of the membranes using these fillers reported increased selectivities. No less than 5 of the membranes show behaviour on, or very near to, the Robeson upper bound. It is very interesting that these membranes are spread along the upper bound do not cross it. One theory could be that these composite membranes are similarly restricted by the Robeson upper bound because the hollow spheres themselves are not directly impacting the permeability but are interacting with the polymer phase, creating rigidified layers or partially blocked pores. This would then mean that it is still the polymer that is ultimately limiting the transport, hence why is does not cross the upper bound. Given that the 6.7 wt.% 160nm C18- MMM crosses the upper bound, this seems like an unlikely theory despite the fact it would explain the points along the upper bound in the C16-MCM-41-PEBAX samples.

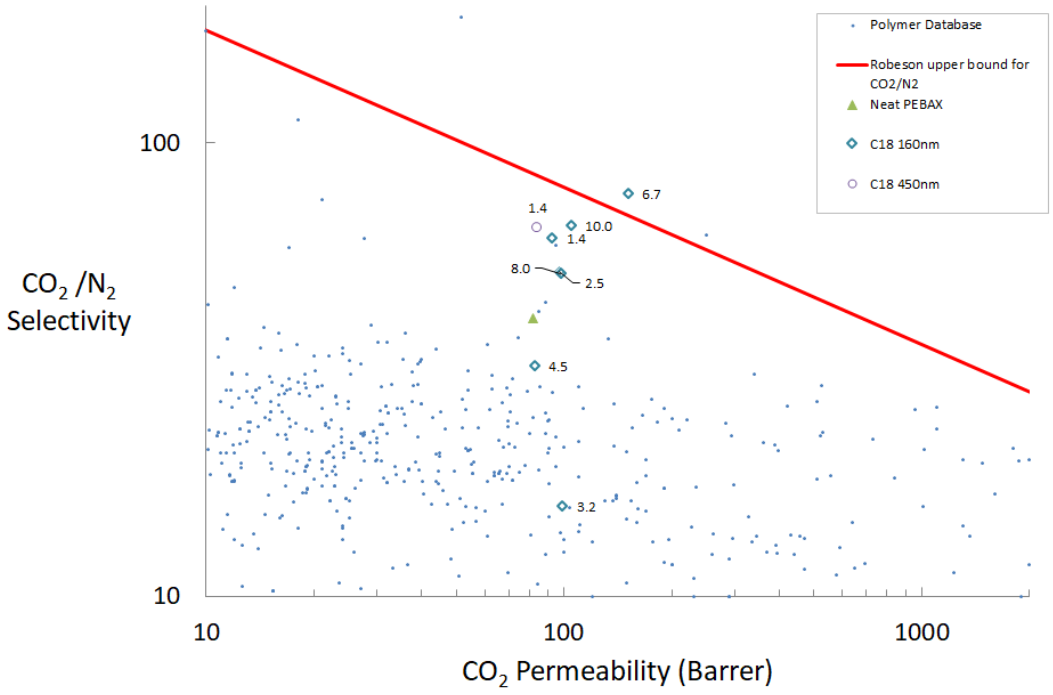

Figure 6.10: The experimental permeation test data for the 160 nm and 450 nm C18-MCM-41-HS-PEBAX membranes. The data labels are the loading by weight of the filler in each membrane.

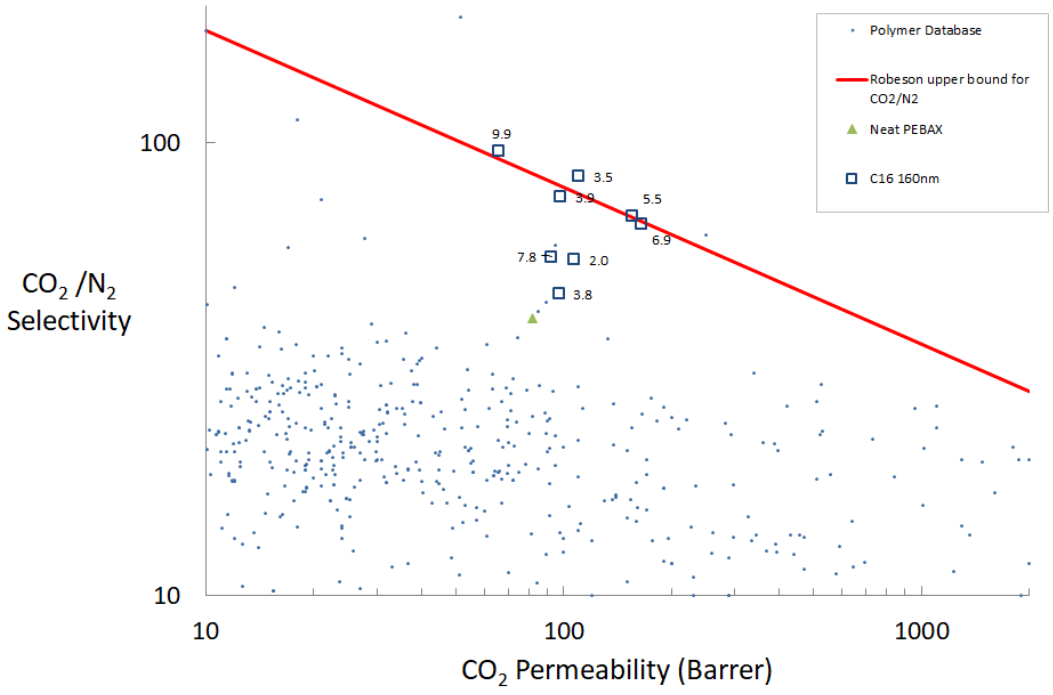

Figure 6.11: The experimental permeation test data for the 160 nm C16-MCM-41-HS-PEBAX membranes. The data labels are the loading by weight of the filler in each membrane.

Table 6.5: Results of the time-lag experiments for the 160 nm C18-MCM-41-HS-PEBAX membranes. All experiments were run at 1 bar upstream pressure.

Loading (wt.%)	Thickness (μm)	Gas	Temperature (°C)	Permeability coefficient (Barrer)	Diffusivity coefficient ($\times 10^{-8}$)
1.4	30	CO_2	35	90 ± 20	14 ± 5
		N_2	35	1.5 ± 0.3	10 ± 4
1.7[1]	35		-	-	-
2.5	31	CO_2	31	100 ± 20	1.6 ± 0.5
		N_2	31	1.9 ± 0.3	8 ± 3
3.2	43	CO_2	33	100 ± 10	27 ± 7
		N_2	33	6.3 ± 0.8	4 ± 1
4.5	25	CO_2	33	80 ± 20	11 ± 5
		N_2	33	2.6 ± 0.5	-[2]
6.1[1]			-	-	-
6.7	71	CO_2	32	150 ± 10	80 ± 10
		CO_2	32	160 ± 10	80 ± 10
		N_2	32	2.0 ± 0.2	44 ± 7
		N_2	32	1.9 ± 0.2	40 ± 6
8.0	42	CO_2	25	100 ± 10	50 ± 10
		CO_2	25	100 ± 10	50 ± 10
		N_2	25	1.9± 0.2	-[2]
		N_2	25	1.9 ± 0.2	-[2]
10.0	26	CO_2	25	110 ± 20	50 ± 30
		CO_2	25	100 ± 20	50 ± 30
		N_2	25	1.6 ± 0.3	-[2]

[1] Membrane possessed insufficient tensile strength to run time-lag experiments.
[2] Diffusivity could not be determined due to indiscernible time lag or due to 'kink' in flux as discussed in section 4.2.3.

Table 6.6: Results of the time-lag experiments for the 160 nm C16-MCM-41-HS-PEBAX membranes. All experiments were run at 1 bar upstream pressure.

Loading (wt.%)	Thickness (μm)	Gas	Temperature (°C)	Permeability coefficient (Barrer)	Diffusivity Coefficient ($\times 10^{-8}$)
2.0	35	CO_2	25	110 ± 10	60 ± 20
		N_2	25	1.9 ± 0.3	30 ± 10
		N_2	25	2.0 ± 0.3	-[2]
3.5	34	CO_2	25	110 ± 10	70 ± 40
		CO_2	25	110 ± 10	70 ± 30
		N_2	25	1.0 ± 0.1	-[2]
		N_2	25	1.7 ± 0.3	13 ± 4
3.8	34	CO_2	25	100 ± 20	28 ± 9
		CO_2	25	90 ± 10	30 ± 10
		N_2	27	1.9 ± 0.3	-[2]
		N_2	26	2.3 ± 0.3	-[2]
3.9	31	CO_2	25	100 ± 10	70 ± 40
		N_2	25	1.3 ± 0.2	-[2]
5.5	47	CO_2	25	150 ± 10	100 ± 30
		CO_2	25	160 ± 20	90 ± 30
		N_2	25	2.3 ± 0.3	9 ± 2
6.9	95	CO_2	25	170 ± 10	110 ± 10.0
		CO_2	25	170 ± 10	-[2]
		N_2	25	2.7 ± 0.2	-[2]
		N_2	25	2.3 ± 0.1	-[2]
7.8[1]	32	CO_2	25	100 ± 20	50 ± 20
		N_2	25	47 ± 7	50 ± 20
7.8	32	CO_2	25	92 ± 10	40 ± 20
		N_2	25	1.7 ± 0.3	5 ± 2
		N_2	25	1.6 ± 0.3	30 ± 10
9.9	19[3]	CO_2	25	70 ± 20	20 ± 10
		N_2	25	0.7 ± 0.2	-[2]
	40[3]	CO_2	25	90 ± 10	-[2]

[1] The low selectivity was indicative of a defect and thus a separate area of the membrane was tested and found to posses a much higher selectivity.

[2] Diffusivity could not be determined due to indiscernible time lag or due to 'kink' in flux as discussed in section 4.2.3.

[3] The 9.9 wt.% membrane produced had a non uniform thickness and as such two differing areas of contrasting thickness were tested separately.

Table 6.7: Results of the time-lag experiments for the 450 nm C18-MCM-41-HS-PEBAX membranes. All experiments were run at 1 bar upstream pressure.

Loading (wt.%)	Thickness (μm)	Gas	Temperature (°C)	Permeability coefficient (Barrer)	Diffusivity Coefficient ($\times 10^{-8}$)
1.4	29	CO_2	32	80 ± 10	14 ± 5
		N_2	32	1.3 ± 0.2	-
3.0	36		-	-	-
3.1	41		-	-	-

[1] Membrane showed unrealistically high flux and selectivity of 1 in permeation tests indicative of a defect or hole.

[2] Diffusivity could not be determined due to indiscernible time lag or due to 'kink' in flux as discussed in section 4.2.3.

6.2.3 A comment on the transport in the hollow spheres

While the transport in the pores is likely governed by Knudsen diffusion, the transport mechanism in the centre of the spheres is less clear. Assuming at steady state, the partial pressure, or chemical potential, is a linear function of the position in the membrane and that the concentration of the diffusing species in the centre of the spheres is at equilibrium with the polymer phase, it can be inferred that the mean free path of gas molecules in the sphere centres increases across the membrane. This is more clearly represented by figure 6.12. This leads to the implication that the transport mechanism in the centre of the spheres changes across the thickness of the membrane.

It is pertinent to note that this does not betray the fundamental theory of the solution-diffusion mechanism in which the total pressure is constant throughout as it is only the partial pressure that is being considered in the centre of the hollow spheres and that the difference in pressure is accounted for by the mechanical pressure exerted by the spheres themselves. This hypothesis also relies on the assumption that the diffusing species in the centre of the sphere is at equilibrium with the polymer phase, something which may not be the case if surface barrier effects occur; given the high porosity of MCM-41 it is deemed unlikely this is the case but could not be confirmed without further information regarding the pore size distribution and density.

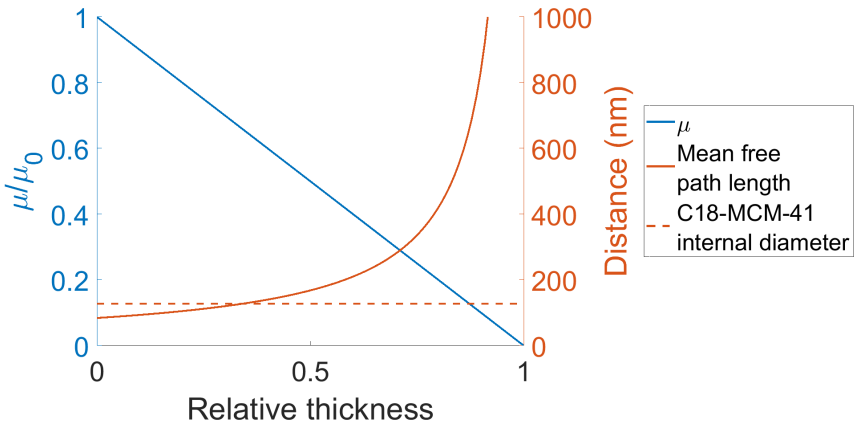

Figure 6.12: Hypothetical mean free path of desorbed gases and effective partial pressure across the membrane at steady-state.

6.3 Discussion

Similar to the ZIF-8 membranes the thicknesses of the MCM-41 hollow sphere membranes produced showed a high variance. As previously discussed in chapter 5 it is thought this is caused by variation in both the casting mixture and casting conditions affecting the viscosity of the solution and that the methodology must be refined to improve the control of these factors.

As mentioned previously in section 4.1.3 the preparation of the MCM-41-HS-PEBAX membranes utilised two different ultrasonic water bath models. Using different models was not desirable for consistency of preparation but was necessary due to equipment limitations. Neither the gas permeation results, nor the SEM images highlight any significant differences between the membranes produced by the two different models.

The CO_2 permeability coefficient of the 160 nm spheres broadly fit into two categories of 'low' permeable membranes with permeability coefficients slightly higher than that of PEBAX (82 to 111 Barrer) and the 'high' permeability outliers (all over 150 Barrer), two of which showed asymmetric distribution of particles and extensive closely packed particle networks. Given these three data points were all of similar loadings around 6 wt.% it is not impossible to postulate that there could be a link between the loading and these high permeability values. The exact cause of this mechanism is not clear and should be answered in future work.

As with the ZIF-8-PEBAX membranes, the densities of the membranes produced were not reported in this work. This work followed that of the study into ZIF-8 and by the point measuring the density was not an established protocol and was omitted due to simple oversight. In future work this should be carried out.

The SEM showed the distribution of the nanosized MCM-41 hollow spheres was generally homogeneous and the filler particles were singularly dispersed. The notable exceptions to this were the 6.7 wt.% C18-MCM-41 and the 6.9 wt.% C16-MCM-41 membranes which were shown to be highly asymmetric with a considerably higher particle density near one external face. While at low magnification these appeared to be clusters similar to the agglomerations seen in the ZIF-8 membranes, at higher magnification it could be seen that the polymer was well interspersed within these dense filler particle regions with only a few isolated voids as seen in the clusters in the 6.9 wt.% C16 sample in figure 6.4e. The morphology of these dense filler particle regions was distinctly different from the isolated clusters seen in the ZIF-8 and as such these features were more appropriately referred to as 'dense particles networks' to distinguish between the two. Within these dense particle networks it seems the proximity and contact of filler particles may simply be due to the loading in this region being close to the packing limit of spheres. While

clustering has been seen in other work utilising unmodified nanoscale MCM-41 in mixed matrix membranes,[176] it is possible the high degree of sphericity of the nanoparticles limits any inter-particle attraction as well as limiting the packing density, similar to what was suggested by Valero et al.[76]

It is speculated that the formation of these dense particle networks in the MCM-41-HS-PEBAX membranes could be due to the mobility of particles and the buoyancy of the hollow spheres due to their inherently low density. It is unclear why these networks would be seen in C16- and C18-MCM-41 membranes, both at similar intermediate filler loadings and neither at higher nor lower loadings. As previously discussed in the ZIF-8 chapter, it is hypothesised the viscosity of the casting solution plays an important role in determining the mobility of the filler.

The membranes in which these dense particle networks were observed reported considerably higher CO_2 permeabilities than the other membranes, around double that of neat PEBAX. Whereas in the ZIF-8 membranes the increase in permeability coefficient was attributed to the voids within the large clusters, here it is thought the proximity of individual filler particles in the dense particle networks allows for the formation of semi-percolating networks, here defined as a network through only part of the thickness of the membrane and subsequently facilitating faster transport through the centre of the hollow spheres. Interestingly the permeability coefficient of nitrogen in these particular membranes did not scale to the same degree.

The 5.5 wt.% and 6.9 wt.% C16-MCM-41-PEBAX membranes showed similarly high CO_2 permeability coefficients despite a clear difference in morphology. In comparison, the 6.9 wt.% sample was shown to be highly asymmetric with SEM, with a dense particle network composed of thousands of hollow spheres near the surface of the membrane. In contrast, the 5.5 wt.% sample was seen to be mostly symmetrical with groupings of perhaps one hundred particles at the most. Thus despite the similar CO_2 permeability coefficient, the morphology of the two was markedly different. It is plausible that the SEM is not necessarily representative given only a few millimetres of each sample could be imaged or that another morphological reason beyond the small groups of particles in the 5.5 wt.% membranes can be attributed to its high CO_2 permeability coefficient.

The thickness of the 9.9 wt.% membrane was not consistent and as such the two different areas (19 and 40 μm) were tested as separate samples. The thicker of the two showed a 28% higher CO_2 permeability coefficient. It is possible that the cause of the discrepancy is that the thickness measured with the micrometer is inaccurate, potentially due to large contaminants present in the membrane or variation in the thickness in the presence of clusters as seen in the ZIF-8 samples (see section 5.4).

The 6.1 wt.% C18-MCM-41-HS-PEBAX membrane presented with widespread voids throughout the cross-section of the membrane. This was the only sample

in which this was seen and also the only membrane which possessed insufficient tensile strength to be tested and the logical conclusion is that decreased contact within the polymer matrix led to a lower tensile strength. The origin of these voids is unclear. With the exception of this membrane the MCM-41 showed very good interaction with PEBAX with no voids seen at the polymer-filler interface and only few randomly located voids of around micron length-scales or smaller. The SEM images showed similarities to that of the work of Wu et. al[56] who also used the same grade of PEBAX with MCM-41 filler particles and saw good interaction between the two phases.

The 3.0 450 nm C18-MCM-41 PEBAX membranes showed strange annular-like structures (figure 6.5). One plausible explanation is that only the exterior filler particles in these groups were able to adhere well with the polymer, and whilst undergoing the polishing and grinding in preparation for SEM analysis, the more central spheres were less strongly bound and displaced. Why this would not have been seen in the other membranes is unclear. Another possible explanation is that these annular-like clusters are actually large MCM-41 hollow spheres damaged by the polishing and grinding process, leaving these fractured ring-like structures where the fragments give the appearance of being formed of numerous smaller particles. Given the diameter of these rings it seems much more likely that this is the case. This is further evidenced by the occurrence of clusters of these rings, which both detracts from the former hypothesis and supports the latter.

The diffusion through the shell pores is likely governed by Knudsen diffusion given the small pore sizes of 3.8 and 4.4 nm for the C16 and C18 hollow spheres respectively. Interestingly, due to the gradient in chemical potential across the membrane, it is thought the diffusion in the internal hollow of the spheres is thought to be Fickian near to the high pressure face of the membrane and at some point change to being governed by Knudsen diffusion, due to the change in the mean free path length of the gases. If there is any truth in this hypothesis, it could lead to the implication that the orientation of the asymmetric membranes plays a much more significant role than would usually be the case with typical mixed matrix membrane with non-hollow filler particles, and hence an interesting avenue of future work could be to intentionally fabricate asymmetric membranes by casting neat PEBAX onto pre-made MMMs and test the permeability relative to the orientation.

It was expected that addition of unmodified MCM-41 alone was unlikely to significantly improve the separation properties of PEBAX. MCM-41 itself shows a solubility selectivity less than that of PEBAX, and since the pore sizes would dictate that Knudsen diffusion is controlling, there would be negligible diffusivity selectivity due to their similar molecular masses of carbon dioxide and nitrogen. The potential benefit of the MCM-41 hollow sphere lies in their shape. As clearly demonstrated by the Robeson plots of the experimental gas permeation data, these

hollow materials can improve the properties in mixed matrix membranes. If the pores of such spheres could be made selective, the hollow spheres could then show even greater selectivity by permitting the transport of the more soluble species through their centres while creating a highly tortuous path for the less favourably admitted species.

As is discussed in section 2.2, estimates have been made using process design models on the required membrane material properties that would be required for carbon capture with membranes to be cost-competitive with the current frontrunner of carbon capture technology, absorption using amines. Roussanaly et al. showed that with a simple two-stage cascade system, a membrane process could economically rival absorption if the membrane had permeances of greater than 1100 gpu and selectivities of over 65. Considering the mixed matrix membrane which had the highest permeability out of all the MCM-41 based materials, estimates on the required thickness to achieve this permeance can be made. The 6.9 wt.% C16-MCM-41-HS-PEBAX MMM had a CO_2 permeability coefficient of 170 Barrer and an ideal selectivity of 68. While the selectivity does indeed meet the criteria, for this material to achieve a permeance of 1100 gpu, it would be required to have a maximum thickness of 0.15 µm. This is less than the diameter of the nanoparticles and thus is impossible that a membrane this thin could be fabricated with these materials. While membranes were produced that approached and even crossed the upper bound, the effect of adding the MCM-41 hollow spheres was to increase the selectivity and thus, these materials may well be better combined with more permeable polymers to increase the selectivity.

6.4 Conclusions and Future Work

- Scanning transmission electron microscopy confirmed the expected shape and morphology of the C16-MCM-41 and C18-MCM-41 hollow spheres.
- Novel nanoscale MCM-41 hollow spheres of with varying pore size and diameter were successfully combined with PEBAX to form mixed matrix membranes via the aforementioned method previously described in Chapter 4.
- The thicknesses of the membranes produced were inconsistent varying from 25 to 95 µm.
- SEM showed the dispersion of the MCM-41 hollow spheres was generally homogeneous and particles were well distributed. Prominent dense particle networks and asymmetry were seen in only two samples of intermediate filler loading: 6.7 wt.% C18-MCM-41-PEBAX and 6.9 wt.% C16-MCM-41-PEBAX.
- SEM elucidated the generally good adhesion between PEBAX MH1657 and MCM-41 hollow spheres.
- Widespread nanoscale voids were seen throughout the cross-section of the membrane the 6.1 wt.% C18-MCM-41-HS-PEBAX membrane which explained its low tensile strength.
- The variation in pore size between the C16- and C18-MCM-41 had minimal effect on the morphology or gas transport of the mixed matrix membranes.
- The 3.0 wt.% 450 nm, prepared for SEM imaging via resin coating, and grinding and polishing, as opposed to fracturing in liquid nitrogen, appeared to show fractured spheres, almost certainly damaged by this alternate method of preparation, highlighting it is not a suitable method of preparation for such materials.
- The permeation coefficients of the MCM-41 hollow sphere PEBAX membranes did not show the same trend as previous work carried out by Wu et. al[56] which also looked at the inclusion of MCM-41 in PEBAX. Given the different shape and pore size of the MCM-41 used in this and literature this is not unexpected.
- It was calculated that using the most permeable MCM-41-HS-PEBAX membrane produced in this work, to meet the material specifications of minimum permeance and selectivity outlined by Roussanaly et al.[74] for membrane carbon capture to rival absorption based technology, the membrane would need to be thinner than the diameter of the nanoparticles and thus virtually impossible to fabricate.

While the results here were far from conclusive, the materials presented show features that ask interesting further questions. Continuing the work of the different diameter hollow spheres could well shine light on the idea of the transport mechanism within the centre of the hollow spheres. This would not only alter the internal diameter of the spheres but it would also change the surface area which, assuming a constant pore density, would alter the number of pores per hollow centre and could therefore be used to investigate any surface barrier effects. This could further be investigated by creating asymmetrical membranes and testing the gas flux dependent on the orientation of the membrane.

Modification of the MCM-41 to narrow the pores could greatly improve the selectivity of the spheres by creating a molecular sieving structure. Functionalisation of the MCM-41 with amines could also show improvements in the selectivity by favouring the transport of CO_2 through the centre of the spheres by virtue of an improved affinity for the filler material.

The combination of MCM-41 hollow spheres in a selective polymer did not have the hoped effect of increasing permeability. In future work these MCM-41-HS fillers should be combined with more permeable polymers.

Chapter 7

Conclusions and Future Work

Carbon capture from large point sources such as coal power stations has been shown to be one of the most cost-effective methods to limit further carbon dioxide emissions in the near future. The current most-developed technology for carbon capture is absorption using amine-based solvents. It has been demonstrated using process simulations that for membrane separation technology to be cost-competitive with amine-based absorption, new membrane materials with higher permeabilities and selectivities should be developed to lessen the financial and energetic costs of the process.

In this study the goal was to develop PEBAX-based mixed matrix membranes for carbon capture applications using novel nanoscale fillers to further develop the understanding of the morphology and gas-transport properties of such materials. PEBAX is a polymer with an inherently high selectivity and so the general approach was to try to increase the permeability of PEBAX using nanoscale fillers. To achieve this goal mixed matrix membranes were successfully developed using two types of nanoscale filler materials: ZIF-8, a type of metal organic framework, and MCM-41 hollow spheres, an ordered mesoporous silica with a hollow sphere geometry and a highly tunable pore structure.

A method of reliably fabricating mixed matrix membranes using PEBAX and the above fillers was successfully developed based on methods from previous literature and observational refinement. The method was not however 100 % reliable and there was notable variation in the thicknesses of membranes produced. This was attributed to variations in the casting conditions such as ambient temperature, humidity and precise control of the casting solution.

The materials were then subsequently characterised primarily using scanning electron microscopy to investigate their morphology and their gas transport properties

successfully determined using a constant volume-variable pressure apparatus.

In the investigation of using ZIF-8 as a filler in PEBAX, both ZIF-8 and a modified ZIF-8 sample were used. The investigation of the morphology highlighted the tendency of the ZIF-8 nanoparticles to form clusters in the ZIF-8-PEBAX membranes at weight loadings above 5 wt.%. Below this loading, the ZIF-8 nanoparticles were homogeneously dispersed as single particles. Good interfacial interactions between PEBAX MH1657 and ZIF-8 were observed showing minimal signs of voids at the polymer-filler interface. Morphological observations led to the hypothesis that the clusters seen in the membranes above 5 wt.% ZIF-8 form during the drying phase of the MMM synthesis, and that the particles are mobile during this phase due to recirculation of the solvent-polymer mixture, caused by local thermal gradients created by evaporating solvent. Predictions of the gas transport properties were calculated using adsorption and diffusivity data of carbon dioxide and nitrogen in ZIF-8 from literature with the ideal Maxwell and Bruggeman models. The gas permeation properties of the ZIF-8 membranes could mostly be explained by the morphology. Below 5 wt.% modest increases in carbon dioxide permeability were closely matched by the permeability coefficients predicted by the ideal models, indicative of ideal behaviour with minimal interfacial defects. This agreed with the morphology observed. The nitrogen permeability coefficient decreased with increasing loading up to 5 wt.% resulting in one highly selective membrane at 4.4 wt.% ZIF-8. This membrane had an ideal selectivity of over 100 and when plotted on a Robeson graph, was above the upper bound. The decrease in nitrogen permeability over the zero to 5 wt.% loading could not be matched by the ideal Maxwell and Bruggeman models even when the filler was modelled as being totally impermeable and it was not clear from the morphology the exact reason for this decrease. Above 5 wt.% loading in the ZIF-8-PEBAX mixed matrix membranes the permeabilities of both gases saw a sharp increase which resulted in decreasing values of ideal selectivity. This could be explained by the presence of the voids that were observed within the clusters.

In an attempt to reduce this clustering a modified ZIF-8 sample was used in conjunction with PEBAX. The ZIF-8 was modified using a high pressure, wet impregnation method using ethylenediamine (ED) by collaborators at Deakin University, Australia. It was expected that the addition of the amine to the ZIF-8 would increase the interaction between the ED-ZIF-8 and the polar groups in the PEBAX. Four mixed matrix membranes formed using ED-ZIF-8 and PEBAX were synthesised up to 12.5 wt.% loadings. This approach was unsuccessful in improving the dispersion of nanoparticles in PEBAX and significant agglomeration of the ED-ZIF-8 nanoparticles was observed using SEM. Significant cracks and voids were also observed within the agglomerations in the ED-ZIF-8-PEBAX mixed matrix membranes. This morphology had the expected effect on the gas permeation

results: as the loading of ED-ZIF-8 increased the permeability coefficients of both gases rose considerably with significant losses in selectivity due to voids. As shown on a Robeson plot, these membranes moved away from the upper bound, which is undesirable for membrane separations. The 12.5 wt.% had an ideal CO_2/N_2 selectivity approaching 1.

While the results with the ED-ZIF-8 did not meet expectations, the unmodified ZIF-8 demonstrated its potential as a filler for the carbon dioxide-nitrogen separation. When the nanoparticles were well dispersed they contributed notably to the selectivity of the composite materials. Future work in these materials should look to improve the dispersion of ZIF-8 so that higher loadings can be accommodated within the polymer matrix without forming voids. Given the ZIF-8 increased the selectivity when ideal interface morphology was observed, it may be more appropriate to incorporate the ZIF-8 nanoparticles into a high permeability polymer.

Three variations of novel MCM-41 hollow spheres (MCM-41-HS) were incorporated into PEBAX in a similar attempt to increase the carbon dioxide permeability coefficient of the composite materials. The three variations of MCM-41-HS were: 160 nm diameter C16-MCM-41-HS with a pore diameter of 3.8 nm, 160 nm diameter C18-MCM-41-HS (pore diameter 4.4 nm) and 450 nm diameter C18-MCM-41-HS (pore diameter 4.4 nm). Multiple mixed matrix membranes were successfully synthesised using the two smaller diameter hollow spheres up to loadings of 10 wt.%. Only one membrane with the larger 450 nm diameter was successfully synthesised and tested.

The investigation into the morphology of the MCM-41-HS-PEBAX membranes generally showed homogeneous dispersion of single hollow spheres across the range of loadings. However in both the 160 nm C16- and C18-MCM-41-HS-PEBAX membranes, at intermediate loadings between 5 and 7 wt.% asymmetry in the distribution of particles was observed with regions of high particle density occurring near one face of the membrane. These membranes coincided with the highest CO_2 gas permeabilities. A model was proposed to describe the transport of gases within the hollow spheres. Despite MCM-41 as a material showing little adsorption or diffusivity-based selectivity for CO_2 over N_2, all of the 160 nm C16-MCM-41-HS-PEBAX membranes reported higher selectivities than neat PEBAX, with 5 out of 8 of these sample displaying properties close to the Robeson upper bound. The maximum CO_2 permeability observed in the MCM-41-HS-PEBAX membranes was 170 Barrer in the 6.9 wt.% 160 nm C16-MCM-41-HS-PEBAX, over double that of neat PEBAX. Using values from literature outlining the permeance and selectivity requirements for economical capture using membranes it was calculated that these materials would need to be produced with a maximum thickness of 150 nm. This value is smaller than that of the diameter of the hollow sphere nanoparticles and thus a membrane so thin would be virtually impossible to produce.

Due to the fact that only a single 450 nm C18-MCM-41-HS-PEBAX membrane was produced the influence of the sphere diameter could not be observed. There was little difference between the CO_2 permeability trends of the 160 nm C16 and C18 samples, although the selectivities of these C16 samples were all higher than those of the 160 nm C18 membranes possibly suggesting the smaller pore size (3.8 vs 4.4 nm) improves selectivity.

Similar to the ZIF-8, the addition of the MCM-41 hollow spheres appeared to improve the selectivity of the composite membrane materials. Thus it is proposed that these should be combined with high permeability polymers such as PIM-1, or PIM-EA-TB, which report permeabilities over 3000 and 7000 respectively[216] but suffer from low selectivities of around 20. This approach could well yield similar improvements in selectivity but with already high-CO_2-permeability membranes. These materials that posses CO_2 permeabilities in the thousands of Barrer may well be more suited to the large flow rates of flue gas produced by a power plant which must be processed.

The investigation into the morphology which suggested that the nanoparticles could be mobile during the drying phase highlights the necessity in the field of mixed matrix membrane to better understand the fluid dynamics and rheology of the casting solutions. In current studies of mixed matrix membranes, the synthesis is often investigated insofar as solvent choice and rarely described with total clarity, and little mention to rheology is given. By further understanding these topics, distribution of filler particles can be better controlled, probably leading to thinner, stronger membranes with better dispersed filler particles. Thus future topics could include determining the dynamic change in viscosity during the drying phase, or to study the influence of nanoparticle loadings on the rheology of polymer solutions. Additionally, many studies in which mixed matrix membranes are synthesised often involve some degree of ultrasonication to break up or deter agglomerations of nanoparticles. But rarely are the specific influences of the ultrasound on the dispersion of nanoparticles determined prior to membrane synthesis.

Several of the composite membranes produced in this study did approach and cross the upper bound, although none of these 'high-performing' membranes possessed sufficiently high permeabilities that could facilitate economical carbon capture using membranes. This study did however successfully implement one of the first studies investigating PEBAX and nanoscale ZIF-8 for carbon capture purposes, showing that high performing membranes with properties above the Robeson upper bound can be produced when the nanoparticles are well dispersed. This study further successfully demonstrated the inclusion of novel MCM-41 hollow spheres in PEBAX to produce mixed matrix membranes, what is thought to be the first of a kind study into MCM-41 in this geometry. Novel evidence of filler particle mobility was also found during the drying phase, suggesting that casting fluid rheology could

well be a promising area of future work.

Appendix A

Calibration of the Constant-Volume Variable Pressure Apparatus

Prior to running experiments with the time-lag apparatus, the volumes of the downstream were calibrated. This was achieved by connecting a closed, one litre volume to the upstream side of the membrane cell and by creating a difference in pressure between the known and downstream volumes and recording the pressure change prior to, and post, equilibrium, the volume of the downstream could be calculated utilising the ideal gas law. The downstream contained three sections: the tubing, the small volume (quoted as 50 cm^3), and the large volume (quoted as 150 cm^3), and thus could be utilised as four different arrangements:

1. the tubing,
2. the tubing plus the small volume,
3. the tubing plus the large volume,
4. the tubing plus both volumes.

Figure A.1 shows a schematic of the apparatus used. A 1 litre ($\pm$ 5 %) volumes was connected via a short length of tubing and a ball valve. A 1 litre volume was used such that it was relatively large compared to the volume of the connecting tubing, minimising the additional uncertainty of the volume of tubing.

The following steps were followed to determine the volume; it was assumed that the pressure in the known volume remained the same when closed.

1. With only the line to the vacuum isolated and all other valves open, the system was filled with nitrogen and the pressure recorded, denoted P_2.

Figure A.1: Schematic showing the setup used to determine the volumes of the downstream volumes.

2. Valve 1 was closed, isolating the known volume and the rest of the system was evacuated for a short time, following which valve 2 was closed, isolating the downstream and the pressure was recorded, denoted P_1.
3. Valve 1 was then opened and the pressure was allowed to reach equilibrium before being recorded, denoted P_{eq}.
4. Steps 2 and 3 were repeated 2-4 times, until insufficient gas remained and then step 1 was carried out to refill the system.

These steps could also be performed by evacuating the whole system and then conversely filling the downstream section with gas. By controlling which valves were open, the different downstream regions could be isolated. Equation A.1 was then used to determine the volume of interest.

$$V_1 = V_2 \frac{P_{eq} - P_2}{P_1 - P_{eq}} \tag{A.1}$$

Table A.1 shows the results of the tests using the attached known volume. The results were highly reproducible and the standard error of the readings well below that of the quoted uncertainty in the known volume of 5%.

All of the volumes determined in table A.1 include a small section of tubing on the upstream side of the cell connecting the attached volume to the cell. Once the volumes of the various sections were known the attached volume could be removed and the valve shut and the experiments repeated using the internal volumes of the downstream and then again with a foil seal in the cell to determine the volume of tubing attached such that it could be subtracted from the other volumes. The results of these tests are shown in table A.2. Finally a summary of the volumes of all four configurations of the downstream are shown in table A.3.

Table A.1: Calibration data

P_1 (mBar)	P_2 (mBar)	Calculated volume (cm^3)
Volume 1: All volumes + conn.; Volume 2: Litre volume		
2.02	1005	231
2.03	1005	231
1.98	1005	230
2.06	1005	231
	Average ± standard error	**231 ± 0.046588831**
Volume 1: Tubing + conn.; Volume 2: Litre volume		
2.02	1005	32
2.02	1005	32
2.03	973	32
2.00	942	32
	Average ± standard error	**32.8 ± 0.01**
Volume 1: Tubing + conn.; Volume 2: Litre volume		
545	0.02	32.8
348	17.3	32.7
722	-0.37	32.9
	Average ± standard error	**32.8 ± 0.04**
Volume 1: Tubing + small volume + conn.; Volume 2: Litre volume		
387	2.96	84.5
455	-0.52	84.6
428	1.81	84.4
	Average ± standard error	**84.5 ± 0.04**
Volume 1: Tubing + large volume + conn.; Volume 2: Litre volume		
361	22.7	181
651	74.3	180
1011	162.4	181
	Average ± standard error	**181 ± 0.32**

Table A.2: Calibration data

P_1 (mBar)	P_2 (mBar)	Calculated volume (cm^3)
Volume 1: Tubing + conn.; Volume 2: Small volume + large volume		
2.02	1004.72	32.8
2.03	862.44	32.7
2.05	1004.6	32.8
2.01	862.11	32.7
2.01	740.3	32.7
2.01	1004.45	32.8
2.02	862.25	32.7
2.01	740.34	32.7
2.02	635.83	32.7
2.00	1004.43	32.8
	Average ± standard error	**32.8 ± 0.01**
Volume 1: Tubing; Volume 2: Small volume + large volume		
1.5	1008	25.0
1.5	895	24.9
1.0	795	24.9
1.3	707	24.9
1.4	628	24.8
1.3	558	24.8
1.4	496	24.8
1.3	441	24.8
1.5	392	24.8
1.3	349	24.8
	Average ± standard error	**24.8 ± 0.02**

Table A.3: Volumes of volumes

Volume	Volume (cm^3)
Tubing	24.8
Small (inc. tubing)	76.5
Large (inc. tubing)	173
Both (inc. tubing)	223

Appendix B

Zeolite 13X in PEBAX

This work was undertaken primarily as a preliminary 'proof-of-concept' type study to establish and refine the method of fabricating mixed matrix membranes with PEBAX and the subsequent gas permeation tests. Zeolite 13X was used as a filler due to its well known high CO_2 capacity and immediate availability at the time of testing.

Preliminary fabrications of neat PEBAX with 2 wt.% polymer in a 70:30 ethanol:water solvent mixture yielded thin membranes with thicknesses of 20 $\pm$ 5 µm. These membranes were highly fragile and difficult to handle without breaking and thus test in the time-lag apparatus. Subsequently higher polymer concentration casting solutions were tested before deciding on the 1:15 polymer:solvent with the solvent being 70:30 ethanol:water by weight.

Three zeolite 13X-PEBAX membranes were successfully synthesised using a procedure similar to that outlined in chapter 4 of 5, 10 and 15 wt.% loading. Instead of using an ultrasonic water bath, however, the filler particles were added after drying in an oven for two hours and then a Waring blender was used for 30 seconds to ensure the casting mixture was homogeneously mixed.

SEM analysis of the materials was carried out by analytical technicians utilising the SEM facilities at JMTC. Figure B.1 shows representative cross-sections of the images taken. High resolution versions can be found in the supplementary electronic files.

Time-lag results were carried out the results of which can be seen in figure B.2. The 5 wt.% membrane was found to be not selective which was indicative of a small crack or hole. A linear increase in CO_2 permeability was observed with neat PEBAX and the 10 and 15 wt.% membranes. The 10 wt.% membrane had the

lowest ideal selectivity which was counterintuitive given the SEM showed it did not possess any voids.

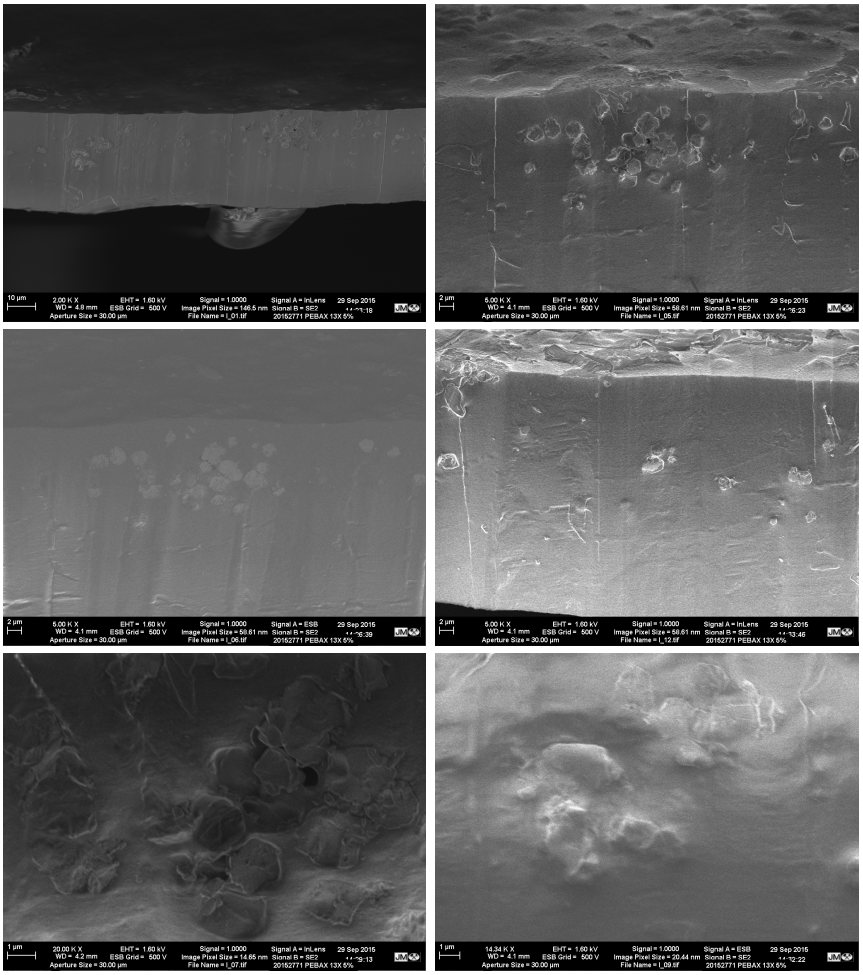

(a) 5wt.%

Figure B.1: SEM images of 13X-PEBAX membranes.

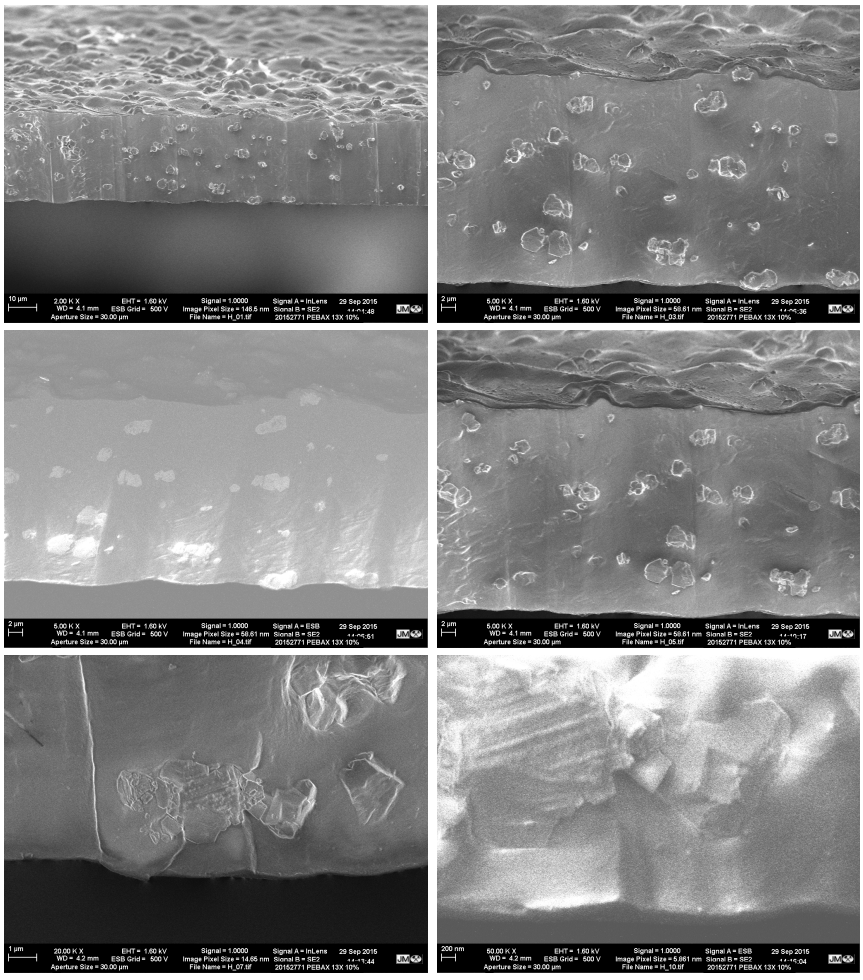

(b) 10wt.%

Figure B.1: SEM images of 13X-PEBAX membranes.

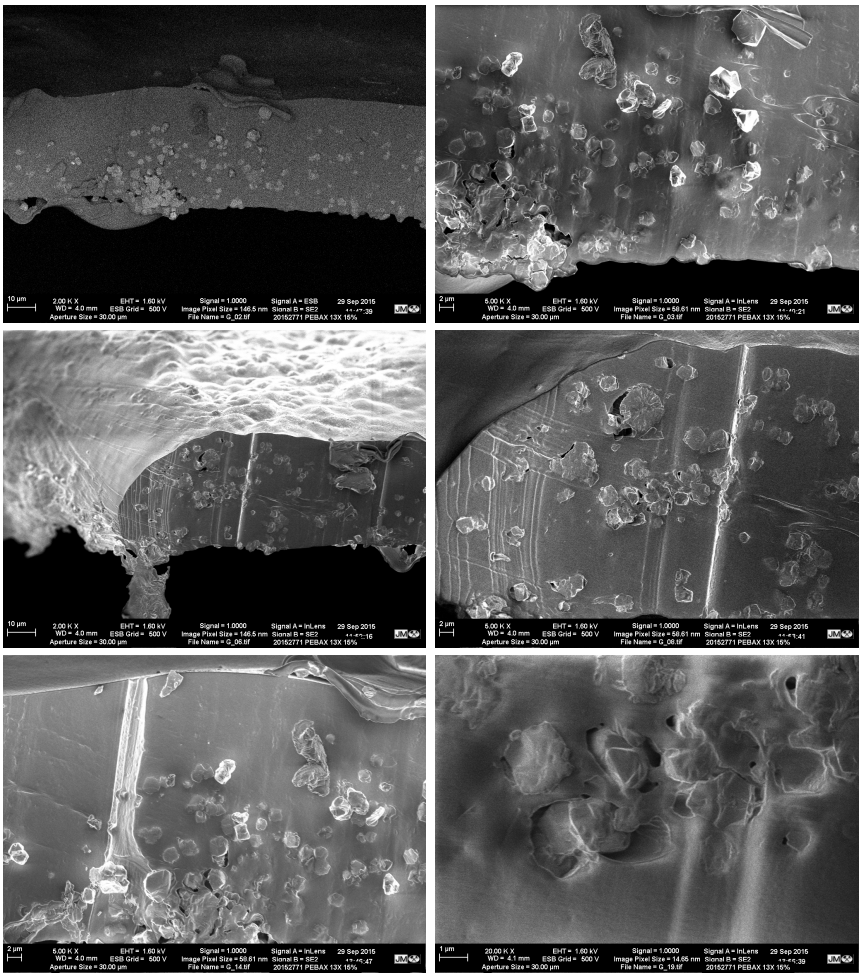

(c) 15wt.%

Figure B.1: SEM images of 13X-PEBAX membranes.

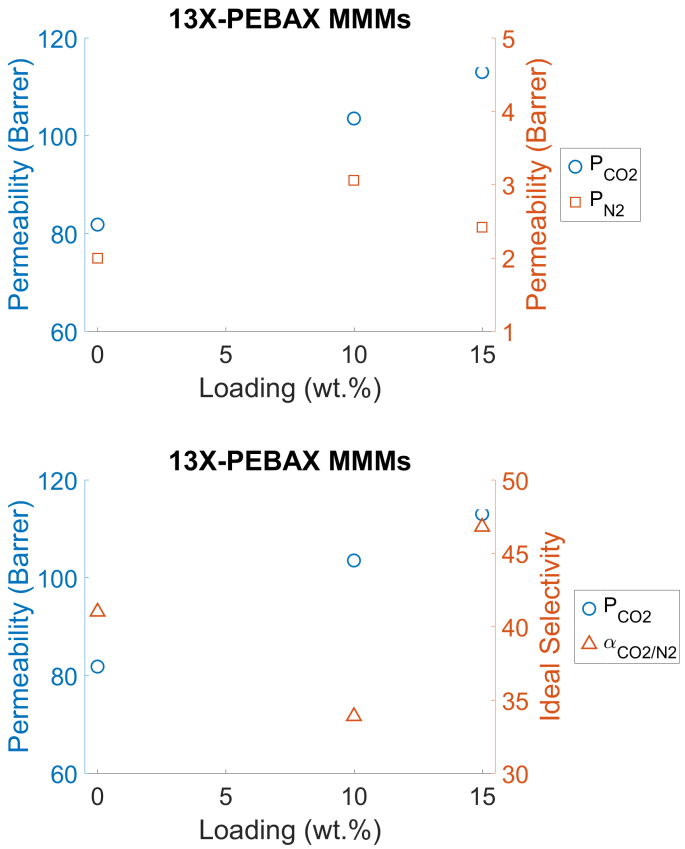

Figure B.2: The CO_2 and N_2 permeability coefficient data, and the ideal CO_2/N_2 selectivity of the zeolite 13X-PEBAX mixed matrix membranes.

References

[1] IPCC, *Climate Change 2007 Synthesis Report*. IPCC, 2008.

[2] M. Esham and C. Garforth, "Agricultural adaptation to climate change: Insights from a farming community in Sri Lanka," *Mitigation and Adaptation Strategies for Global Change*, vol. 18, no. 5, pp. 535–549, 2013.

[3] L. Mudd, Y. Wang, C. Letchford, and D. Rosowsky, "Hurricane wind hazard assessment for a rapidly warming climate scenario," *Journal of Wind Engineering and Industrial Aerodynamics*, vol. 133, pp. 242–249, 2014.

[4] C. Schannwell, N. E. Barrand, and V. Radi??, "Future sea-level rise from tidewater and ice-shelf tributary glaciers of the Antarctic Peninsula," *Earth and Planetary Science Letters*, vol. 453, pp. 161–170, 2016.

[5] IPCC, *Managing the risks of extreme events and disasters to advance climate change adaptation*. Cambridge University Press, 2012.

[6] G. J. van Oldenborgh, K. van der Wiel, A. Sebastian, R. Singh, J. Arrighi, F. Otto, K. Haustein, S. Li, G. Vecchi, and H. Cullen, "Attribution of extreme rainfall from Hurricane Harvey, August 2017," *Environmental Research Letters*, vol. 12, no. 12, p. 124009, 2017.

[7] P. A. Stott, D. A. Stone, and M. R. Allen, "Human contribution to the European heatwave of 2003 Peter," *Nature*, vol. 432, 2004.

[8] D. J. Hartmann, A. M. G. Klein Tank, M. Rusticucci, L. V. Alexander, S. Brönnimann, Y. A. R. Charabi, F. J. Dentener, E. J. Dlugokencky, D. R. Easterling, A. Kaplan, B. J. Soden, P. W. Thorne, M. Wild, and P. Zhai, "Observations: Atmosphere and Surface," *Climate Change 2013: The Physical Science Basis. Contribution of Working Group I to the Fifth Assessment Report of the Intergovernmental Panel on Climate Change*, pp. 159–254, 2013.

[9] B. Marzeion, J. G. Cogley, K. Richter, and D. Parkes, "Attribution of global glacier mass loss to anthropogenic and natural causes," *Science*, vol. 345, no. 6199, pp. 919–921, 2014.

[10] K. Hille, "2016 Climate Trends Continue to Break Records," 2016.

[11] J. Hansen, R. Ruedy, M. Sato, and K. Lo, "Global surface temperature change," *Rev. Geophys.*, vol. 48, no. 4, p. RG4004, 2010.

[12] GISTEMP Team, "GISS Surface Temperature Analysis (GISTEMP)," 2016.

[13] T. Crowther, K. Todd-Brown, C. Rowe, W. Wieder, J. Carey, M. Machmuller, L. Snoek, S. Fang, G. Zhou, S. Allison, J. Blair, S. Bridgham, A. Burton, Y. Carrillo, P. Reich, J. Clark, A. Classen, F. Dijkstra, B. Elberling, B. Emmett, M. Estiarte, S. Frey, J. Guo, J. Harte, L. Jiang, B. Johnson, G. Kröel-Dulay, K. Larsen, H. Laudon, J. Lavallee, Y. Luo, M. Lupascu, L. Ma, S. Marhan, A. Michelsen, J. Mohan, S. Niu, E. Pendall, J. Penuelas, L. Pfeifer-Meister, C. Poll, S. Reinsch, L. Reynolds, I. Schmidth, S. Sistla, N. Sokol, P. Templer, K. Treseder, J. Welker, and M. Bradford, "Quantifying global soil carbon losses in response to warming," *Nature*, 2016.

[14] Arctic Council, G. Peterson, and J. C. Rocha, "Arctic Resilience Report Chapter 3," tech. rep., Stockholm Environment Institute and Stockholm Resilience Centre, 2016.

[15] G. Myhre, D. Shindell, F.-M. Bréon, W. Collins, J. Fuglestvedt, J. Huang, D. Koch, J.-F. Lamarque, D. Lee, B. Mendoza, T. Nakajima, A. Robock, G. Stephens, T. Takemura, and H. Zhang, "Anthropogenic and Natural Radiative Forcing," *Climate Change 2013: The Physical Science Basis. Contribution of Working Group I to the Fifth Assessment Report of the Intergovernmental Panel on Climate Change*, pp. 659–740, 2013.

[16] IPCC, "Climate Change 2007 The Physical Science Basis. Contribution of Working Group I to the Fourth Assessment Report of the Intergovernmental Panel on Climate Change," tech. rep., IPCC, 2007.

[17] NOAA, "Monthly mean atmospheric carbon dioxide at Mauna Loa Observatory, Hawaii," 2016.

[18] UNFCCC, "Entry into force," 2016.

[19] United Nations/Framework Convention on Climate Change, "Paris Agreement," *21st Conference of the Parties*, p. 3, 2015.

[20] R. McKie, "Scientists warn world will miss key climate target," 2016.

[21] International Energy Agency, "World Energy Outlook," tech. rep., IEA, 2016.

[22] S. L'Orange Seigo, S. Dohle, and M. Siegrist, "Public perception of carbon capture and storage (CCS): A review," *Renewable and Sustainable Energy Reviews*, vol. 38, pp. 848–863, 2014.

[23] R. Oxburgh, "Lowest cost decarbonisation for the UK: The critical role of CCS. Report to the Secretary of State for Business, Energy and Industrial Strategy from the Parliamentary Advisory Group on Carbon Capture and Storage (CCS).," Tech. Rep. September, Parliamentary Advisory Group on CCS, 2016.

[24] D. Clarke and ETI, "Letter to Angus Neil MP," 2015.

[25] IEA and OECD, "Energy Technology Perspectives 2010," tech. rep., IEA, 2010.

[26] M. E. Boot-Handford, J. C. Abanades, E. J. Anthony, M. J. Blunt, S. Brandani, N. Mac Dowell, J. R. Fernandez, M.-C. M.-C. Ferrari, R. Gross, J. P. Hallett, R. S. Haszeldine, P. Heptonstall, A. Lyngfelt, Z. Makuch, E. Mangano, R. T. J. Porter, M. Pourkashanian, G. T. Rochelle, N. Shah, J. G. Yao, P. S. Fennell, J. R. Fernández, M.-C. M.-C. Ferrari, R. Gross, J. P. Hallett, R. S. Haszeldine, P. Heptonstall, A. Lyngfelt, Z. Makuch, E. Mangano, R. T. J. Porter, M. Pourkashanian, G. T. Rochelle, N. Shah, J. G. Yao, and P. S. Fennell, "Carbon capture and storage update," *Energy & Environmental Science*, vol. 7, no. 1, pp. 130–189, 2014.

[27] R. S. Haszeldine, "Carbon capture and storage. How Green Can Black Be?," *Science*, vol. 325, no. 5948, pp. 1647–1652, 2009.

[28] M. Kanniche, R. Gros-Bonnivard, P. Jaud, J. Valle-Marcos, J. M. Amann, and C. Bouallou, "Pre-combustion, post-combustion and oxy-combustion in thermal power plant for CO2 capture," *Applied Thermal Engineering*, vol. 30, no. 1, pp. 53–62, 2010.

[29] T. C. Merkel, H. Lin, X. Wei, and R. Baker, "Power plant post-combustion carbon dioxide capture: An opportunity for membranes," *Journal of Membrane Science*, vol. 359, no. 1-2, pp. 126–139, 2010.

[30] C. Kunze and H. Spliethoff, "Assessment of oxy-fuel, pre- and post-combustion-based carbon capture for future IGCC plants," *Applied Energy*, vol. 94, pp. 109–116, 2012.

[31] BP, "BP Statistical Review of World Energy - Full report," Tech. Rep. June, BP, 2016.

[32] R. Khalilpour, K. Mumford, H. Zhai, A. Abbas, G. Stevens, and E. S. Rubin, "Membrane-based carbon capture from flue gas: A review," *Journal of Cleaner Production*, vol. 103, pp. 286–300, 2015.

[33] SaskPower, "Boundary Dam Carbon Capture Project Fact Sheet," 2014.

[34] K. Stéphenne, "Start-up of world's first commercial post-combustion coal fired ccs project: Contribution of shell cansolv to saskpower boundary dam iccs project," *Energy Procedia*, vol. 63, pp. 6106–6110, 2014.

[35] L. M. Romeo, I. Bolea, and J. M. Escosa, "Integration of power plant and amine scrubbing to reduce CO2 capture costs," *Applied Thermal Engineering*, vol. 28, no. 8-9, pp. 1039–1046, 2008.

[36] M. T. Ho, G. W. Allinson, and D. E. Wiley, "Reducing the Cost of CO2 Capture from Flue Gases Using Pressure Swing Adsorption," *Industrial & Engineering Chemistry Research*, vol. 47, no. 14, pp. 4883–4890, 2008.

[37] M. Lucquiaud and J. Gibbins, "Retrofitting {CO2} capture ready fossil plants with post-combustion capture. Part 1: Requirements for supercritical pulverized coal plants using solvent-based flue gas scrubbing," *Proceedings of the Institution of Mechanical Engineers, Part A: Journal of Power and Energy*, vol. 223, no. 3, pp. 213–226, 2009.

[38] D. Aaron and C. Tsouris, "Separation of CO2 from Flue Gas: A Review," *Separation Science and Technology*, vol. 40, no. 1, pp. 321–348, 2005.

[39] J. Blamey, E. J. Anthony, J. Wang, and P. S. Fennell, "The calcium looping cycle for large-scale CO2 capture," *Progress in Energy and Combustion Science*, vol. 36, no. 2, pp. 260–279, 2010.

[40] T. C. Merkel, M. Zhou, and R. W. Baker, "Carbon dioxide capture with membranes at an IGCC power plant," *Journal of Membrane Science*, vol. 389, pp. 441–450, feb 2012.

[41] A. Brunetti, E. Drioli, Y. M. Lee, and G. Barbieri, "Engineering evaluation of CO2 separation by membrane gas separation systems," *Journal of Membrane Science*, vol. 454, pp. 305–315, mar 2014.

[42] R. Baker, *Membrane technology and applications*. John Wiley & Sons, 2nd ed., 2004.

[43] R. Spillman, "Economics of gas separation membrane processes," *Membrane Separations Technology. Principle and Applications*, 1995.

[44] MTR, "NITROGEN REMOVAL FROM NATURAL GAS: NITROSEP™."

[45] MTR, "CO2 Removal From Natural Gas."

[46] Fujifilm, "Gas Membrane — Apura™ Gas Separation Membrane Element."

[47] L. Zhao, E. Riensche, L. Blum, and D. Stolten, "Multi-stage gas separation membrane processes used in post-combustion capture: Energetic and economic analyses," *Journal of Membrane Science*, vol. 359, no. 1–2, pp. 160–172, 2010.

[48] X. Zhang, X. He, and T. Gundersen, "Post-combustion carbon capture with a gas separation membrane: Parametric study, capture cost, and exergy analysis," *Energy and Fuels*, vol. 27, no. 8, pp. 4137–4149, 2013.

[49] W. J. Koros and R. Mahajan, "Pushing the limits on possibilities for large scale gas separation: Which strategies?," *Journal of Membrane Science*, vol. 181, no. 1, p. 141, 2001.

[50] L. M. Robeson, "Correlation of separation factor versus permeability for polymeric membranes," *Journal of Membrane Science*, vol. 62, no. 2, pp. 165–185, 1991.

[51] L. M. Robeson, "The upper bound revisited," *Journal of Membrane Science*, vol. 320, pp. 390–400, jul 2008.

[52] A. Thornton, L. Robeson, and B. Freeman, "The Membrane Database," 2012.

[53] S. Kasahara, E. Kamio, and H. Matsuyama, "Improvements in the CO2 permeation selectivities of amino acid ionic liquid-based facilitated transport membranes by controlling their gas absorption properties," *Journal of Membrane Science*, vol. 454, pp. 155–162, mar 2014.

[54] A. Hussain and M.-B. Hägg, "A feasibility study of {CO2} capture from flue gas by a facilitated transport membrane," *Journal of Membrane Science*, vol. 359, pp. 140–148, sep 2010.

[55] C. Zhang, Z. Wang, Y. Cai, C. Yi, D. Yang, and S. Yuan, "Investigation of gas permeation behavior in facilitated transport membranes: Relationship between gas permeance and partial pressure," *Chemical Engineering Journal*, vol. 225, pp. 744–751, jun 2013.

[56] H. Wu, X. Li, Y. Li, S. Wang, R. Guo, Z. Jiang, C. Wu, Q. Xin, and X. Lu, "Facilitated transport mixed matrix membranes incorporated with amine functionalized MCM-41 for enhanced gas separation properties," *Journal of Membrane Science*, vol. 465, pp. 78–90, sep 2014.

[57] L. Deng, T.-J. Kim, and M.-B. Hägg, "Facilitated transport of CO2 in novel PVAm/PVA blend membrane," *Journal of Membrane Science*, vol. 340, pp. 154–163, sep 2009.

[58] J.-N. Shen, C.-C. Yu, G.-N. Zeng, and B. van der Bruggen, "Preparation of a Facilitated Transport Membrane Composed of Carboxymethyl Chitosan and Polyethylenimine for CO2/N2 Separation.," *International journal of molecular sciences*, vol. 14, pp. 3621–38, jan 2013.

[59] J. Huang, J. Zou, and W. S. W. Ho, "Carbon Dioxide Capture Using a CO 2 -Selective Facilitated Transport Membrane," *Ind. Eng. Chem. Res.*, pp. 1261–1267, 2008.

[60] Y. Zhao and W. Winston Ho, "Steric hindrance effect on amine demonstrated in solid polymer membranes for CO2 transport," *Journal of Membrane Science*, vol. 415-416, pp. 132–138, oct 2012.

[61] D. F. Sanders, Z. P. Smith, R. Guo, L. M. Robeson, J. E. McGrath, D. R. Paul, and B. D. Freeman, "Energy-efficient polymeric gas separation membranes for a sustainable future: A review," *Polymer*, vol. 54, pp. 4729–4761, aug 2013.

[62] T.-S. Chung, L. Y. Jiang, Y. Li, and S. Kulprathipanja, "Mixed matrix membranes (MMMs) comprising organic polymers with dispersed inorganic fillers for gas separation," *Progress in Polymer Science*, vol. 32, no. 4, pp. 483–507, 2007.

[63] C. M. Zimmerman, A. Singh, and W. J. Koros, "Tailoring mixed matrix composite membranes for gas separations," *Journal of Membrane Science*, vol. 137, no. 1–2, pp. 145–154, 1997.

[64] M. Arjmandi and M. Pakizeh, "Mixed matrix membranes incorporated with cubic-MOF-5 for improved polyetherimide gas separation membranes: Theory and experiment," *Journal of Industrial and Engineering Chemistry*, vol. 20, pp. 3857–3868, sep 2014.

[65] F. Dorosti, M. R. Omidkhah, M. Z. Pedram, and F. Moghadam, "Fabrication and characterization of polysulfone/polyimide–zeolite mixed matrix membrane for gas separation," *Chemical Engineering Journal*, vol. 171, no. 3, pp. 1469–1476, 2011.

[66] M. G. De Angelis and G. C. Sarti, "Gas sorption and permeation in mixed matrix membranes based on glassy polymers and silica nanoparticles," *Current Opinion in Chemical Engineering*, vol. 1, pp. 148–155, may 2012.

[67] M. G. De Angelis, R. Gaddoni, and G. C. Sarti, "Gas Solubility, Diffusivity, Permeability, and Selectivity in Mixed Matrix Membranes Based on PIM-1 and Fumed Silica," *Industrial & Engineering Chemistry Research*, vol. 52, no. 31, pp. 10506–10520, 2013.

[68] A. Halim, Q. Fu, Q. Yong, P. A. Gurr, S. E. Kentish, and G. G. Qiao, "Soft polymeric nanoparticle additives for next generation gas separation membranes," *J. Mater. Chem. A*, vol. 2, no. 14, pp. 4999–5009, 2014.

[69] S. A. Hashemifard, A. F. Ismail, and T. Matsuura, "Mixed matrix membrane incorporated with large pore size halloysite nanotubes (HNT) as filler for gas separation: experimental.," *Journal of colloid and interface science*, vol. 359, pp. 359–70, jul 2011.

[70] T.-S. Chung, S. S. Chan, R. Wang, Z. Lu, and C. He, "Characterization of permeability and sorption in Matrimid/C60 mixed matrix membranes," *Journal of Membrane Science*, vol. 211, pp. 91–99, jan 2003.

[71] M. J. C. Ordoñez, K. J. Balkus, J. P. Ferraris, and I. H. Musselman, "Molecular sieving realized with ZIF-8/Matrimid mixed-matrix membranes," *Journal of Membrane Science*, vol. 361, no. 1-2, pp. 28–37, 2010.

[72] S. Basu, A. Cano-Odena, and I. F. J. Vankelecom, "MOF-containing mixed-matrix membranes for CO2/CH4 and CO2/N2 binary gas mixture separations," *Separation and Purification Technology*, vol. 81, no. 1, pp. 31–40, 2011.

[73] R. Surya Murali, A. Ismail, M. Rahman, and S. Sridhar, "Mixed matrix membranes of Pebax-1657 loaded with 4A zeolite for gaseous separations," *Separation and Purification Technology*, vol. 129, pp. 1–8, may 2014.

[74] S. Roussanaly, R. Anantharaman, K. Lindqvist, H. Zhai, and E. Rubin, "Membrane properties required for post-combustion CO2 capture at coal-fired power plants," *Journal of Membrane Science*, vol. 511, pp. 250–264, 2016.

[75] V. I. Bondar, B. D. Freeman, and I. Pinnau, "Gas transport properties of poly(ether-b-amide) segmented block copolymers," *Journal of Polymer Science, Part B: Polymer Physics*, vol. 38, no. 15, pp. 2051–2062, 2000.

[76] M. Valero, B. Zornoza, C. Téllez, and J. Coronas, "Mixed matrix membranes for gas separation by combination of silica MCM-41 and MOF NH2-MIL-53(Al) in glassy polymers," *Microporous and Mesoporous Materials*, vol. 192, pp. 23–28, jul 2014.

[77] W. J. Koros and G. k. Fleming, "Membrane-Based Gas Separation," *Journal of Membrane Science*, vol. 83, no. 1, pp. 1–80, 1993.

[78] T. C. Merkel, R. Blanc, I. Ciobanu, B. Firat, A. Suwarlim, and J. Zeid, "Silver salt facilitated transport membranes for olefin/paraffin separations: Carrier instability and a novel regeneration method," *Journal of Membrane Science*, vol. 447, pp. 177–189, 2013.

[79] J. G. Wijmans and R. W. Baker, "the Solution-Diffusion Model - a Review," *Journal of Membrane Science*, vol. 107, no. 1-2, pp. 1–21, 1995.

[80] R. M. Barrer, "Diffusivities in glassy polymers for the dual mode sorption model," *Journal of Membrane Science*, vol. 18, no. 0, pp. 25–35, 1984.

[81] L. Zhao, E. Riensche, R. Menzer, L. Blum, and D. Stolten, "A parametric study of CO2/N2 gas separation membrane processes for post-combustion capture," *Journal of Membrane Science*, vol. 325, pp. 284–294, nov 2008.

[82] D. Bocciardo, M. C. Ferrari, and S. Brandani, "Modelling and multi-stage design of membrane processes applied to carbon capture in coal-fired power plants," *Energy Procedia*, vol. 37, no. 0, pp. 932–940, 2013.

[83] M.-c. Ferrari, D. Bocciardo, and S. Brandani, "Integration of multi-stage membrane carbon capture processes to coal-fired power plants using highly permeable polymers," *Green Energy and Environment*, 2016.

[84] Massaschusetts Institute of Technology, "Carbon Capture and Sequestration Technologies Program," 2016.

[85] B. Hu and H. Zhai, "The cost of carbon capture and storage for coal-fired power plants in China," *International Journal of Greenhouse Gas Control*, vol. 65, no. January, pp. 23–31, 2017.

[86] T. C. Merkel, X. Wei, Z. He, L. S. White, J. G. Wijmans, and R. W. Baker, "Selective exhaust gas recycle with membranes for CO2 capture from natural gas combined cycle power plants," *Industrial and Engineering Chemistry Research*, vol. 52, pp. 1150–1159, 2013.

[87] A. M. Arias, M. C. Mussati, P. L. Mores, N. J. Scenna, J. A. Caballero, and S. F. Mussati, "Optimization of multi-stage membrane systems for CO2 capture from flue gas," *International Journal of Greenhouse Gas Control*, vol. 53, pp. 371–390, 2016.

[88] N. C. Mat and G. G. Lipscomb, "Membrane process optimization for carbon capture," *International Journal of Greenhouse Gas Control*, vol. 62, no. November 2016, pp. 1–12, 2017.

[89] D. R. Paul and D. R. Kemp, "The diffusion time lag in polymer membranes containing adsorptive fillers," *Journal of Polymer Science: Polymer Symposia*, vol. 41, no. 1, pp. 79–93, 1973.

[90] S. Kulprathipanja, N. N. Li, and R. H. Nelson, "Separation of fluids by means of mixed matrix membranes," *US Patent 4,740,219*, 1988.

[91] M. Jia, K. V. Peinemann, and R. D. Behling, "Molecular sieving effect of the zeolite-filled silicone rubber membranes in gas permeation," *Journal of Membrane Science*, vol. 57, no. 2-3, pp. 289–292, 1991.

[92] J. M. Duval, B. Folkers, M. H. V. Mulder, G. Desgrandchamps, and C. A. Smolders, "Adsorbent filled membranes for gas separation. Part 1. Improvement of the gas separation properties of polymeric membranes by incorporation of microporous adsorbents," *Journal of Membrane Science*, vol. 80, no. 1, pp. 189–198, 1993.

[93] T. M. Gür, "Permselectivity of zeolite filled polysulfone gas separation membranes," *Journal of Membrane Science*, vol. 93, pp. 283–289, sep 1994.

[94] M. G. Süer, N. Baç, and L. Yilmaz, "Gas permeation characteristics of polymer-zeolite mixed matrix membranes," *Journal of Membrane Science*, vol. 91, no. 1–2, pp. 77–86, 1994.

[95] P. Goh, A. Ismail, S. Sanip, B. Ng, and M. Aziz, "Recent advances of inorganic fillers in mixed matrix membrane for gas separation," *Separation and Purification Technology*, vol. 81, pp. 243–264, oct 2011.

[96] M. P. Bernal, J. Coronas, M. Menéndez, and J. Santamaría, "Separation of CO2/N2 mixtures using MFI-type zeolite membranes," *AIChE Journal*, vol. 50, no. 1, pp. 127–135, 2004.

[97] M. Hussain and A. König, "Mixed-Matrix Membrane for Gas Separation: Polydimethylsiloxane Filled with Zeolite," *Chemical Engineering & Technology*, vol. 35, pp. 561–569, mar 2012.

[98] J. P. Boom, I. G. M. Pünt, H. Zwijnenberg, R. De Boer, D. Bargeman, C. a. Smolders, and H. Strathmann, "Transport through zeolite filled polymeric membranes," *Journal of Membrane Science*, vol. 138, no. 2, pp. 237–258, 1998.

[99] K. Zarshenas, A. Raisi, and A. Aroujalian, "Mixed matrix membrane of nano-zeolite NaX/poly (ether-block-amide) for gas separation applications," *Journal of Membrane Science*, vol. 510, pp. 270–283, 2016.

[100] T. W. Pechar, S. Kim, B. Vaughan, E. Marand, M. Tsapatsis, H. K. Jeong, and C. J. Cornelius, "Fabrication and characterization of polyimide–zeolite L mixed matrix membranes for gas separations," *Journal of Membrane Science*, vol. 277, no. 1–2, pp. 195–202, 2006.

[101] D. Bastani, N. Esmaeili, and M. Asadollahi, "Polymeric mixed matrix membranes containing zeolites as a filler for gas separation applications: A review," *Journal of Industrial and Engineering Chemistry*, vol. 19, pp. 375–393, mar 2013.

[102] N. Kosinov, J. Gascon, F. Kapteijn, and E. J. M. Hensen, "Recent developments in zeolite membranes for gas separation," *Journal of Membrane Science*, vol. 499, pp. 65–79, 2016.

[103] D. Q. Vu, W. J. Koros, and S. J. Miller, "Mixed matrix membranes using carbon molecular sieves: II. Modeling permeation behavior," *Journal of Membrane Science*, vol. 211, pp. 335–348, jan 2003.

[104] D. Q. Vu, W. J. Koros, and S. J. Miller, "Effect of condensable impurity in CO2/CH4 gas feeds on performance of mixed matrix membranes using carbon molecular sieves," *Journal of Membrane Science*, vol. 221, pp. 233–239, aug 2003.

[105] A. Ahmad, Z. Jawad, S. Low, and S. Zein, "A cellulose acetate/multi-walled carbon nanotube mixed matrix membrane for CO2/N2 separation," *Journal of Membrane Science*, vol. 451, pp. 55–66, feb 2014.

[106] C. H. Park, E. Tocci, E. Fontananova, M. A. Bahattab, S. A. Aljlil, and E. Drioli, "Mixed matrix membranes containing functionalized multiwalled carbon nanotubes: Mesoscale simulation and experimental approach for optimizing dispersion," *Journal of Membrane Science*, vol. 514, pp. 195–209, 2016.

[107] S. Kim, L. Chen, J. K. Johnson, and E. Marand, "Polysulfone and functionalized carbon nanotube mixed matrix membranes for gas separation: Theory and experiment," *Journal of Membrane Science*, vol. 294, pp. 147–158, may 2007.

[108] D. Zhao, J. Ren, H. Li, X. Li, and M. Deng, "Gas separation properties of poly(amide-6-b-ethylene oxide)/amino modified multi-walled carbon nanotubes mixed matrix membranes," *Journal of Membrane Science*, vol. 467, pp. 41–47, oct 2014.

[109] Y. Zhao, B. T. Jung, L. Ansaloni, and W. W. Ho, "Multiwalled carbon nanotube mixed matrix membranes containing amines for high pressure CO2/H2 separation," *Journal of Membrane Science*, vol. 459, pp. 233–243, jun 2014.

[110] A. F. Bushell, M. P. Attfield, C. R. Mason, P. M. Budd, Y. Yampolskii, L. Starannikova, A. Rebrov, F. Bazzarelli, P. Bernardo, J. Carolus Jansen, M. Lanč, K. Friess, V. Shantarovich, V. Gustov, and V. Isaeva, "Gas permeation parameters of mixed matrix membranes based on the polymer of intrinsic microporosity PIM-1 and the zeolitic imidazolate framework ZIF-8," *Journal of Membrane Science*, vol. 427, pp. 48–62, jan 2013.

[111] Y. Dai, J. R. Johnson, O. Karvan, D. S. Sholl, and W. J. Koros, "Ultem®/ZIF-8 mixed matrix hollow fiber membranes for CO2/N2 separations," *Journal of Membrane Science*, vol. 401–402, no. 0, pp. 76–82, 2012.

[112] V. Nafisi and M.-B. Hägg, "Development of dual layer of ZIF-8/PEBAX-2533 mixed matrix membrane for CO2 capture," *Journal of Membrane Science*, vol. 459, pp. 244–255, jun 2014.

[113] S. Shahid and K. Nijmeijer, "High pressure gas separation performance of mixed-matrix polymer membranes containing mesoporous Fe(BTC)," *Journal of Membrane Science*, vol. 459, pp. 33–44, jun 2014.

[114] B. Zornoza, C. Tellez, J. Coronas, J. Gascon, and F. Kapteijn, "Metal organic framework based mixed matrix membranes: An increasingly important field of research with a large application potential," *Microporous and Mesoporous Materials*, vol. 166, pp. 67–78, jan 2013.

[115] J. Y. Lee, R. B. Thompson, D. Jasnow, and A. C. Balazs, "Effect of Nanoscopic Particles on the Mesophase Structure of Diblock Copolymers," *Macromolecules*, vol. 35, pp. 4855–4858, 2002.

[116] A. C. Balazs, T. Emrick, and T. P. Russell, "Nanoparticle Polymer Composites: Where Two Small Worlds Meet," *Science*, vol. 314, no. 5802, pp. 1107–1110, 2006.

[117] A. Ebneyamini, H. Azimi, F. H. Tezel, and J. Thibault, "Modelling of mixed matrix membranes: Validation of the resistance-based model," *Journal of Membrane Science*, vol. 543, no. August, pp. 361–369, 2017.

[118] H. Vinh-Thang and S. Kaliaguine, "Predictive Models for Mixed-Matrix Membrane Performance: A Review," *Chemical Reviews*, vol. 113, no. 7, pp. 4980–5028, 2013.

[119] J. C. Maxwell, *Treatise on Electricity and Magnetism*. Oxford University Press, 1873.

[120] E. E. Gonzo, M. L. PARENTIS, and J. C. GOTTIFREDI, "Estimating models for predicting effective permeability of mixed matrix membranes," *Journal of Membrane Science*, vol. 277, pp. 46–54, jun 2006.

[121] N. Bryan, E. Lasseuguette, M. van Dalen, N. Permogorov, A. Amieiro, S. Brandani, and M.-C. Ferrari, "Development of Mixed Matrix Membranes Containing Zeolites for Post-combustion Carbon Capture.," *Energy Procedia*, vol. 63, pp. 160–166, 2014.

[122] R. Mahajan and W. J. Koros, "Mixed matrix membrane materials with glassy polymers. Part 1," *Polymer Engineering & Science*, vol. 42, no. 7, pp. 1420–1431, 2002.

[123] R. Pal, "Permeation models for mixed matrix membranes.," *Journal of colloid and interface science*, vol. 317, pp. 191–8, jan 2008.

[124] L. Hao, P. Li, T. Yang, and T.-S. S. Chung, "Room temperature ionic liquid/ZIF-8 mixed-matrix membranes for natural gas sweetening and post-combustion {CO2} capture," *Journal of Membrane Science*, vol. 436, pp. 221–231, jun 2013.

[125] V. Bruggeman, "Berechnung verschiedener physikalischer Konstanten von heterogenen Substanzen. I. Dielektrizitätskonstanten und Leitfähigkeiten der Mischkörper aus isotropen Substanzen [Calculation of various physical constants of heterogeneous substances . I. dielectri," *Annalen der physik*, vol. 461, no. 8, pp. 665–679, 1935.

[126] S. A. Hashemifard, A. F. Ismail, and T. Matsuura, "Prediction of gas permeability in mixed matrix membranes using theoretical models," *Journal of Membrane Science*, vol. 347, no. 1–2, pp. 53–61, 2010.

[127] T. T. Moore and W. J. Koros, "Non-ideal effects in organic–inorganic materials for gas separation membranes," *Journal of Molecular Structure*, vol. 739, pp. 87–98, apr 2005.

[128] M. Fang, C. Wu, Z. Yang, T. Wang, Y. Xia, and J. Li, "ZIF-8/PDMS mixed matrix membranes for propane/nitrogen mixture separation: Experimental result and permeation model validation," *Journal of Membrane Science*, sep 2014.

[129] T. C. Merkel, B. D. Freeman, R. J. Spontak, Z. He, I. Pinnau, P. Meakin, and A. J. Hill, "Ultrapermeable, Reverse-Selective Nanocomposite Membranes," *Science*, vol. 296, no. 5567, pp. 519–522, 2002.

[130] M. M. Rahman, S. Shishatskiy, C. Abetz, P. Georgopanos, S. Neumann, M. M. Khan, V. Filiz, and V. Abetz, "Influence of temperature upon properties of tailor-made PEBAX® MH 1657 nanocomposite membranes for post-combustion CO2 capture," *Journal of Membrane Science*, vol. 469, pp. 344–354, nov 2014.

[131] C.-C. Chen, W. Qiu, S. J. Miller, and W. J. Koros, "Plasticization-resistant hollow fiber membranes for CO2/CH4 separation based on a thermally crosslinkable polyimide," *Journal of Membrane Science*, vol. 382, pp. 212–221, oct 2011.

[132] X. Ren, J. Ren, and M. Deng, "Poly(amide-6-b-ethylene oxide) membranes for sour gas separation," *Separation and Purification Technology*, vol. 89, pp. 1–8, mar 2012.

[133] C. a. Scholes, J. Bacus, G. Q. Chen, W. X. Tao, G. Li, A. Qader, G. W. Stevens, and S. E. Kentish, "Pilot plant performance of rubbery polymeric membranes for carbon dioxide separation from syngas," *Journal of Membrane Science*, vol. 389, pp. 470–477, feb 2012.

[134] B. Kraftschik, W. J. Koros, J. Johnson, and O. Karvan, "Dense film polyimide membranes for aggressive sour gas feed separations," *Journal of Membrane Science*, vol. 428, pp. 608–619, feb 2013.

[135] W. Yave, A. Car, K.-V. V. Peinemann, M. Q. Shaikh, K. Rätzke, and F. Faupel, "Gas permeability and free volume in poly(amide-b-ethylene oxide)/polyethylene glycol blend membranes," *Journal of Membrane Science*, vol. 339, pp. 177–183, sep 2009.

[136] X. Ren, J. Ren, H. Li, S. Feng, and M. Deng, "Poly (amide-6-b-ethylene oxide) multilayer composite membrane for carbon dioxide separation," *International Journal of Greenhouse Gas Control*, vol. 8, no. 0, pp. 111–120, 2012.

[137] S. Armstrong, B. Freeman, A. Hiltner, and E. Baer, "Gas permeability of melt-processed poly(ether block amide) copolymers and the effects of orientation," *Polymer*, vol. 53, no. 6, pp. 1383–1392, 2012.

[138] A. Car, C. Stropnik, W. Yave, and K. V. Peinemann, "Pebax/polyethylene glycol blend thin film composite membranes for CO2 separation: Performance with mixed gases," *Separation and Purification Technology*, vol. 62, no. 1, pp. 110–117, 2008.

[139] S. Shahid, K. Nijmeijer, S. Nehache, I. Vankelecom, A. Deratani, and D. Quemener, "MOF-mixed matrix membranes: Precise dispersion of MOF particles with better compatibility via a particle fusion approach for enhanced gas separation properties," *Journal of Membrane Science*, vol. 492, pp. 21–31, 2015.

[140] A. Car, C. Stropnik, W. Yave, and K. V. Peinemann, "PEG modified poly(amide-b-ethylene oxide) membranes for CO2 separation," *Journal of Membrane Science*, vol. 307, pp. 88–95, jan 2008.

[141] G. Dong, J. Hou, J. Wang, Y. Zhang, V. Chen, and J. Liu, "Enhanced CO2/N2 separation by porous reduced graphene oxide/Pebax mixed matrix membranes," *Journal of Membrane Science*, vol. 520, pp. 860–868, 2016.

[142] Y. Dai, X. Ruan, Z. Yan, K. Yang, M. Yu, H. Li, W. Zhao, and G. He, "Imidazole functionalized graphene oxide/PEBAX mixed matrix membranes for efficient CO2 capture," *Separation and Purification Technology*, vol. 166, pp. 171–180, 2016.

[143] J. H. Kim and Y. M. Lee, "Gas permeation properties of poly(amide-6-b-ethylene oxide)–silica hybrid membranes," *Journal of Membrane Science*, vol. 193, no. 2, pp. 209–225, 2001.

[144] H. Lin and B. D. Freeman, "Gas solubility, diffusivity and permeability in poly(ethylene oxide)," *Journal of Membrane Science*, vol. 239, no. 1, pp. 105–117, 2004.

[145] P. Jan Roman, F. Detlev, K. Thomas, and P. Klaus-Viktor, "Gas permeation measurement under defined humidity via constant volume/variable pressure method," *Journal of Membrane Science*, vol. 389, pp. 343–348, 2012.

[146] D. Zhao, J. Ren, H. Li, K. Hua, and M. Deng, "Poly(amide-6-b-ethylene oxide)/SAPO-34 mixed matrix membrane for CO2 separation," *Journal of Energy Chemistry*, vol. 23, pp. 227–234, mar 2014.

[147] N. L. Le, Y. Wang, and T.-S. Chung, "Pebax/POSS mixed matrix membranes for ethanol recovery from aqueous solutions via pervaporation," *Journal of Membrane Science*, vol. 379, pp. 174–183, sep 2011.

[148] K. S. Park, Z. Ni, A. P. Côté, J. Y. Choi, R. Huang, F. J. Uribe-Romo, H. K. Chae, M. O'Keeffe, and O. M. Yaghi, "Exceptional chemical and thermal stability of zeolitic imidazolate frameworks.," *Proceedings of the National Academy of Sciences of the United States of America*, vol. 103, no. 27, pp. 10186–91, 2006.

[149] L. S. Lai, Y. F. Yeong, T. L. Chew, K. K. Lau, and M. S. Azmi, "CO2 and CH4 gas permeation study via zeolitic imidazolate framework (ZIF)-8 membrane," *Journal of Natural Gas Science and Engineering*, vol. 34, pp. 509–519, 2016.

[150] C. Chmelik, "Characteristic Features of Molecular Transport in MOF ZIF-8 as revealed by IR Microimaging," *Microporous and Mesoporous Materials*, pp. 1–8, 2015.

[151] R. Mueller, S. Zhang, C. Zhang, R. Lively, and S. Vasenkov, "Relationship between long-range diffusion and diffusion in the ZIF-8 and polymer phases of a mixed-matrix membrane by high field NMR diffusometry," *Journal of Membrane Science*, vol. 477, pp. 123–130, mar 2015.

[152] V. Nafisi and M. B. Hägg, "Gas separation properties of ZIF-8/6FDA-durene diamine mixed matrix membrane," *Separation and Purification Technology*, vol. 128, pp. 31–38, 2014.

[153] H. Bux, C. Chmelik, J. M. Van Baten, R. Krishna, and J. Caro, "Novel MOF-membrane for molecular sieving predicted by IR-diffusion studies and molecular modeling," *Advanced Materials*, vol. 22, no. 42, pp. 4741–4743, 2010.

[154] D. Peralta, G. Chaplais, J. L. Paillaud, A. Simon-Masseron, K. Barthelet, and G. D. Pirngruber, "The separation of xylene isomers by ZIF-8: A demonstration of the extraordinary flexibility of the ZIF-8 framework," *Microporous and Mesoporous Materials*, vol. 173, pp. 1–5, 2013.

[155] D. I. Kolokolov, A. G. Stepanov, and H. Jobic, "Mobility of the 2-Methylimidazolate Linkers in ZIF-8 Probed by 2H NMR: Saloon Doors for the Guests," *Journal of Physical Chemistry C*, vol. 119, no. 49, pp. 27512–27520, 2015.

[156] K. Zhang, R. P. Lively, C. Zhang, R. R. Chance, W. J. Koros, D. S. Sholl, and S. Nair, "Exploring the framework hydrophobicity and flexibility of zif-8: From biofuel recovery to hydrocarbon separations," *Journal of Physical Chemistry Letters*, vol. 4, no. 21, pp. 3618–3622, 2013.

[157] D. Fairen-Jimenez, S. A. Moggach, M. T. Wharmby, P. A. Wright, S. Parsons, and T. Düren, "Opening the gate: Framework flexibility in ZIF-8 explored by experiments and simulations," *Journal of the American Chemical Society*, vol. 133, no. 23, pp. 8900–8902, 2011.

[158] T. Chokbunpiam, R. Chanajaree, T. Remsungnen, O. Saengsawang, S. Fritzsche, C. Chmelik, J. Caro, W. Janke, and S. Hannongbua, "N2 in ZIF-8: Sorbate induced structural changes and self-diffusion," *Microporous and Mesoporous Materials*, vol. 187, pp. 1–6, 2014.

[159] C. Chmelik and J. K??rger, "The predictive power of classical transition state theory revealed in diffusion studies with MOF ZIF-8," *Microporous and Mesoporous Materials*, vol. 225, pp. 128–132, 2016.

[160] L. Zhang, G. Wu, and J. Jiang, "Adsorption and Diffusion of CO 2 and CH 4 in Zeolitic Imidazolate Framework-8: Effect of Structural Flexibility," *The Journal of Physical Chemistry C*, p. 140411102121001, 2014.

[161] C. Chmelik, J. van Baten, and R. Krishna, "Hindering effects in diffusion of CO 2/CH 4 mixtures in ZIF-8 crystals," *Journal of Membrane Science*, vol. 397-398, pp. 87–91, 2012.

[162] S. Hwang, W. S. Chi, S. J. Lee, S. H. Im, J. H. Kim, and J. Kim, "Hollow ZIF-8 nanoparticles improve the permeability of mixed matrix membranes for CO2/CH4 gas separation," *Journal of Membrane Science*, vol. 480, pp. 11–19, 2015.

[163] P. D. Sutrisna, J. Hou, H. Li, Y. Zhang, and V. Chen, "Improved operational stability of Pebax-based gas separation membranes with ZIF-8: A comparative study of flat sheet and composite hollow fibre membranes," *Journal of Membrane Science*, vol. 524, no. July 2016, pp. 266–279, 2017.

[164] S. Park, W. R. Kang, H. T. Kwon, S. Kim, M. Seo, J. Bang, S. hyup Lee, H. K. Jeong, and J. S. Lee, "The polymeric upper bound for N2/NF3 separation and beyond; ZIF-8 containing mixed matrix membranes," *Journal of Membrane Science*, vol. 486, pp. 29–39, jul 2015.

[165] C. Zhang, Y. Dai, J. R. Johnson, O. Karvan, and W. J. Koros, "High performance ZIF-8/6FDA-DAM mixed matrix membrane for propylene/propane separations," *Journal of Membrane Science*, vol. 389, pp. 34–42, feb 2012.

[166] M. Benzaqui, R. Semino, N. Menguy, F. Carn, T. Kundu, J. M. Guigner, N. B. McKeown, K. J. Msayib, M. Carta, R. Malpass-Evans, C. Le Guillouzer, G. Clet, N. A. Ramsahye, C. Serre, G. Maurin, and N. Steunou, "Toward an Understanding of the Microstructure and Interfacial Properties of PIMs/ZIF-8 Mixed Matrix Membranes," *ACS Applied Materials and Interfaces*, vol. 8, no. 40, pp. 27311–27321, 2016.

[167] E. M. Mahdi and J. C. Tan, "Mixed-matrix membranes of zeolitic imidazolate framework (ZIF-8)/Matrimid nanocomposite: Thermo-mechanical stability and viscoelasticity underpinning membrane separation performance," *Journal of Membrane Science*, vol. 498, pp. 276–290, 2016.

[168] J. A. Thompson, K. W. Chapman, W. J. Koros, C. W. Jones, and S. Nair, "Sonication-induced Ostwald ripening of ZIF-8 nanoparticles and formation of ZIF-8/polymer composite membranes," *Microporous and Mesoporous Materials*, vol. 158, pp. 292–299, aug 2012.

[169] N. Jusoh, Y. F. Yeong, K. K. Lau, and A. M. Shariff, "Mixed Matrix Membranes Comprising of ZIF-8 Nanofillers for Enhanced Gas Transport Properties," *Procedia Engineering*, vol. 148, pp. 1259–1265, 2016.

[170] N. Jusoh, Y. F. Yeong, W. L. Cheong, K. K. Lau, and A. M. Shariff, "Facile fabrication of mixed matrix membranes containing 6FDA-durene polyimide and ZIF-8 nanofillers for CO2 capture," *Journal of Industrial and Engineering Chemistry*, vol. 44, pp. 164–173, 2016.

[171] H. Li, L. Tuo, K. Yang, H. K. Jeong, Y. Dai, G. He, and W. Zhao, "Simultaneous enhancement of mechanical properties and CO2 selectivity of ZIF-8 mixed matrix membranes: Interfacial toughening effect of ionic liquid," *Journal of Membrane Science*, vol. 511, pp. 130–142, 2016.

[172] N. Jusoh, Y. F. Yeong, K. K. Lau, and A. M. Shariff, "Transport properties of mixed matrix membranes encompassing zeolitic imidazolate framework 8 (ZIF-8) nanofiller and 6FDA-durene polymer: Optimization of process variables for the separation of CO2 from CH4," *Journal of Cleaner Production*, vol. 8, 2017.

[173] M. Amirilargani and B. Sadatnia, "Poly(vinyl alcohol)/zeolitic imidazolate frameworks (ZIF-8) mixed matrix membranes for pervaporation dehydration of isopropanol," *Journal of Membrane Science*, vol. 469, pp. 1–10, nov 2014.

[174] J. S. Beck, J. C. Vartuli, W. J. Roth, M. E. Leonowicz, C. T. Kresge, K. D. Schmitt, C. T. W. Chu, D. H. Olson, E. W. Sheppard, S. B. McCullen, J. B. Higgins, and J. L. Schlenker, "A new family of mesoporous molecular sieves prepared with liquid crystal templates," *Journal of the American Chemical Society*, vol. 114, no. 27, pp. 10834–10843, 1992.

[175] S. Y. Lee and S. J. Park, "A review on solid adsorbents for carbon dioxide capture," *Journal of Industrial and Engineering Chemistry*, vol. 23, pp. 1–11, 2015.

[176] S. Kim and E. Marand, "High permeability nano-composite membranes based on mesoporous MCM-41 nanoparticles in a polysulfone matrix," *Microporous and Mesoporous Materials*, vol. 114, pp. 129–136, sep 2008.

[177] C. G. Sonwane and S. K. Bhatia, "Structural characterization of MCM-41 over a wide range of length scales," *Langmuir*, vol. 15, no. 8, pp. 2809–2816, 1999.

[178] B. D. Reid, F. A. Ruiz-trevino, I. H. Musselman, K. J. Balkus, and J. P. Ferraris, "Gas Permeability Properties of Polysulfone Membranes Containing the Mesoporous Molecular Sieve MCM-41," *Chem. Mater.*, no. 7, pp. 2366–2373, 2001.

[179] M. R. Mello, D. Phanon, G. Q. Silveira, P. L. Llewellyn, and C. M. Ronconi, "Amine-modified MCM-41 mesoporous silica for carbon dioxide capture," *Microporous and Mesoporous Materials*, vol. 143, no. 1, pp. 174–179, 2011.

[180] X. Wang, L. Chen, and Q. Guo, "Development of hybrid amine-functionalized MCM-41 sorbents for CO2 capture," *Chemical Engineering Journal*, vol. 260, pp. 573–581, 2014.

[181] B. Zornoza, C. Téllez, and J. Coronas, "Mixed matrix membranes comprising glassy polymers and dispersed mesoporous silica spheres for gas separation," *Journal of Membrane Science*, vol. 368, no. 1-2, pp. 100–109, 2011.

[182] A. Galve, D. Sieffert, C. Staudt, M. Ferrando, C. Güell, C. Téllez, and J. Coronas, "Combination of ordered mesoporous silica MCM-41 and layered titanosilicate JDF-L1 fillers for 6FDA-based copolyimide mixed matrix membranes," *Journal of Membrane Science*, vol. 431, pp. 163–170, 2013.

[183] P. Burmann, B. Zornoza, C. Téllez, and J. Coronas, "Mixed matrix membranes comprising {MOFs} and porous silicate fillers prepared via spin coating for gas separation," *Chemical Engineering Science*, vol. 107, pp. 66–75, apr 2014.

[184] A. L. Khan, C. Klaysom, A. Gahlaut, and I. F. J. Vankelecom, "Polysulfone acrylate membranes containing functionalized mesoporous MCM-41 for CO2 separation," *Journal of Membrane Science*, vol. 436, pp. 145–153, 2013.

[185] B. Zornoza, C. Téllez, J. Coronas, O. Esekhile, and W. J. Koros, "Mixed matrix membranes based on 6FDA polyimide with silica and zeolite microsphere dispersed phases," *AIChE Journal*, vol. 61, no. 12, pp. 4481–4490, 2015.

[186] H. Tan, Y. Wu, Y. Zhou, Z. Liu, and T. Li, "Pervaporative recovery of n-butanol from aqueous solutions with MCM-41 filled PEBA mixed matrix membrane," *Journal of Membrane Science*, vol. 453, pp. 302–311, 2014.

[187] G. Dong, H. Li, and V. Chen, "Challenges and opportunities for mixed-matrix membranes for gas separation," *J. Mater. Chem. A*, vol. 1, no. 15, pp. 4610–4630, 2013.

[188] S. Rafiq, L. Deng, and M.-B. Hägg, "Role of Facilitated Transport Membranes and Composite Membranes for Efficient CO ₂ Capture - A Review," *ChemBioEng Reviews*, vol. 3, no. 2, pp. 68–85, 2016.

[189] R. Ameloot, F. Vermoortele, W. Vanhove, M. B. J. Roeffaers, B. F. Sels, and D. E. De Vos, "Interfacial synthesis of hollow metal?????"organic framework capsules demonstrating selective permeability," *Nature Chemistry*, vol. 3, no. 5, pp. 382–387, 2011.

[190] D. K. Roh, S. J. Kim, W. S. Chi, J. K. Kim, and J. H. Kim, "Dual-functionalized mesoporous TiO(2) hollow nanospheres for improved CO(2) separation membranes.," *Chemical communications (Cambridge, England)*, vol. 50, no. 43, pp. 5717–20, 2014.

[191] J. Cravillon, S. Münzer, S.-j. Lohmeier, A. Feldhoff, and K. Huber, "Rapid Room-Temperature Synthesis and Characterization of Nanocrystals of a Prototypical Zeolitic Imidazolate Framework- Supporting Information," *Chemistry of Materials*, vol. 21, no. 8, pp. 1–21, 2009.

[192] Z. Zhang, S. Xian, Q. Xia, H. Wang, Z. Li, and J. Li, "Enhancement of CO2 Adsorption and CO2/N2 Selectivity on ZIF-8 via Postsynthetic Modification," *AIChE Journal*, vol. 59, no. 6, pp. 2195–2206, 2013.

[193] G. Qi, Y. Wang, L. Estevez, A. K. Switzer, X. Duan, X. Yang, and E. P. Giannelis, "Facile and scalable synthesis of monodispersed spherical capsules with a mesoporous shell," *Chemistry of Materials*, vol. 22, no. 9, pp. 2693–2695, 2010.

[194] M. Naseri, S. F. Mousavi, T. Mohammadi, and O. Bakhtiari, "Synthesis and gas transport performance of MIL-101/Matrimid mixed matrix membranes," *Journal of Industrial and Engineering Chemistry*, vol. 29, pp. 249–256, 2015.

[195] A. Ismail, S. Hashemifard, and T. Matsuura, "Facilitated transport effect of Ag+ ion exchanged halloysite nanotubes on the performance of polyetherimide mixed matrix membrane for gas separation," *Journal of Membrane Science*, vol. 379, pp. 378–385, sep 2011.

[196] B. Seoane, C. Téllez, J. Coronas, and C. Staudt, "NH2-MIL-53(Al) and NH2-MIL-101(Al) in sulfur-containing copolyimide mixed matrix membranes for gas separation," *Separation and Purification Technology*, vol. 111, pp. 72–81, jun 2013.

[197] Fisher Scientific, "Fisher Scientific Ultrasonic Baths," 2009.

[198] T. T. Moore, S. Damle, P. J. Williams, and W. J. Koros, "Characterization of low permeability gas separation membranes and barrier materials; design and operation considerations," *Journal of Membrane Science*, vol. 245, pp. 227–231, dec 2004.

[199] S. W. Rutherford and D. D. Do, "Review of time lag permeation technique as a method for characterisation of porous media and membranes," *Adsorption*, vol. 3, no. 4, pp. 283–312, 1997.

[200] J. Crank, *The mathematics of diffusion*. Oxford: Oxford University Press, 2nd editio ed., 1975.

[201] S. J. B. Reed, "Instrumentation," in *Scanning electron microscopy*, ch. 3, pp. 21–40, Cambridge: Cambridge University Press, 2005.

[202] S. J. B. Reed, "Electron–specimen interactions," in *Scanning electron microscopy*, ch. 2, pp. 7–20, Cambridge: Cambridge University Press, 2005.

[203] S. J. B. Reed, "Scanning electron microscopy," in *Scanning electron microscopy*, ch. 4, pp. 41–75, Cambridge: Cambridge University Press, 2005.

[204] J. A. Gibson, *The development of functionalised porous carbon materials for the separation of carbon dioxide from gas mixtures*. PhD thesis, University of Edinburgh, 2016.

[205] E. Pantatosaki, G. Megariotis, A. K. Pusch, C. Chmelik, F. Stallmach, and G. K. Papadopoulos, "On the impact of sorbent mobility on the sorbed phase equilibria and dynamics: A study of methane and carbon dioxide within the zeolite imidazolate framework-8," *Journal of Physical Chemistry C*, vol. 116, no. 1, pp. 201–207, 2012.

[206] H. Huang, W. Zhang, D. Liu, B. Liu, G. Chen, and C. Zhong, "Effect of temperature on gas adsorption and separation in ZIF-8: A combined experimental and molecular simulation study," *Chemical Engineering Science*, vol. 66, no. 23, pp. 6297–6305, 2011.

[207] J. McEwen, J. D. Hayman, and a. Ozgur Yazaydin, "A comparative study of CO2, CH4 and N2 adsorption in ZIF-8, Zeolite-13X and BPL activated carbon," *Chemical Physics*, vol. 412, pp. 72–76, 2013.

[208] J. Pérez-Pellitero, H. Amrouche, F. R. Siperstein, G. Pirngruber, C. Nieto-Draghi, G. Chaplais, A. Simon-Masseron, D. Bazer-Bachi, D. Peralta, and N. Bats, "Adsorption of CO2, CH4, and N2 on zeolitic imidazolate frameworks: Experiments and simulations," *Chemistry - A European Journal*, vol. 16, no. 5, pp. 1560–1571, 2010.

[209] M. Majumder, C. S. Rendall, J. A. Eukel, J. Y. L. Wang, N. Behabtu, C. L. Pint, T. Y. Liu, A. W. Orbaek, F. Mirri, J. Nam, A. R. Barron, R. H. Hauge, H. K. Schmidt, and M. Pasquali, "Overcoming the "coffee-stain" effect by compositional marangoni-flow-assisted drop-drying," *Journal of Physical Chemistry B*, vol. 116, no. 22, pp. 6536–6542, 2012.

[210] A. Stannard, "Dewetting-mediated pattern formation in nanoparticle assemblies," *Journal of Physics: Condensed Matter*, vol. 23, no. 8, p. 083001, 2011.

[211] U. Thiele, I. Vancea, a. J. Archer, M. J. Robbins, L. Frastia, a. Stannard, E. Pauliac-Vaujour, C. P. Martin, M. O. Blunt, and P. J. Moriarty, "Modelling approaches to the dewetting of evaporating thin films of nanoparticle suspensions.," *Journal of physics. Condensed matter : an Institute of Physics journal*, vol. 21, no. 26, p. 264016, 2009.

[212] K. Jacobs, S. Herminghaus, and K. R. Mecke, "Thin liquid polymer films rupture via defects," *Langmuir*, vol. 14, no. 4, pp. 965–969, 1998.

[213] J. Schindelin, I. Arganda-Carreras, E. Frise, V. Kaynig, M. Longair, T. Pietzsch, S. Preibisch, C. Rueden, S. Saalfeld, B. Schmid, J.-Y. Tinevez, D. J. White, V. Hartenstein, K. Eliceiri, P. Tomancak, and A. Cardona, "Fiji: an open-source platform for biological-image analysis.," *Nature methods*, vol. 9, no. 7, pp. 676–82, 2012.

[214] J. Schindelin, C. T. Rueden, M. C. Hiner, and K. W. Eliceiri, "The ImageJ ecosystem: An open platform for biomedical image analysis," *Molecular Reproduction and Development*, vol. 82, no. 7-8, pp. 518–529, 2015.

[215] B. Marler, U. Oberhagemann, S. Vortmann, and H. Gies, "Influence of the sorbate type on the XRD peak intensities of loaded MCM-41," *Microporous Materials*, vol. 6, pp. 375–383, 1996.

[216] J. Liu, X. Hou, H. B. Park, and H. Lin, "High-Performance Polymers for Membrane CO2/N2Separation," *Chemistry - A European Journal*, vol. 22, no. 45, pp. 15980–15990, 2016.